Title

Early effects of acute joint injury, the beginnings of Post-Traumatic Osteoarthritis

Author

Leale, Dustin

Publication Date

2023

Peer reviewed|Thesis/dissertation

Early Effects of Acute Joint Injury,
the Beginnings of Post-Traumatic Osteoarthritis
By

DUSTIN M. LEALE
DISSERTATION

Submitted in partial satisfaction of the requirements for the degree of

DOCTOR OF PHILOSOPHY

in

Integrative Pathobiology

in the

OFFICE OF GRADUATE STUDIES

of the

UNIVERSITY OF CALIFORNIA

DAVIS

Approved:

Dominik Haudenschild, Chair

Natalia Vapniarsky-Arzi

Gabriela Loots

Committee in Charge

2023

TABLE OF CONTENTS

TABLE OF FIGURES

TABLE OF TABLES

ABBREVIATIONS

OA - Osteoarthritis

PTOA – Post traumatic osteoarthritis

AIR – Acute injury response

scRNA-seq – Single-cell RNA sequencing

cDNA – Complementary DNA

mRNA – Messenger RNA

PBS – Phosphate Buffered Saline

PC – Principal component

PCA – Principal component analysis

UMI – Unique molecular identifier

UMAP – Uniform manifold approximation and projection

sNuc-Seq - Single nucleus sequencing

NK (cells) - Natural killer (cells)

ACL – Anterior cruciate ligament

IHC – Immunohistochemistry

H&E – Hematoxylin and eosin (histology)

DEGs – Differentially expressed genes

GO – Gene Ontology

Th1 - T helper cell type 1

Th2 - T helper cell type 2

ECM – Extracellular matrix

DCs – Dendritic cells

IL – Interleukin

DAMPs – Damage associated molecular patterns

DMM – Destabilization of the medial meniscus

ACL-T – Anterior cruciate ligament transection

ACL-R – Anterior cruciate ligament repair

p-ACL-T – Partial anterior cruciate ligament transection

ICRS – International Cartilage Repair Society

BMSC – Bone marrow stem cells

IA – Intra-Articular

TP – Total protein

TNCC – Total nucleated cell count

CBC – Complete blood count

CDK9 – Cyclin-dependent kinase 9

PLGA – Polylactic-co-glycolic acid

SF – Synovial fluid

DMSO – Dimethyl sulfoxide

LDH – Lactate dehydrogenase

IACUC – Institutional animal care and use committee

HPLC/MS - High Performance liquid chromatography / Mass Spectrometry

ACKNOWLEDGEMENTS

Science is full of assessment, measurement, and judgment. This process drives us to make progress, be better, or at least acknowledge where we can't - for now. When assessing our own work, it's easy to become your own harshest critic, internalizing every flaw and the weight of every milligram of missed potential. Whether it's in a manuscript, dataset or even in my own woodworking, it's easy to dismiss our accomplishments through the intimate awareness of their shortcomings. In this regard, I particularly want to thank my advisor Dominik for pulling me back and reminding me that my work is novel, valid and valuable. I thank him for extending me expectations and understanding in equal measure.

I am very thankful for the steady presence of Jasper Yik. He was often able to point me in the right direction when I was adrift at times, whether it was navigating a protocol, a presentation or paragraph. This work simply does not exist in isolation, and I thank the member of the Haudenschild Lab who's contributions, foundations and feedback have shaped it: Linan, Gabe, Yihan, and Song Yang have all positively shaped my experiences through the pandemic and contributed much to this work.

Thanks to Integrative Pathobiology and the people who make it what it is, I really do enjoy having to explain what the heck it means every time it comes up. Erin Kent, who is the beating heart of the group who earnestly serves us students with joy and dedication.

I'm thankful for Alice Wong, who has the curious but charming habit of befriending lifeguards and turning them into scientists. The Arzis, beginning with Boaz, a role model, who cemented my future in science, and has mastered the motto of "Work Hard, Play Hard"; and Natasha who has continued to watch over my work as I prepare to finish this stage of my life. Thanks to the top-notch dinner companions at conferences: Blaine Christiansen, Damian Genetos, and Clare Yellowley who always were always kind, honest, and generous. I'm overjoyed that my last committee member, Gabriela Loots, has

finally made UC Davis her home. She has been instrumental in finishing this work and I always look forward to her research.

I want to acknowledge and thank the friends who have been my companions and have become like family in this journey: Konrad Franco, Michael & Tessie Stewart, Maxwell Marple & Beck Ehrlich, Michael (2) Lee, and Jacob Steenis. I'm so grateful to those who've shared this time with me and made Davis home: James Hasbany, Morgan Vaught, Abigail McInnes, Thomas Steele, Bryce Cook, Will Shaddix and Kali Kecskemeti.

Finally - I can't neglect my family. My parents are source of unabating support and love – I may take this for granted sometimes, and for that I apologize. However, I know in my bones that they would go to the end of the earth for my brother and me. My brother Derek, who I will always quibble with, but I know that we will always be on each other's team. To my family – thank you for this, and your love and patience as I make my way through this life.

ABSTRACT

Osteoarthritis (OA) is a degenerative disease of the joints, with significant burden on humans and animals alike. OA is increasingly understood as having an inflammatory pathology, as many immune processes and inflammation create a deleterious environment within the joint. Cartilage and chondrocytes have very poor regenerative capacity and are thus susceptible to degeneration in this inflammatory environment. Cell-to-cell communication between both immune and stromal cells, which contribute to prolonged inflammation in the joint, form a key component of OA. Such cross-talk highlights the need to study the joint as an organ, inclusive of stromal and immune cells. To date, there are no disease modifying drugs for PTOA or OA, and surgical repair of joint structure and tissues is inadequate to reverse this inflammatory joint environment.

Like many inflammatory diseases, the largest risk factor for developing OA is age, however the next largest risk factor is injury to a joint, known as post-traumatic osteoarthritis (PTOA). Trauma to a joint initiates inflammation and immune infiltration by the release of damage-associated molecular patterns, and alarmins. These are released from disrupted tissues and stressed—or dying—cells. This event may only occur once in the lifetime of a joint. However, this event makes the joint more likely to develop OA in the following years and decades. The acute injury response (AIR) of joint tissues has not been characterized in the first twenty-four hours as most studies have followed the progression of PTOA starting in the days, weeks, and months post-injury.

A crucial tool for assessing changes occurring in a tissue is transcriptomics. Though the advancements in single-cell transcriptomics (scRNA-seq) have been momentous in recent years, orthopedics lagged other fields in its adoption. For scRNA-seq, cells must be extracted - alive and with minimal perturbation however the tissues of the joint are highly heterogeneous and require different digestion for the hard and soft tissues. This has been a hurdle for the implementation of scRNA-seq in joint tissues. To fully

capture the transcriptome of the knee as an organ, both the soft and hard tissues would need to be included, without over-digestion of soft tissue cells.

Chapter One details a novel protocol for the preparation of mouse knee tissues for single-cell RNA sequencing. A novel two-stage digest was devised and validated to create a single-cell suspension. This suspension is comparable to the traditional bulk preparation of cryo-pulverization, in which the cells from growth plate to growth plate are sequenced. This two stage digest allows softer tissue cells to exit the digest conditions while subjecting hard tissue to more aggressive enzymatic digestion. This work has demonstrated the ability to generate highly viable cells from both soft and hard tissues within the joint, to wholistically capture the joint as an organ in a single digest.

With this methodology, Chapter Two characterizes the AIR in mouse knees with a combination of bulk and single-cell sequencing, to study potential origins of PTOA. The bulk transcriptional changes occurring in the joint twenty-four hours after injury were characterized. In the first hour, only fifty-four genes were upregulated, which continued in a growing cascade of transcriptional changes through four, eight and twenty-four hours. During the first four hours a pattern of early transcription factors was followed by signaling associated genes. Further, this study identified the cells present within the knee after injury and indicated a diverse expression of AIR genes between stromal and immune cells, as well as revealing synovial fibroblasts as a notable population due to the expression of a high amount of AIR genes.

Moving from small-animal models, Chapter Three reviews surgical models of PTOA in sheep to determine the optimal models to employ for future work. Sheep make a good choice of animal model as their knee joint has very similar biomechanical properties to human knees and they are cheaper and easier to handle than other large animal models. This review details the advantages and disadvantages of seven surgically inducible PTOA models. Key findings were the relative time-course, severity of

subsequent PTOA, and prior uses of specific models to inform researchers deciding on appropriate surgical methods to suit the needs of their study.

Chapter Four further develops this study by establishing the tolerability and pharmacokinetics of a potential treatment formulation in equine middle carpal joints. Prior research in the Haudenschild Lab has shown that early application of transcriptional inhibitors post-injury can attenuate knee degeneration in animal models. Flavopiridol is an inhibitor of Cdk9 which is necessary for transcription and has been shown to reduce PTOA development post-injury. In four healthy horses, intra-articular administration of an extended-release flavopiridol microparticle formulation was well-tolerated with detectable levels of flavopiridol in the synovial fluid for approximately 4-weeks post administration and negligible systemic exposure. In equine synovial cells and chondrocytes, flavopiridol successfully suppressed the response to inflammatory stimulus (IL-1B) at low doses with no notable cytotoxicity. This study lays the groundwork for testing the beneficial effects of flavopiridol in horses going forward.

Overall, this dissertation adds to our understanding of trauma in the knee and models of PTOA. I have developed new protocols for wholistically sequencing the murine knee; characterized the AIR in a small animal model; reviewed the field of ovine PTOA models; and assessed the safety and dosage of a potential anti-inflammatory therapy in horses.

CHAPTER I: A two-stage digestion of healthy whole murine knee joints for single-cell RNA sequencing

Dustin M. Leale, Linan Li, Matthew L. Settles

Keith Mitchell, Lutz Froenicke, Jasper H.N. Yik, Dominik R. Haudenschild

This work was published November 26, 2022

In the journal

Osteoarthritis and Cartilage Open

https://doi.org/10.1016/j.ocarto.2022.100321

ABSTRACT

Objective

Single-cell RNA sequencing (scRNA-seq) is a powerful technology that can be applied to the cells populating the whole knee in the study of joint pathology. The knee contains cells embedded in hard structural tissues, cells in softer tissues and membranes, and immune cells. This creates a technical challenge in preparing a viable and representative cell suspension suitable for use in scRNA-seq in minimal time, where under-digestion may exclude cells in hard tissues, over-digestion may damage soft tissue cells, and prolonged digestion may induce phenotypic drift. We developed a rapid two-stage digestion protocol to overcome these difficulties.

Design

A two-stage digest consisting of first collagenase IV, an intermediate cell recovery, then collagenase II on the remaining hard tissue. Cells were sequenced on the 10x Genomics platform.

Results

We observed consistent cell numbers and viable single cell suspensions suitable for scRNA-seq analysis. Comparison of contralateral knees and separate mice showed reproducible cell yields and gene expression patterns by similar cell-types. A diverse collection of structural and immune cells were captured with a majority from immune origins. Two digestions were necessary to capture all cell-types.

Conclusions

The knee contains a diverse mixture of stromal and immune cells that may be crucial for the study of osteoarthritis. The two-stage digestion presented here reproducibly generated highly viable and representative single-cell suspension for sequencing from the whole knee. This protocol facilitates transcriptomic studies of the joint as a complete organ.

INTRODUCTION

Osteoarthritis (OA) is the most common degenerative joint disease affecting 30%-50% of people over 65 years old. OA is a complex disease of the whole joint, involving different joint tissues and cell types, including cells of the synovium, cartilage, subchondral bone, meniscus, tendons, fat pad, and ligaments [1, 2]. Degeneration of joint tissues is driven primarily by inflammation, through activation of immune cells, through the cross-talk between tissues, and specifically, through interactions between immune cells and the different structural cells [3-6]. It is becoming increasingly clear that immune cell functions are modulated by their interactions with a variety of structural cells that express tissue-specific immune regulators and cytokine signaling molecules [7]. Historically, gene expression studies in OA mainly focused on isolation of individual cell types and rarely examine the effects of tissue cross-talk within different joint tissues. Therefore, it is important to design new studies to elucidate the interaction and cross-talk between immune and structural cells within the joint. This will provide new insight into understanding OA pathogenesis and developing effective treatments.

Conventional microarray or bulk-RNA sequencing analyses of mixed joint tissues lack the ability to determine cell type-specific gene expression. This is largely overcome by the advent of single-cell RNA Sequencing (scRNA-seq) technology, which reveals gene expression profiles of individual cells. scRNA-seq has quickly become the gold standard for defining cell states and phenotypes in many tissues. However, the joint is a unique organ as it contains both hard (bone/cartilage/ligament) and soft (synovium/fat/tendon) tissues, which create a challenge during extraction of cells embedded in different tissue matrices. Cells residing within the synovium and other “soft” matrices are readily extracted with mild digestive enzymes, while other cells deeply embedded in cartilaginous and bony “hard” matrices require much harsher digestion with more aggressive collagenases that could damage soft tissue cells [8-

10]. Thus, conventional single-step methods for cell extraction used in other organs/tissues, such as liver or lungs, are not suitable for joint tissues.

In this study, we developed a sequential two-step digestion protocol to isolate representative cells from all tissues in whole mouse joints. Cells embedded in soft tissues were first extracted and removed under mild enzymatic conditions, while the remaining cells embedded in hard tissues were subsequently extracted under aggressive enzymatic conditions designed for bony tissues. Digestive enzyme concentrations were optimized to minimize time, stress response, and transcriptional shift during processing. The isolated cells were then analyzed by scRNA-seq to determine individual gene expression profiles specific for known cell types found within the joint.

MATERIALS AND METHODS

Mice

Healthy adult male C57BL6 mice, n=2, (The Jackson Laboratory, Bar Harbor, ME, US) aged 23-25 weeks were used in this study. All animal procedures were approved by the Institutional Animal Care and Use Committee (IACUC) at the University of California, Davis. No statistical method was used to predetermine sample size. No experiments were performed on living mice.

Microdissection

Immediately following euthanasia with carbon dioxide asphyxiation, mice were submerged in ice-cold 70% ethanol, and then washed in ice-cold PBS. The skin on the hind limb was removed to expose the knee joint, then the surrounding muscles were carefully dissected with scissors to expose the joint capsule. The knee joint was then excised by cutting the tibia and femur adjacent to the growth plates and transferred to a 60-mm petri dish containing ice-cold PBS. Under a dissecting microscope, the remaining muscles were carefully trimmed until the joint capsule and growth plates were clearly visible.

An incision was made along the femoral and tibial growth plates. The remaining joint tissues (typically weighting about 80mg) included the femoral growth plate, ligaments, synovial lining, patella, meniscus, and the tibial growth plate, were then transferred to a dry petri dish and minced with a scalpel. Time from animal euthanasia to minced knee tissue was approximately 10 minutes per knee.

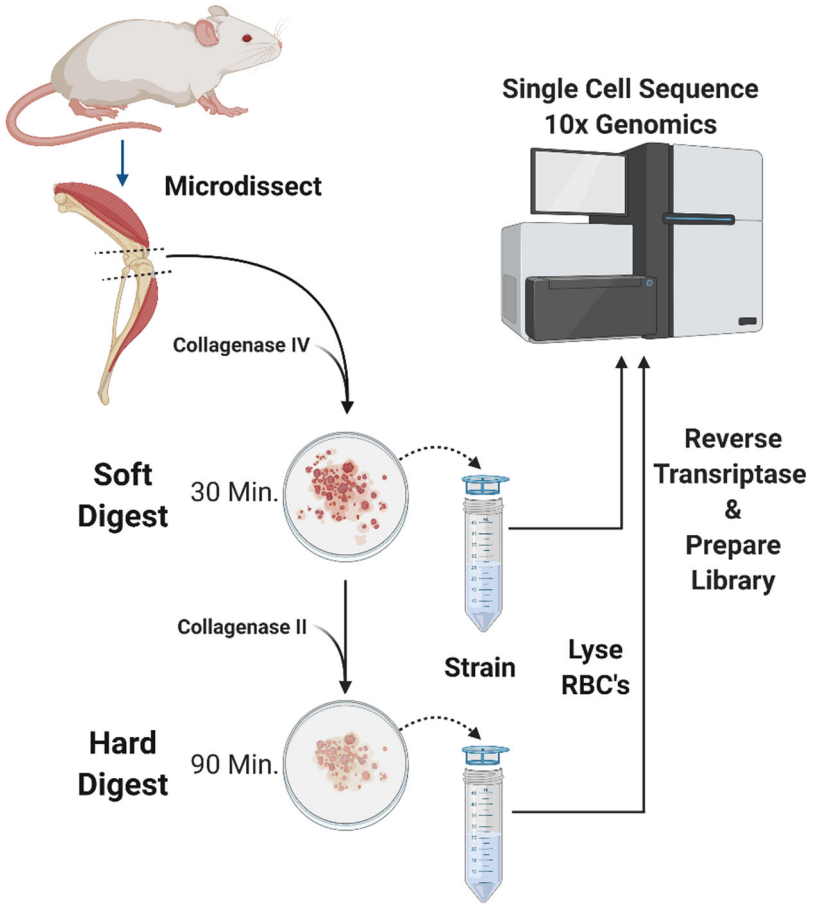

Figure 1.1: A workflow of cell isolation from soft and hard tissues for scRNA-seq. See Materials and Method for details.

Soft and Hard Tissue Digestion

The two-step digestion protocol is illustrated in Figure 1.1. Briefly, the minced knee tissue was first subjected to a mild enzymatic digestion step designed to disassociate soft tissues, in 5 mL of 1%

collagenase IV (1600 U mL^{-1}) (Thermo Fisher Scientific, Carlsbad, CA, US) (w/v) in DMEM with 5% FBS. The soft digestion was carried out at 37 ^{o}C, with constant orbital rotation at 90 RPM. After 30 minutes the media containing the released cells from soft tissues was aspirated, the remaining undigested tissues were then rinsed with 10 ml room temperature DMEM/5% FBS. The aspirated media and rinse media were strained twice through a 70 µm cell strainer (Falcon, Corning Incorporated) and further processed immediately for red blood cell lysis as described below. The remaining tissue was subjected to a second enzymatic digestion step for hard tissues, in 5 mL of 2% (w/v) collagenase II (2500 U mL^{-1}) (Worthington Biochemical, Lakewood, NJ, US) in DMEM with 5% FBS. The hard tissue digestion was carried out at 37 ^{o}C with constant rotation for 90 minutes. At the completion of the hard digestion, cells were aspirated, rinsed, and strained as described above.

Red Blood Cell Lysis

Immediately after straining, cells from soft or hard tissue digests were centrifuged at 300 x g for 5 minutes at 4 ^{o}C. To lyse the red blood cells, the cells were resuspended 10 ml ice-cold ACK lysis buffer (Life Technologies, Carlsbad, CA, US), followed by 10 minutes incubation on ice following the recommendations of 10x Genomics for tissue dissociation. Cells were centrifuged and washed with 10 ml ice-cold DMEM/5% FBS, and resuspended in 1 ml ice-cold DMEM/5% FBS. The single-cell suspension was transferred on ice to the DNA Technologies and Expression Analysis Core Laboratory at UC Davis.

The entire process from both knees of one mouse was performed in less than 2.5 hours, resulting in two independent samples of single-cell suspension, one from soft tissue digest and one from hard tissue digest, per knee for a total of 4 samples (Figure 1.1).

Assessment of Cell Viability, Quantity, and Quality

The single-cell suspension (100 µl) was passed through a 40 µm cell strainer (Flowmi, SP Scienceware, Wayne, NJ, US) to remove debris and cellular aggregates. The samples were then visualized, and the

number of live cells counted with a Luna-FL cell counter/imager (Logos Biosystems, Anyang, South Korea) under brightfield and fluorescence (Acridine Orange/Propidium Iodide) settings.

Library Preparation and sc-RNA Sequencing

Barcoded transcriptome libraries were prepared from the single-cell suspensions using the Chromium Next GEM Single Cell 3' Kit v3.1 (10X Genomics, Pleasanton, CA, US) according to the manufacturer's instructions. Briefly, approximately 17,000 cells per sample were loaded onto a Chromium Next GEM Chip G and encapsulated into nanodroplets on a Chromium Controller microfluidic system, resulting in the mRNA barcoding of ~10,000 single cells per sample. After reverse transcription, the barcoded cDNA was purified with DynaBeads (Invitrogen, Carlsbad, CA, US). After PCR amplification, the quality of the cDNA was verified by micro-capillary gel electrophoresis using a Bioanalyzer 2100 (Agilent, Santa Clara, CA, US). The amplified cDNA was fragmented and converted to 3' gene expression profiling sequencing libraries. The fragment lengths of the sequencing libraries were assessed on a Bioanalyzer. The libraries were quantified by fluorometry on a Qubit instrument (Life Technologies, Carlsbad, CA, US) and qPCR with a Kapa Library Quant kit (Kapa Biosystems-Roche, Basel, Switzerland). Pooled libraries were sequenced on a NovaSeq 6000 sequencer (Illumina, San Diego, CA, US) with paired-end reads. The sample processing targeted 10,000 cells per sample and a depth of 40,000 reads per cell.

Data Filtering

The sequencing data were processed using Cell Ranger version 5.0.1 (10X Genomics, Pleasanton, CA, US) with the mouse reference package mm10 (GENCODE vM23/Ensembl 98). To maintain the most important features of the dataset and high-quality cells, further analysis was performed only on cells expressing at least 300 genes, and only on genes that were expressed in at least 10 cells. Cell cycle was determined using the "scran" R-Package [11]. Mitochondrial gene expression was calculated for the data as a proportion of total gene expression per cell. Cells with greater than 90% mitochondrial gene

expression (indicative of damaged cells) were excluded. A highly inclusive mitochondrial DNA threshold was chosen intentionally to visualize the distribution of mitochondrial DNA content that was observed within the joint samples. To identify possible cell-doublets in the data, we counted cells with total genes (nFeature_RNA) that exceeded a threshold of 7800 using Seurat [12].

Dataset integration and Cell Clustering

Following the single-cell expression assignment, Seurat (Satija Lab, New York, US Version 4.0.1) was used to further analyze the data [13]. The four files output from Cell Ranger (Left knee-soft digest, left knee-hard digest, right knee-soft digest, right knee-hard digest) from each mouse were combined into one object for each mouse in Seurat for analysis going forward. Gene expression measurements were normalized with LogNormalize for each cell, multiplied by a scale factor (10,000 by default), and log-transformed. To better standardize the dataset, regression analysis was performed using the number of Unique Molecular Identifiers (UMIs), the number of genes, and the cell cycle stage. Due to the fact that mitochondrial gene expression has been shown to be a feature of some cells, mitochondrial gene expression was not included in the regression analysis, as this may mask the changes observed in these genes. To combine datasets from multiple mice a set of mutually variable anchors were found between the individually processed mice datasets. These anchors were then used to integrate the two datasets using the IntegrateData command of Seurat, and the combined dataset was then scaled. A Principal Component Analysis (PCA)-based clustering technique was performed in Seurat, at first using 50 PCs to be more inclusive of rare cell types [14, 15]. In the final analysis presented here, 10 PCs were chosen to simplify presentation of the data. The final number of PCs used was determined by using an elbow, or scree plot generated by the ElbowPlot command, and observing the point at which the y values between points stops changing significantly. Uniform Manifold Approximation and Projection (UMAP) was chosen to display the combined datasets [16].

Statistical Analysis

For tables one and two, means and standard deviations were calculated for multiple samples. Bioinformatics of single cell data were handled in Seurat version 4.0.1 with default values.

RESULTS

Cell Yield and Viability

The quantity and quality of cells isolated from the soft and hard tissue digestions were assessed for their suitability for scRNA-seq analysis. On average, about 6.5 million and 5 million cells were isolated in each knee from the soft tissues and hard tissues, respectively (Table 1.1). Cell viability was at least 87%, and the samples were mostly free of debris and cell clusters (Figure 1.2). These results indicate that the two-step digestion protocol yields highly viable single-cell suspension suitable for scRNA-seq.

Soft Tissue Digest		Hard Tissue Digest	
Cell Number (Millions)	Viability (%)	Cell Number (Millions)	Viability (%)
6.5 ± 0.5	92.4 ± 0.9	4.9 ± 0.6	87.2 ± 7.2

Table 1.1: Cell yields and viability from soft and hard joint tissues. The total number and viability of cells isolated from soft or hard knee tissues. Data represented the average ± SD from 4 knees (2 left + 2 right from 2 mice)

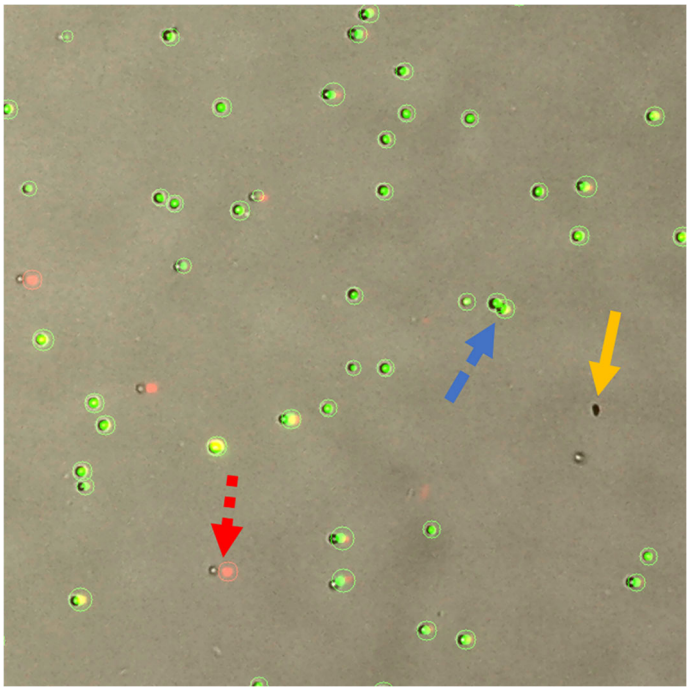

Figure 1.2: Viability and Quality of single-cell suspension. Fluorescence staining of live (Acridine Orange, green) and dead (Propidium Iodide, red) cells, overlaid on brightfield microscopy. The single-cell suspension consisted of mostly live cells (single green dots) and was mostly free of cell clusters (blue dashed arrow), dead cells (red smaller dashed arrow), and debris (orange arrow). The image from LUNA-FL imager shows an area of about 5 mm2.

Quality Control of scRNA-seq Data

The quality of scRNA-seq data was assessed first by determining the mitochondrial gene content relative to total expressed genes. The mitochondrial gene profiles in all samples were comparable, regardless of the tissue origins (i.e. soft or hard tissues; left or right knees), (Figure 1.3). Most of the sequenced cells within each sample were derived from cells containing less than 10% mitochondrial gene contents, an example threshold of 20% is displayed. Further, the digestion protocols yielded almost exclusively single-cells. Using a cutoff of 7800 genes/cell to indicate possible doublets, we observed only 14 cells out of

~33 thousand exceeded this threshold [12]. A low mitochondrial content indicates viable cells [17], thus these results corroborated with the high viability values determined above (Figure 1.2).

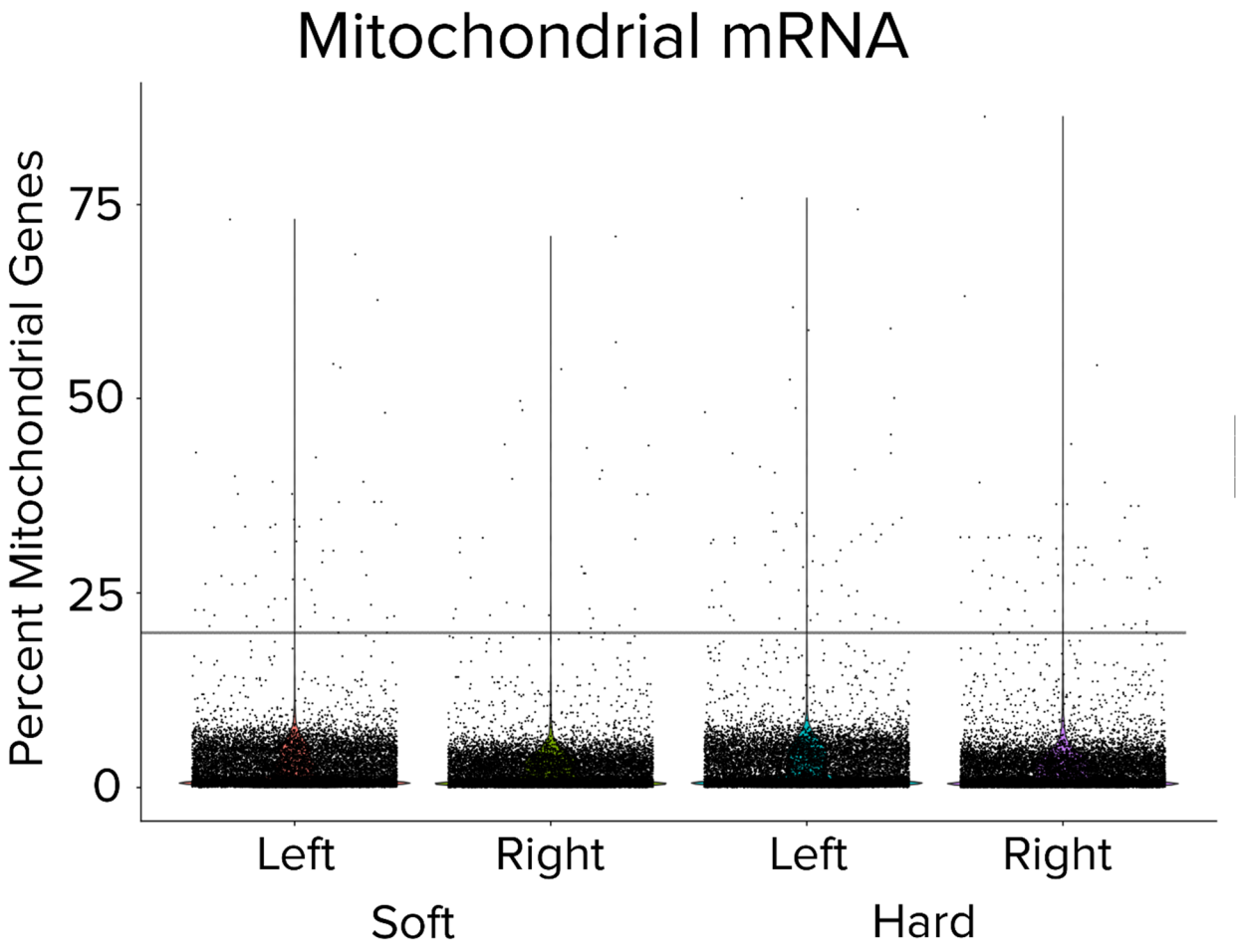

Figure 1.3: Mitochondrial DNA content of single cells. Violin plots of percent mitochondrial DNA within each digest, a line at 20% is shown as an example cut-off threshold. Each dot represented one cell. Data was obtained from sequencing four knee digests from two mice for a total of eight digests.

The quality of the scRNA-seq data was further assessed using the numeric properties of the sequencing read information with Cell Ranger. As shown in Table II, over 8000 cells from each sample were sequenced to a depth of at least 40,000 reads per cell. A UMI count of at least 4000 across all samples

indicated a complex library with sufficient starting materials. Thus, the depth and breadth of these sequencing data indicate that the digestion protocol yielded a high quality library with sufficient complexity for further analysis.

		Cells Sequenced	Mean Reads per Cell	Median Genes per Cell	Median UMI Counts per Cell
Soft Digest	Left	9,477	39,759	1,425	4,543
	Right	8,955	55,046	1,474	4,700
Hard Digest	Left	7,903	63,438	1,286	4,581
	Right	8,165	48,229	1,204	3,977

Table 1.2: Sequencing depth and quality control metrics. Shown were the total number of cells sequenced per sample, as well as mean reads, median genes, and UMI counts per cell. Data shown from one mouse.

Reproducibility between contralateral knees and individual mice

Reproducibility between samples is a critical aspect of protocol development. Using the combined datasets from each mouse, we compared gene expression profiles in cell samples isolated from contralateral knees and between two mice. Reproducibility is indicated by samples having similar UMAP projections and gene expression patterns (shown as 11 different clusters, each represented by a different color) (Figure 1.4A). For soft tissues, data from both the left and right legs projected similar clustering and gene expression patterns (Figure 1.4A). Cell populations present in the left were also present in the right, and vice versa. The same was also true for the cell populations from the hard tissues. When splitting the dataset by mouse of origin, the resulting UMAP projections are again similar (Figure 1.4B). In contrast, when comparing between the soft and hard tissue digests, there were marked differences in

the UMAP projections, indicating that unique cell types are isolated by the soft- and hard-tissues digestion protocols.

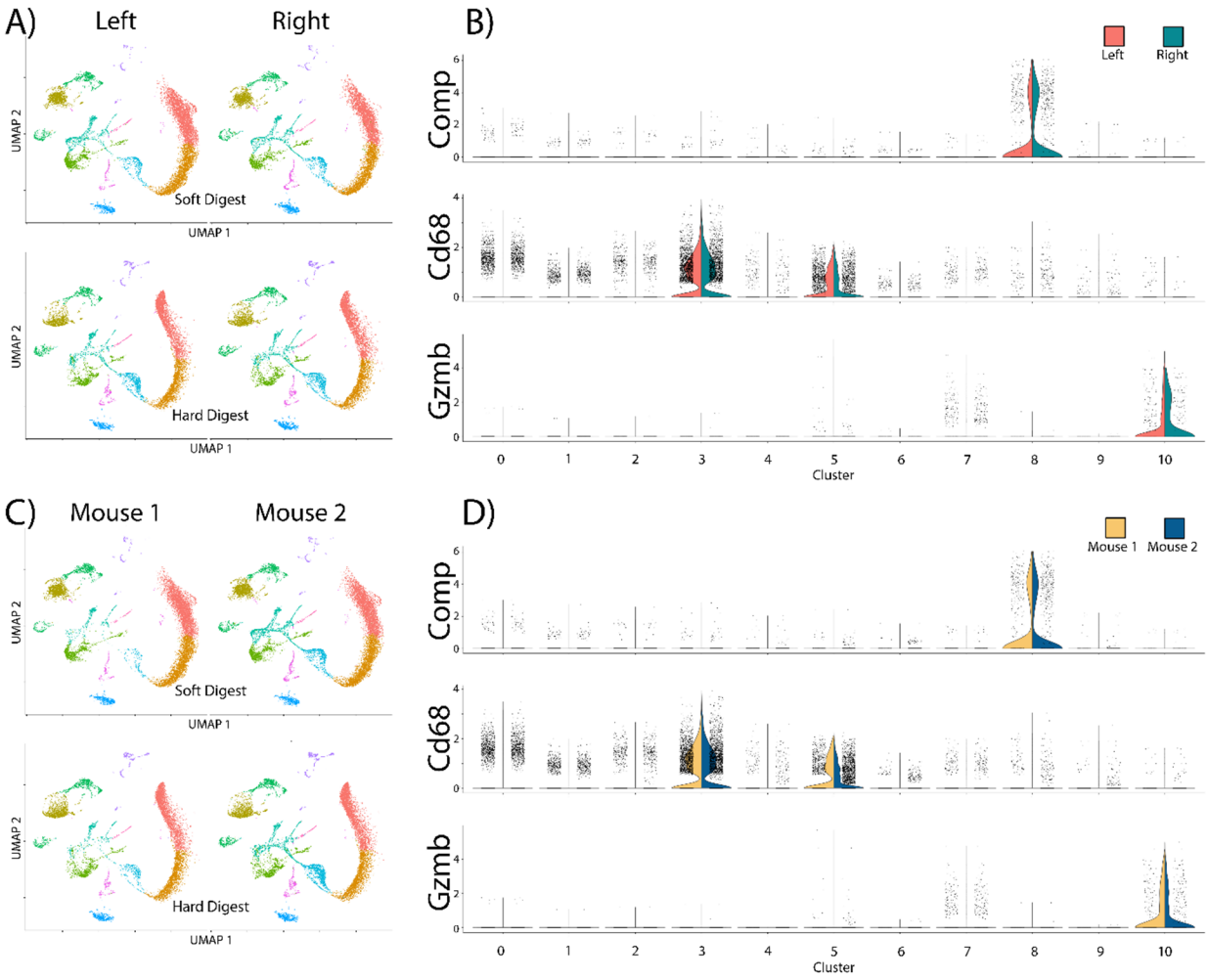

Figure 1.4: Reproducibility is demonstrated by the comparisons between contralateral knees and individual mice in both the Soft and Hard tissue digests. A) Uniform Manifold Approximation and Projection (UMAP) of single-cell RNA sequencing scRNA-seq data split by soft and hard digests from left and right knees. B) Split (Left knee/Right knee) Violin plots show expression of selected genes in different clusters. Selected genes: cartilage oligomeric matrix protein (*Comp*); *Cd68*; and Granzyme B (*Gzmb*). C) UMAP of single-cell RNA sequencing scRNA-seq data split by cells from soft and hard digests

from Mouse 1 or Mouse 2 D) Split (Mouse 1/Mouse 2) Violin plots show expression of selected genes in different clusters. Data from two mice shown.

A final test of reproducibility was to determine the expression of marker genes known to be expressed in different cell-types unique or common in soft and hard tissues. The selected genes and their cellular origins are: 1) cartilage oligomeric matrix protein (*Comp*), chondrocytes, synovium, and other structural cells; 2) *Cd68*, monocytes; and 3) Granzyme B (*Gzmb*), Natural killer (NK) and other cytotoxic immune cells. Comp is expected to be present only in non-immune, structural tissues, whereas *Cd68* and *Gzmb* are expected to be present in immune cells, which may include resident cells within the knee tissues. The violin plots (Figure 1.4C) showed that these 3 selected marker genes were present equally in both left and right knees and equally between mice (Figure 1.4D). However, each marker gene was only found in specific cell clusters. These results indicate that unique cells specific to the soft or hard tissues were reproducibly obtained from our two-step cell isolation protocol, and that both steps are required for the isolation of cells representative of all joint tissues.

Cell Type-Specific Genes were Present in the Corresponding Hard and Soft Tissues

To determine if our digestion protocol captured representative cells from both hard and soft tissues, we used UMAP projections of the combined dataset to visualize the presence of selected marker genes for different cell types. The established marker genes and cell-types were as follows: 1) aggrecan (*Acan*), chondrocytes or meniscal cells; 2) collagen type 1a (*Col1a1*), osteoblasts; 3) T-Cell Receptor Alpha Constant (*Trac*), T and NK cells; 4) Lymphocyte Antigen 6 Family Member G6D (*Ly6g*), monocytes and neutrophils; 5) Adhesion G Protein-Coupled Receptor E1 (*Adgre1* also known as the F4/80 antigen), macrophages, and 6) *Cd79a*, B cells (Figure 1.5A). Cd45 (*Ptprc*) was used to identify hematopoietic cells. To assess the cellular composition of the sample, we calculated the number of cells expressing each signature gene. When examining all cells in the combined dataset, 0.4% expressed *Acan*, 4.1% expressed

Col1a1, 3.2% expressed *Trac*, 37.3% expressed *Ly6g*, 7% expressed *Adgre1*, 19.8% expressed *Cd79a*, and 85.1% expressed *Cd45* (Figure 1.5A). When these cell-type specific marker genes were visualized with the UMAP projections, each gene was present predominately within one or two clusters, indicating the presence of these different cell types (Figure 1.5B).

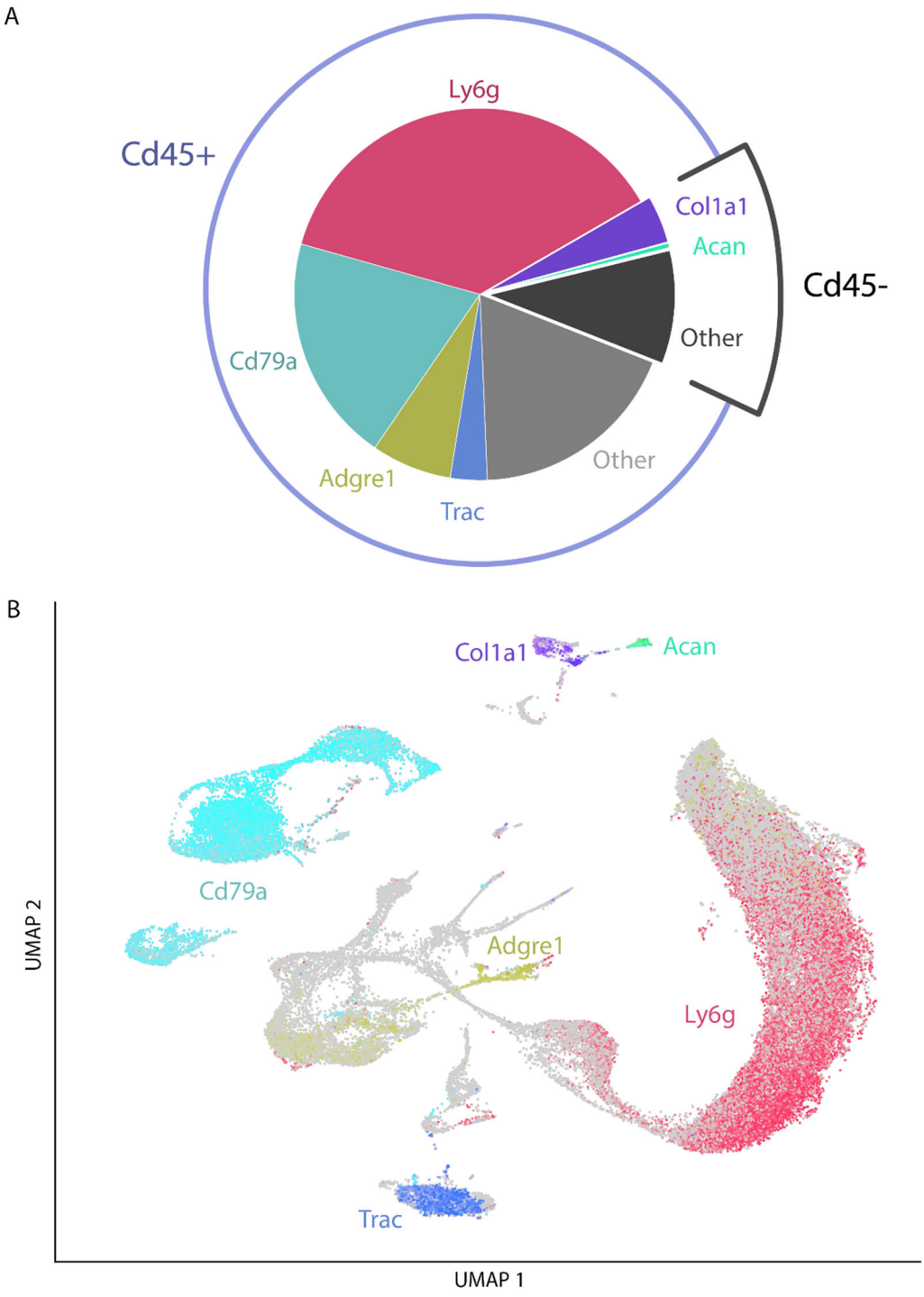

Figure 1.5: Expression of selected marker genes. A) Percentage of cells expressing selected marker genes. *Cd45* expression is shown around the pie chart. Each gene was indicated by a different color: *Acan* (bright teal), *Col1a1* (purple), *Trac* (blue), *Adgre* (gold), *Ly6g* (red), and *Cd79a* (cyan). B) Uniform

Manifold Approximation and Projection of combined hard and soft tissues obtained from four knees from two mice, same color labels as above.

We next confirmed whether each marker gene originated from cell-types expected in the soft or hard tissue digests. The percentage of expression of each marker gene originating from soft or hard digest was determined (Figure 1.6). Immune cell markers (*Ly6g*, *Adgre1*, *Trac*, and *Cd79a*) expected in both soft and hard tissues were distributed similarly among cells isolated from soft and hard digest. In contrast, markers of osteocytes (*Col1a1*) and chondrocytes (*Acan*) were predominant within cells isolated from the hard tissue digest (Figure 1.6). Taken together, these data indicate that cell-type specific markers are found within the expected tissue types, thus validating the two-step digestion protocol for the isolation of different cell types from both hard and soft tissues.

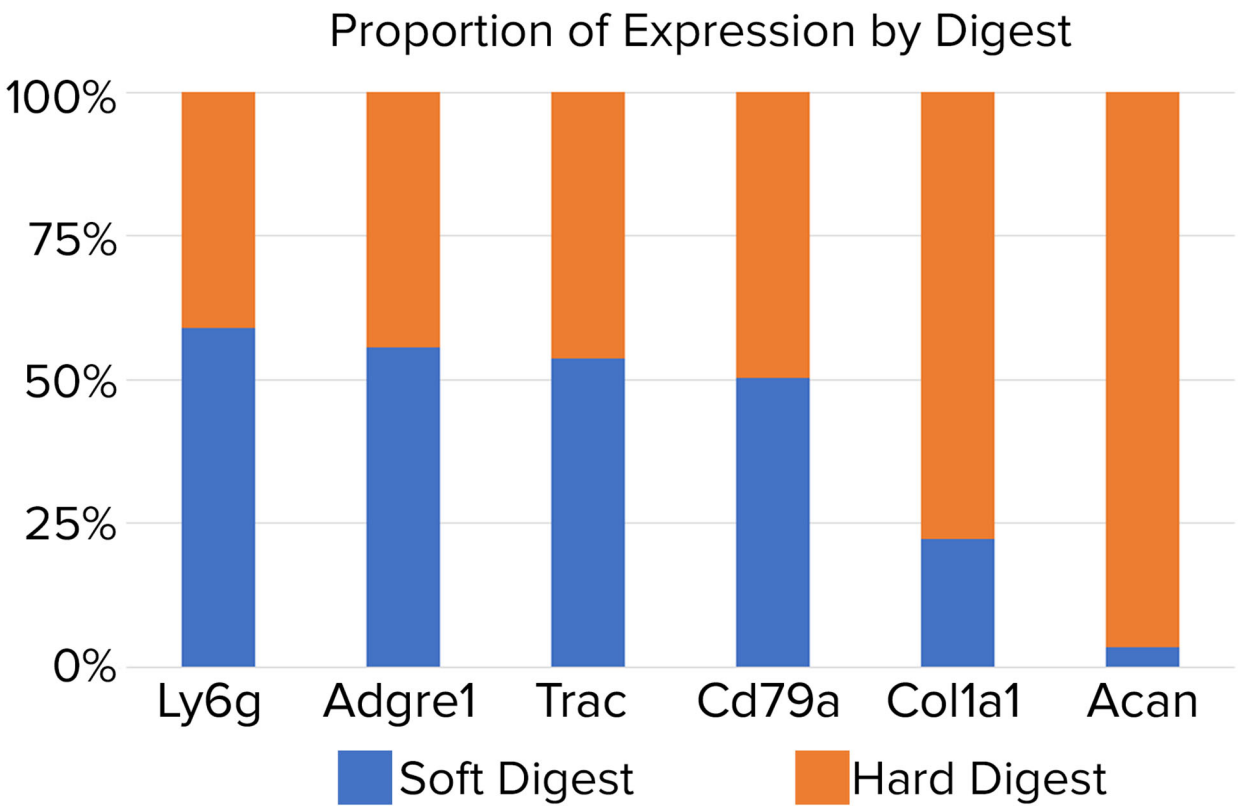

Figure 1.6: Relative expression of genes in soft and hard digests. Percentage of expression of selected genes originating from soft or hard digests. Combined data from four knees from two mice.

DISCUSSION

Recent years have seen a proliferation of scRNA-seq studies targeting specific cell populations that are isolated from different joint tissues, such as chondrocytes, synoviocytes, macrophages, and other immune cells. However, few transcriptomic studies provide a holistic approach to characterize all the different cell-types across whole joints, limiting our ability to study the physiological consequences of their tissue cross-talk. This is in part due to the presence of both soft and hard joint tissues that require different digestive enzymes for cell extraction. We developed and validated a two-step digestion protocol tailored for whole joint analysis, to isolate the tissue-specific cell types while preserving their viability (Table 1.1, Figures 1.2 and 1.3). Analysis of scRNA-seq data with UMAP projections showed that representative cell types within their respective tissue origins were present, with high reproducibility between different cell samples isolated from different knees and different mice (Figures 1.4-1.6).

The technology for transcriptomic analysis of mouse knee joints has evolved, from the microarray analysis in the early 2000s [18], more recently progressing to bulk RNA-seq analysis [19], and now to single-cell RNA-seq. Historically, the dissection of the mouse knee joint was performed similarly for either microarray or bulk RNA-seq analyses. The tissues analyzed generally included structures between the distal femoral growth plate and the proximal tibial growth plate. Due to the small size of each tissue in mouse joints transcriptome studies on individual tissues were generally performed in larger animal models. These whole tissue assays gave insight into the overall trends within the joint but could not identify the contributing cell-types. Several methods were developed to isolate only particular cells of interest, including the use of physical segmentation of the knee to focus on chondrocyte-rich regions [20, 21], the use of cell enrichment or depletion in suspension to separate immune cells from

stromal cells [19, 22, 23], or the culture of isolated cells [24]. Another alternative new sequencing technology is single nuclei RNA-sequencing (sNuc-Seq). This technique processes only nuclei and the RNA found within and can be performed on frozen and undigested tissues [25], however only human synovium and porcine cartilage explants have been studied this way in the joint [26, 27]. Techniques used to filter or only sequence parts of the joint allow a more focused sample containing a larger proportion of "desired" cells but may miss the activities of the excluded cell populations and the crosstalk that exists within the whole joint environment. Our protocol is consistent with that used previously in microarray and bulk RNA-seq studies. Thus, the scRNA-seq data obtained from our protocol should be directly comparable to existing microarray or bulk RNA-seq data.

To our surprise, immune cells constituted the majority of cells within the whole joint digest - with 85% of cells expressing the universal hematopoietic marker *Cd45*. The percentage of immune cells in the knee is higher than those observed in other tissues studied by scRNA-seq [28-30]. In cells isolated from human lungs, 6-20% were immune cells [31]. In human skin biopsies immune cells contributed 6-40% [32]. A broad survey of human tissues using scRNA-seq found that the liver contained 45% immune cells; in the eye 31% of cells were fibroblasts and 25% were immune cells; bone marrow contained 44% NK & T cells and a large portion of B and hematopoietic stem-cells, as well as neutrophils and monocytes [33]. Among these studies in different tissues, immune cells were between 5-45% of all cells. A recent study using digested mouse knees found that 78.4% to 70.4% of cells were *Cd-45* positive using flow cytometry, with neutrophils composing the majority of those cells [34]. *Cd-45* positive high immune cell component of our whole joint samples may be explained by the presence of bone marrow, which is a primary hematopoietic organ. In support of this, we found high percentages of cells expressing the universal B-cell marker *Cd79a* (19.4%), and *Rag1* and *Rag2* (4.7%) (data not shown), Rag expression takes place within the bone marrow [35]. Previous studies in the murine knee have shown Cd45 via immunostaining and flow cytometry of immune and progenitor cells within the synovium, bone marrow,

and subchondral bone [36, 37], one study which digested subchondral bone chips identified 36% of cells as *Cd45+* [38]. Further, large populations of neutrophils (*S100a8+*, *S100a9+*, *Ly6g+*, >25% data not shown) are present within our samples. The mix of developing B-cells and large number of neutrophils suggest a strong component of bone marrow within the samples, as these cells, and other immune cells, arise from marrow [39]. Although it is established that immune cells are the biggest drivers of inflammation in the joint [40-44], the quantity and composition of these cells within the knee has been difficult to discern until now. Our results suggest that the contribution of immune cells to the whole-joint transcriptome may have been underappreciated in previous microarray or bulk RNA-seq studies.

A limitation of this study is that transcription drift is possible during the enzymatic digestions [45]. Bone in particular remains challenging to digest and contains diverse cell populations that are sensitive to transcription drift [46, 47]. Even with prior mechanical disruption of bony tissues, extensive enzymatic dissociation is still required [48] and mechanical disruption may lead to its own phenotypic artifacts [49-51]. Due to the necessity of enzymatic digestion of knee tissues at 37^{o}c some transcriptional drift is inevitable, as the cells are biologically active at these temperatures, and may increase stress related genes in response to these conditions [52, 53]. To reduce phenotypic drift, we minimized the overall time of cells in the digest required for the two-step cell isolation protocol. During all stages that do not require enzymatic digestion, samples were chilled on ice. Neonatal mouse kidneys have been digested using a protease with high activity in the cold, which substantially reduced digestion artifacting, but this has not been demonstrated in more complex and difficult to digest tissues [54]. Inhibition of transcription during digestion is one potential tool shown to reduce this artifacting [53]. Despite this challenge, there is evidence of phenotypic stability in chondrocytes and osteocytes, even with prolonged overnight tissue digestion protocols [55-58]. Cell identification remains a complex challenge, the genes selected are suggestive of broad cell categories and are not meant to provide definitive cell identities. Additionally, the inclusion of circulating blood within the joint and samples may account for a portion of

the neutrophils and other immune cells found within the samples. Future work could include an IV perfusion of PBS prior to sacrifice to eliminate these populations in the final samples. The scRNA-seq data was generated with a combined 8 tissue digests of 4 healthy stifle joints from 2 mice. While there is a limitation in the number of biological (mouse) replicates, the two-stage digestion method generated scRNA-seq expression data that was reproducible and consistent across all 4 joints. In future studies, we may consider reducing the effect of biological variability by combining multiple mouse limb digests into a pooled sample prior to library preparation and sequencing. The low number of chondrocytes in the whole-joint relative to other cells could increase the difficulty in determining subtle differences that may exist within these populations. With this approach, there is the potential limitation of missing rarer structural cell-types due to the quantity of immune cells in whole knee digests.

Having established a reproducible protocol for whole joint transcriptomics analysis, our current focus will be on the comparison between joints from different conditions. For example, to study the contributions of individual cell-types in healthy and arthritic joints, sex-related differences, early OA or post-traumatic OA, induced OA models, and the assessment of therapeutic efficacy. Other future work includes the identification of cells using machine learning algorithms [59, 60]. Different subtypes of cells, especially macrophages, have demonstrated pro- or anti-inflammatory roles in the joint depending on polarization [61-65]. Transcriptomic data from whole joints could enable the study of immune-stromal cell cross-talk, as these interactions have important implications for OA [66], bone cells [1, 67], macrophages [68], synoviocytes [69, 70], and NK-cells [71].

In summary, we developed a protocol that reproducibly captures cell-types from soft and hard tissues, generating viable single-cell suspensions and preserving both stromal and immune cells for scRNA-seq. We observed an abundance of immune cells from diverse lineages, as well as chondrocytes and other key structural cells of the knee tissues.

ACKNOWLEDGEMENTS

This research was supported in part by Department of Defense award PR171305 and departmental funds to DRH. The sequencing library preparation and the sequencing were carried out at the UC Davis Genome Center DNA Technologies and Expression Analysis Core, supported by NIH Shared Instrumentation Grant 1S10OD010786-01.

CONTRIBUTIONS

Dustin M Leale – Wet protocol design, acquisition of data, drafting of the article, interpretation of data, revising intellectual content.

Linan Li – Wet protocol design, acquisition of pilot data.

Matt Settles – Bioinformatics design and analysis, statistical expertise.

Keith Mitchell – Processing of read data. Bioinformatic analysis and toolmaking.

Lutz Froenicke - Administrative, technical, or logistic support, sequencing expertise, revising of technical content.

Jasper Yik – Interpretation of data, revising intellectual content, administrative, technical, or logistic support

Dominik Haudenschild – Conception of study, design, interpretation of data, revising intellectual content. Obtaining of funding, administrative, technical, or logistic support.

Role of the funding source

Department of Defense PR171305 and departmental funds to DRH.

Competing interests

No commercial funding was received for the work. The University of California has patents and pending patents on some of the findings, with Drs. Haudenschild and Yik listed as inventors. Drs. Haudenschild and Yik are co-founders of Tesio Pharmaceuticals, Inc, which is in the process of licensing related intellectual property from The University of California.

CHAPTER II: Transcriptomic analysis of the knee following ACL-rupture in murine PTOA model reveals dynamic Acute Injury Response and insight into immune-stromal crosstalk during the first twenty-four hours after injury.

Dustin M. Leale, Yik HN Jasper, Dominik R. Haudenschild

This work will be submitted to the journal:

Osteoarthritis and Cartilage

November

ABSTRACT

Objective:

The development of post-traumatic osteoarthritis is well characterized in the days, weeks and months that follow injury; however, the initial injury period is not well documented. This study aims to characterize the Acute Injury Response (AIR) in the murine knee joint, identify the major signals, and identify the cell-types within the knee that may be responsible.

Design:

Using a non-surgical ACL rupture injury model in mice, injured knee joints underwent bulk-RNA sequencing at 1, 4, 8, and 24 hours (n=4/time) post-injury and differentially regulated genes (DEGs) were identified compared to controls. The knees of one mouse were sequenced 3 hours post-injury at the single-cell level to determine possible cell-types contributing to the DEGs observed in the bulk data.

Results:

At one hour, 54 genes were upregulated, this grew at each timepoint to 311 genes at 24 hours. A trend of early transcription factor expression cascading into cytokine and chemokine signaling, followed by chemotaxis, cell infiltration and angiogenesis was found over the first 24 hours. Immune and stromal cells expressed different outgoing AIR signals after injury, with many AIR pathways potentially originating from stromal cells, particularly synovial fibroblasts.

Conclusions:

The Acute Injury Response is highly dynamic, with major inflammatory cytokines and chemokines first appearing one hour post-injury. Immune cells and stromal cells both have roles in expression of AIR genes. This study provides targets for further study or potential intervention.

Keywords: PTOA, joint injury, cross-talk, Acute Injury Response, transcriptomics

Running Headline: Acute Injury Response of the murine knee

INTRODUCTION

Osteoarthritis (OA) is the most common form of joint disease and the leading cause of disability in the US[72, 73]. With aging populations and the increasing burden of OA-related disability, understanding the underlying mechanisms driving this condition has become a significant focus of research. A single occurrence of joint injury can significantly increase the risk of developing post-traumatic osteoarthritis (PTOA) [74, 75]. It is estimated that approximately 12% of all OA cases are attributable to trauma[74, 75]. PTOA can arise from various joint injuries, including ligament tears, fractures, and dislocations[76]. These injuries initiate a cascade of pathological events that lead to the breakdown of articular cartilage, alteration of joint biomechanics, and immune cell infiltration[77] that promotes the development of chronic inflammation. Importantly, PTOA is often more severe and progresses at an accelerated rate compared to non-traumatic forms of OA.[78] Current treatments rely on managing patient pain and joint mobility, however these measures treat only symptoms and do not prevent further deterioration of joint tissues or disease progression[76, 79, 80]. This underscores the need for comprehensive investigations into the cellular and molecular events associated with joint injury that lead to OA.

Despite its critical role in subsequent disease progression, the precise mechanisms by which injury leads to the development of OA remain largely unknown. Most studies of PTOA have not assessed the joint earlier than twenty-four hours post-injury, and instead focus on the development of PTOA in the weeks post-injury. In the weeks and months following injury, PTOA development follows general patterns of low-grade inflammation, cellular infiltration, cytokine signaling, inflammatory phenotypes of joint cells such as chondrocytes and synoviocytes, and proinflammatory crosstalk between different joint tissues [81-85]. However, the timeline of the Acute Injury Response (AIR) remains unclear in the joint. In this study we define the AIR to encompasses the initial bulk-transcriptional changes that occur within the joint during the first twenty-four hours following injury or trauma.

To gain insights into the processes driving PTOA development, we employed bulk RNA sequencing to analyze the gene expression profiles in mouse knees during the first twenty-four hours following ACL-rupture injury. This approach allowed us to identify a list of differentially expressed genes associated with the AIR. Further, we employed Single Cell RNA sequencing (scRNA-seq) techniques to the whole joint in an effort to map the cell populations that may be effecting these observed changes. We aim to characterize the relative roles of immune and stromal cells and identify specific cell populations responsible for driving the observed bulk gene expression changes associated with PTOA. This integrative approach will provide valuable insights into the molecular and cellular processes underlying the initiation and progression of PTOA, opening new avenues for therapeutic interventions and improved patient outcomes.

Since joint injury provides the initial push towards degenerative OA development, we investigated the changes that joint cells undergo during the acute injury period using a mouse ACL-rupture injury model. We show that the AIR is a highly dynamic event initially involving a small number of initial transcriptomic changes at one hour which cascades over the next twenty-four hours. Stromal synovial cells are notable responders to joint trauma at three hours post-injury, but a wide variety of immune and stromal cells may be contributing to this cascade.

MATERIALS AND METHODS

Injury Model

All animals were maintained and used in accordance with NIH guidelines and approved by UC Davis Institutional Animal Care and Use Committee. Adult male C57BL6 mice (The Jackson Laboratory, Bar Harbor, ME, US) aged 12-15 weeks were used in this study.

For all mice receiving ACL injury the right knee was injured by application of a single mechanical compression to induce ACL rupture as previously described [86]. This injury model creates ACL rupture

via transient anterior subluxation of the tibia and has been shown to reliably induce PTOA within 4 weeks[86]. Mice were isoflurane-anesthetized during injury, and a single dose of buprenorphine (0.05 mg/kg) was administered immediately after injury. Mice in the uninjured group were anesthetized and placed in the tibial compression device before being returned to cages. Euthanasia was accomplished by CO2 asphyxiation.

Bulk RNA-seq of Mouse Knees

At 1, 4, 8, and 24 hours after injury, mice were sacrificed (n=4 per timepoint, and 4 uninjured mice) and the right knees were dissected and prepared as previously described [87]. After removal of skin and muscle surround the knee the region between the distal femoral growth plate and the proximal tibial growth plate was removed for RNA isolation. The removed knee tissue was then snap frozen by liquid nitrogen and pulverized by pestle and mortar under liquid nitrogen.

Total RNA was isolated from the pulverized knees using RNeasy Mini Kits (Qiagen Valencia, CA) following manufacturers recommendations. Samples were then sequenced with the 3'-Tag-RNA-Seq method on an Ilummina NextSeq500 system with single-end 80 bp reads (Illumina San Diego, CA) at the UC Davis DNA Technologies Core facility.

Bulk RNA-seq data processing and Analysis

Sequence data were preprocessed using htstream[88] (Version 1.3.3) including adapter and quality trimming, and aligned to GRCm39 using STAR version 2.7.9a and Ensembl 105 annotations. Normalization factors were calculated using TMM[89] and used to define adjusted library sizes for calculation of counts per million reads (CPM). Normalization of gene expression was performed using the limma voom[90], which log-transforms data, estimates the mean-variance relationship and computes weights in preparation for linear modeling. Differential expression analyses were conducted using limma-voom with the model ~ 0 + interaction (treatment, time). For each pairwise comparison, genes with

Benjamini-Hochberg adjusted p-values less than or equal to 0.05 are considered differentially expressed. Gene Ontology analysis was performed via enrichr [91], the GO Biological Processes (2023), GO Cellular Component (2023), and GO Molecular Function libraries were utilized [92, 93], and an adjusted p-value > 0.05 was used as a cutoff.

scRNA-seq Tissue Preparation

Three hours after injury, one mouse was sacrificed and both knees were prepared for scRNA-seq as previously described [94]. Immediately following euthanasia with carbon dioxide asphyxiation, mice were submerged in ice-cold 70% ethanol, and then washed in ice-cold PBS before limb dissection. The knee joint was then excised by cutting the tibia and femur adjacent to the growth plates and trimmed similarly to the knees for bulk-seq. The tissue was digested in two stages, red blood cells were lysed and the cell suspensions strained [94]. The suspension was then passed to the UC Davis DNA Technologies Core facility for library preparation and sequencing.

Library preparation and scRNA sequencing

Barcoded transcriptome libraries were prepared from the single-cell suspensions using the Chromium Next GEM Single Cell 3' Kit v3.1 (10X Genomics, Pleasanton, CA, US) according to the manufacturer's instructions. Briefly, approximately 17,000 cells per sample were loaded onto a Chromium Next GEM Chip G and encapsulated into nanodroplets on a Chromium Controller microfluidic system, resulting in the mRNA barcoding of ~10,000 single cells per sample. After reverse transcription, the barcoded cDNA was purified with DynaBeads (Invitrogen, Carlsbad, CA, US). After PCR amplification, the quality of the cDNA was verified by micro-capillary gel electrophoresis using a Bioanalyzer 2100 (Agilent, Santa Clara, CA, US). The amplified cDNA was fragmented and converted to 3' gene expression profiling sequencing libraries. The fragment lengths of the sequencing libraries were assessed on a Bioanalyzer. The libraries were quantified by fluorometry on a Qubit instrument (Life Technologies, Carlsbad, CA, US) and qPCR

with a Kapa Library Quant kit (Kapa Biosystems-Roche, Basel, Switzerland). Pooled libraries were sequenced on a NovaSeq 6000 sequencer (Illumina, San Diego, CA, US) with paired-end reads. The sample processing targeted 10,000 cells per sample and a depth of 40,000 reads per cell.

Data filtering, integration, and clustering

Single-cell data was filtered and integrated as previously described[94]. The filtering process helps eliminate poor quality reads, dying cells, and potential doublets. The mouse knees were sequenced across four runs, one run each for the soft and hard digests of each knee digest, and the datasets were integrated to combine the left and right knees, and hard and soft digests of each knee. A Principal Component Analysis (PCA)-based clustering technique was performed in Seurat.

To better visualize and identify the CD45 negative populations. Cells within clusters lacking Cd45 (excluding the platelets/erythrocytes and proliferating cluster) were reclustered in Seurat to better define the cells and populations present. First the clusters were subsetted from the main dataset, then expression scaled within the subset. On this subset of cells principal component analysis (PCA) was run, a UMAP generated for visualization, and the cells were reclustered by FindClusters for analysis. The clusters were then assigned new identities based on expression of marker genes and these identities were ported back to the main dataset. This subsetting and reclustering method was also applied to the monocyte and macrophage containing clusters.

Data Analysis scRNA-seq

Clusters were split by left and right knee for analysis. To compare visually the expression of previously identified AIR genes, the scRNA seq data was plotted using complexheatmap[95]. Left and right knee expression was plotted by circles representing percentage of cells expressing a gene and expression level of those genes by cluster by the Heatmap() function, these plots were then visually merged, with each knee being represented by a half-circle. To better group the features and potentially highlight any

expression patterns in Figure 3, the rows were split by K-means partitioning using “row_km=3”[96]. Gene Ontologies were performed on the resulting groups of genes as before. On a cluster by cluster basis the left (control) and right (injured) knee expressions were compared for differential gene expression using limma voom (~LeftRight * Digest) to account for the longer digest on expression[97] .

The r package Cellchat[98] was employed to assess cell-cell communication within the single-cell dataset. Conversion of the Seurat object dataset and preparation of the CellChat object and inference of signaling was consistent with recommendations by the CellChat workflow. To focus analysis on the AIR, only pathways which included genes found on the one and four hour AIR gene lists were analyzed. Outgoing signal river plots was generated at the pattern numbers (four) at which cophenetic and silhouette measure scores decreased simultaneously. Chord plots were generated with *netvisual_chord(obj, signaling = AIR.paths…)* and river plots with *netanalysis_river(obj, pattern = “outgoing”, signaling = AIR.paths…).*

For comparison of synovial fibroblast sub-populations we used three additional scRNA-seq datasets: Chou C. et al (2020)[69], Sebastian A. et al (2022)[34], and Knights et al (2023)[99]. Datasets were downloaded from NCBI GenBank and synovial cell populations identified by expression of *Col1a1*, *Thbs4*, *Pdgfra* and *Prg4*, these cells were subsetted and reclustered as shown in Supplemental Figure 1. Next to focus on a specific subset of cells the expression of the genes *Has1*, *Prg4*, *Col22a1*, and *Tspan15* were plotted to highlight the cells of interest. The subset of stromal cells from this study was used for comparison.

Histology and Immunohistochemistry

At one and four hours after injury, mice were sacrificed (n=4 per timepoint, and 4 uninjured mice) limbs dissected as before. The right limbs were affixed to foam to maintain neutral knee position and placed in 4% paraformaldehyde for 24 hours, the fixed knees were then stored in ethanol until being decalcified

for three days in Immunocal (StatLab, Texas, USA) and embedded in paraffin. Before staining, slides were baked lying flat for 2 hours at 65 °c. Antigen retrieval was performed with Unitrieve following manufacturer protocols (NB325 Innovex Biosciences, Richmond, CA. USA) and application of Protinase K (Abcam, Massachusetts, USA) for 5 minutes at 37°c [100]. (Millipore-Sigma, 5 mg/ml, 1000 units/mg stock) for 10 minutes at 37°c. Afterwards, primary antibodies were incubated overnight at 4°C in a dark humid-chamber. Primary Antibodies: IL-33 (1:100, from supplier provided stock solution, Invitrogen, PA5-47007), HAS1 (1:100, from 500 ug/mL stock, Invitrogen, PA5-95599), PRG4 (1:200, from 1mg/mL stock, Novus Biologicals , Centennial, CO, USA , NBP1-19048), MT2A (1:200, from 1 mg/mL stock, Invitrogen, PA5-102549). Secondary antibodies were incubated for 2 hours at room temperature in a dark, humid chamber at 1:500 dilution. Images were captured on a Leica DMi8 microscope.

RESULTS

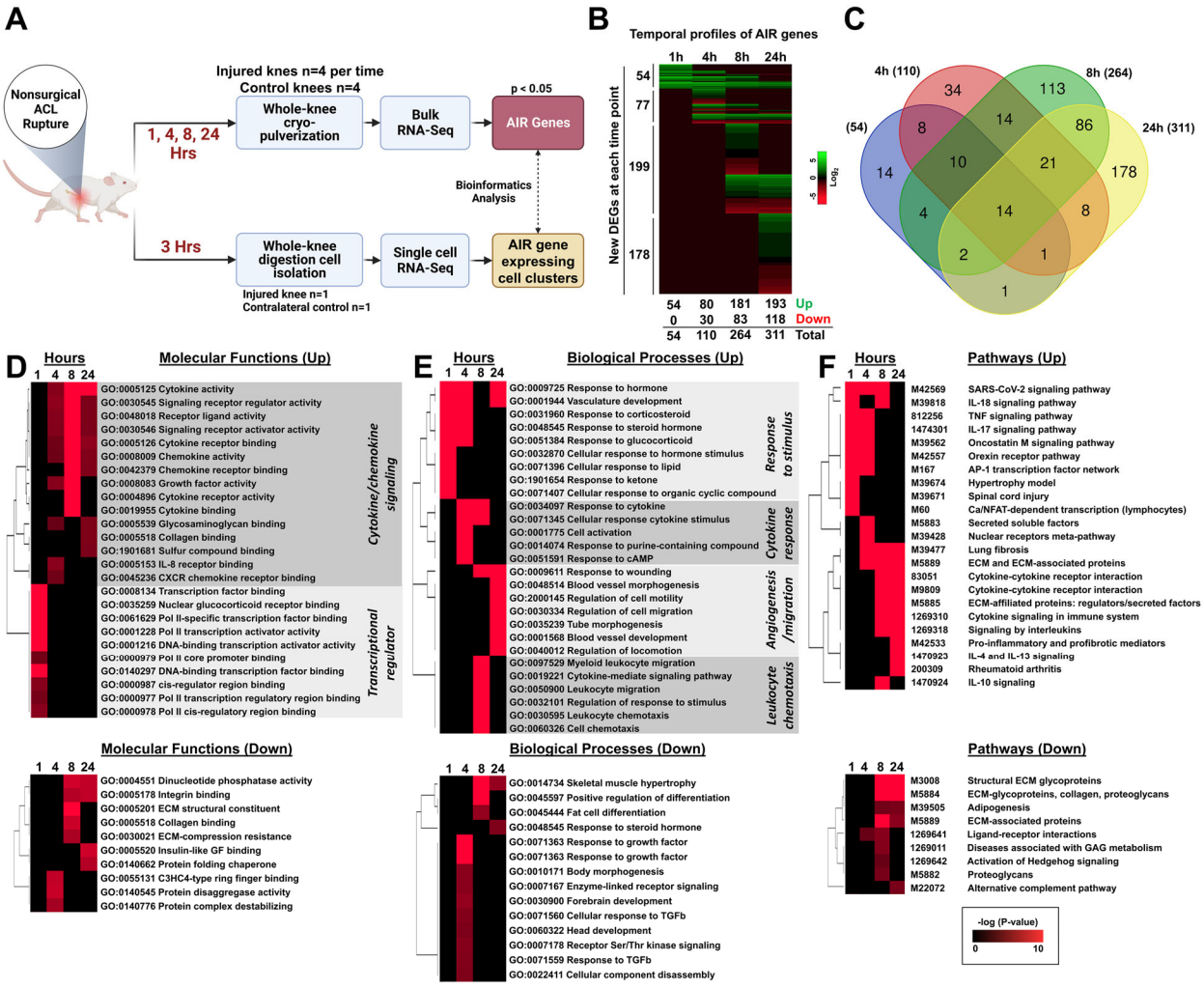

Figure 2.1: Whole Knee level changes after injury define the Acute Injury Response in the first 24 hours after injury. *A. Overview of mouse knee sequencing experiments (see methods). B. Temporal Heatmap of DEGs in the murine knee at 1, 4, 8, and 24 hours. C. Venn Diagram of DEGs for each timepoint of bulk sequencing. D. Molecular function ontology heatmaps for up and down regulated AIR genes at each timepoint. E. Biological processes ontology heatmaps for up and down regulated AIR genes at each timepoint. F. Ontological analysis of pathways associated with up and down regulated AIR genes at each timepoint.*

To establish the broad pattern of response genes that define the AIR, we performed bulk sequencing on whole murine knees 1, 4, 8, and 24 hours after nonsurgical ACL rupture. Experiments are outlined in Figure 2.1A, for details see the Methods section. Differentially Expressed Genes (DEGs) were identified based on expression compared to uninjured control limbs. Supplemental Table 1 contains the full list of DEGs at each timepoint. The temporal up and down regulation of these DEGs identified by bulk sequencing is shown in Figure 2.1B. DEGs that span multiple timepoints are indicated by continuing lines across the x axis while new DEGs are added to the bottom of the chart over time. We found an expanding number of genes at each timepoint creating a cascading "fan-shape" of plotted AIR genes. Initially 54 genes are upregulated at one hour, but this number increases to 110 DEGs at 4 hours, 264 DEGs at 8 hours, and 311 DEGs at 24 hours. No genes were downregulated one hour post injury. Four hours post-injury the number of DEGs increases to 110, including the downregulation of 30 new genes. The number of shared and unique AIR genes between timepoints is shown in Figure 2.1C. Fourteen genes remained elevated for all timepoints following injury.

Table 2.1: AIR Genes by Temporal Expression**.** n=4/group/time point (except naïve controls at time 0 only). Transcriptomes at 1-24h points were individually compared to naïve controls at time 0. DEGs =Differentially expressed genes (defined as adjusted p values <0.0549 compared to controls). logFC = fold change in log2, a negative number means higher expression compared to controls, and vice versa. Unique genes first detected at each time points were color coded.

1 hour			4 hour			8 hour			24 hour		
Gene	logFC	AveExpr	Gene	logFC	AveExpr	Gene	logFC	AveExpr	Gene	logFC	AveExpr
Fosb	-5.19	1.19	*Cxcl1*	-5.82	2.95	*Cxcl1*	-6.43	2.95	*Arg1*	-8.67	0.78
Cxcl1	-5.06	2.95	*Cxcl2*	-5.01	3.15	*Cxcl2*	-6.25	3.15	*Ccl7*	-4.94	3.50
Cxcl2	-4.56	3.15	*Ccl7*	-3.76	3.50	*Arg1*	-5.93	0.78	*Il11*	-4.80	0.71
Has1	-3.49	3.07	*Il6*	-3.41	1.67	*Ccl7*	-5.10	3.50	*Saa1*	-4.10	0.90
Il6	-3.16	1.67	*Ereg*	-3.31	0.83	*Saa1*	-5.03	0.90	*Cxcl5*	-3.81	4.95
Acod1	-3.09	2.29	*Has1*	-3.24	3.07	*Cxcl3*	-5.02	0.07	*Cxcl1*	-3.80	2.95
Fos	-2.95	4.49	*Fosl1*	-3.16	0.21	*Cxcl5*	-4.69	4.95	*Serpine1*	-3.71	4.52
Ccn1	-2.78	3.48	*Mt2*	-3.02	8.38	*Il6*	-4.45	1.67	*Ereg*	-3.63	0.83
Ptgs2	-2.62	1.38	*Serpine1*	-2.98	4.52	*Ereg*	-4.08	0.83	*Ankrd1*	-3.60	4.13
Serpine1	-2.56	4.52	*Tnfaip6*	-2.55	4.80	*Ptgs2*	-3.93	1.38	*Ccl2*	-3.29	4.39
Tnfaip6	-2.47	4.80	*Ptx3*	-2.43	4.67	*Ccl2*	-3.60	4.39	*Cxcl3*	-3.15	0.07
Egr1	-2.37	5.75	*Ccn1*	-2.39	3.48	*Serpine1*	-3.60	4.52	*Pdpn*	-2.97	5.87

Atf3	-2.27	2.70	*Pdk4*	-2.28	3.30	*Mmp3*	-3.59	4.03	*Timp1*	-2.94	5.29
Errfi1	-2.11	5.38	*Maff*	-2.25	2.04	*Il11*	-3.57	0.71	*Mmp3*	-2.90	4.03
Ddit4	-1.97	4.75	*Sox11*	-2.17	1.20	*Tnfaip6*	-3.47	4.80	*Rrad*	-2.84	1.91
Gm49839	-1.88	3.19	*Mt1*	-2.14	8.31	*Has1*	-3.33	3.07	*Hmga2*	-2.81	1.24
Apold1	-1.85	4.14	*Ddit4*	-2.04	4.75	*Mt2*	-3.25	8.38	*Dbp*	-2.60	2.26
Per1	-1.85	3.57	*Ccn2*	-1.92	5.93	*Pdpn*	-2.99	5.87	*Mt2*	-2.55	8.38
Dusp1	-1.76	5.65	*Errfi1*	-1.75	5.38	*Fosl1*	-2.96	0.21	*Ptx3*	-2.53	4.67
Socs3	-1.75	4.48	*Socs3*	-1.74	4.48	*Hmga2*	-2.85	1.24	*Msr1*	-2.49	4.73
Nr4a1	-1.74	4.15	*Gm49839*	-1.73	3.19	*Acod1*	-2.84	2.29	*Has1*	-2.47	3.07
Mt2	-1.74	8.38	*Gm16845*	-1.66	1.98	*Cd14*	-2.78	2.81	*Chl1*	-2.34	4.27
Ptx3	-1.74	4.67	*Il33*	-1.65	3.95	*Timp1*	-2.76	5.29	*Tnfaip6*	-2.29	4.80
Egr2	-1.70	1.66	*Fkbp5*	-1.60	5.75	*Ptx3*	-2.66	4.67	*Ptgs2*	-2.28	1.38
Nr4a3	-1.66	2.40	*Cxcl5*	-1.58	4.95	*Il33*	-2.55	3.95	*Tnfrsf12a*	-2.26	1.52
Nr4a2	-1.58	4.58	*Per1*	-1.55	3.57	*Pdk4*	-2.39	3.30	*Chrnb1*	-2.15	1.23
Il1b	-1.57	5.40	*Mmp19*	-1.47	3.45	*Mt1*	-2.39	8.31	*Ccr5*	-2.12	3.57
Adamts1	-1.43	5.66	*Ifi205*	-1.44	4.12	*Tnfrsf12a*	-2.38	1.52	*Plau*	-2.10	3.10
Junb	-1.33	6.50	*Cirbp*	-1.44	5.03	*Gm13889*	-2.31	3.96	*Flnc*	-1.96	3.58
Mt1	-1.30	8.31	*Fos*	-1.41	4.49	*Socs3*	-2.29	4.48	*Il33*	-1.96	3.95
P2ry10	-1.24	3.35	*Pdpn*	-1.34	5.87	*Kcnj2*	-2.29	2.49	*Trim63*	-1.94	5.88
Ier3	-1.09	5.30	*Fst*	-1.34	4.57	*Ccl3*	-2.26	1.08	*Has2*	-1.86	0.98
Angptl4	-1.08	4.67	*Gfpt2*	-1.33	4.01	*Slc39a14*	-2.24	4.09	*Mmp19*	-1.86	3.45
Cd83	-1.07	3.61	*Il15ra*	-1.27	3.62	*Snhg6*	-2.24	1.95	*Slc39a14*	-1.83	4.09
Trib1	-1.07	6.13	*Il1r2*	-1.26	4.81	*Maff*	-2.21	2.04	*C3ar1*	-1.81	4.72
Cebpb	-1.06	6.03	*Hopx*	-1.23	3.13	*Il1b*	-2.18	5.40	*Cxcl14*	-1.80	6.93
Trem1	-1.06	4.83	*Thbd*	-1.21	5.98	*Inhba*	-2.13	6.65	*Serpina3n*	-1.78	3.66
Egr3	-1.04	3.30	*Hbegf*	-1.21	6.05	*Rrad*	-2.13	1.91	*Mt1*	-1.71	8.31
Arg2	-1.03	3.00	*Inhba*	-1.20	6.65	*Ccl4*	-2.11	2.76	*Sod3*	-1.68	4.32
Il1r2	-1.01	4.81	*Btf3l4*	-1.19	2.91	*Ccn1*	-2.00	3.48	*Ms4a6d*	-1.68	4.85
Gfpt2	-1.01	4.01	*Egr1*	-1.19	5.75	*Plau*	-1.93	3.10	*Socs3*	-1.67	4.48
Sik1	-1.01	3.72	*Apold1*	-1.15	4.14	*Tm4sf1*	-1.91	5.34	*Eda2r*	-1.66	2.56
Hbegf	-0.93	6.05	*Dusp1*	-1.12	5.65	*Ier3*	-1.88	5.30	*Nek6*	-1.65	3.56
Ugdh	-0.81	6.12	*Ier3*	-1.09	5.30	*Serpina3n*	-1.87	3.66	*Vgll3*	-1.63	2.65
Rcan1	-0.76	4.84	*Il1b*	-1.06	5.40	*Gprc5a*	-1.82	1.68	*Gjb3*	-1.58	0.78
Clec4d	-0.74	5.89	*Ugdh*	-1.06	6.12	*Mmp19*	-1.78	3.45	*Fbln2*	-1.56	4.39
Tsc22d3	-0.74	6.74	*Foxred2*	-1.06	2.97	*Ccn2*	-1.74	5.93	*Slco2a1*	-1.55	3.63
Nfkbia	-0.73	8.56	*Adamts1*	-1.01	5.66	*Kcne4*	-1.73	2.65	*Gm13889*	-1.54	3.96
Pim3	-0.69	5.92	*Angptl4*	-1.01	4.67	*Igfbp3*	-1.73	3.00	*Kcne4*	-1.50	2.65
Ifrd1	-0.69	6.83	*Pik3ip1*	-0.97	4.81	*Fos*	-1.72	4.49	*Bcat1*	-1.49	2.48
Sgk1	-0.68	5.60	*Abt1*	-0.94	3.70	*Ucp3*	-1.72	2.72	*Inhba*	-1.47	6.65
Klf4	-0.63	6.93	*Emp1*	-0.92	7.55	*Ankrd1*	-1.70	4.13	*Crlf1*	-1.45	1.78
Klf9	-0.63	7.90	*Btla*	-0.92	4.30	*Adamts4*	-1.66	2.77	*Tm4sf1*	-1.43	5.34
Thbd	-0.54	5.98	*Srxn1*	-0.89	5.49	*Cxcl14*	-1.62	6.93	*Clec4n*	-1.39	3.41
			Junb	-0.89	6.50	*Myf6*	-1.58	3.24	*Fkbp11*	-1.39	2.99
			Sdc4	-0.85	6.15	*Slco2a1*	-1.58	3.63	*Vcan*	-1.35	6.48
			Tsc22d3	-0.84	6.74	*Vcan*	-1.57	6.48	*Cirbp*	-1.34	5.03
			Fgl2	-0.78	6.54	*Ms4a6d*	-1.55	4.85	*Tacc2*	-1.33	5.92
			Tlr13	-0.76	4.32	*Trim63*	-1.50	5.88	*Klhl40*	-1.31	4.32
			Parn	-0.72	4.52	*Adamts1*	-1.47	5.66	*Pcsk5*	-1.31	3.54
			Cebpb	-0.71	6.03	*Nek6*	-1.45	3.56	*Snai1*	-1.29	3.20
			Klf9	-0.70	7.90	*Clec4n*	-1.43	3.41	*P2ry6*	-1.28	2.53
			Klf13	-0.69	7.18	*Gfpt2*	-1.38	4.01	*Mir22hg*	-1.26	5.01
			Tarsl2	-0.67	4.72	*Angptl4*	-1.37	4.67	*1700086O0*	-1.23	2.56
			Uap1	-0.66	6.64	*Msr1*	-1.36	4.73	*Nr1d2*	-1.20	5.61
			Slc25a30	-0.66	5.40	*Junb*	-1.34	6.50	*Tgfbi*	-1.19	7.34
			Sgk1	-0.60	5.60	*Errfi1*	-1.30	5.38	*Ier3*	-1.17	5.30
			Cd300lf	-0.60	6.18	*Hbegf*	-1.26	6.05	*Cyp26b1*	-1.16	4.81
			Crispld2	-0.60	7.17	*Flnc*	-1.23	3.58	*Mustn1*	-1.16	4.06
			Glul	-0.58	8.57	*Ifi205*	-1.22	4.12	*Il1b*	-1.15	5.40
			Zbtb22	-0.55	4.91	*Sdc4*	-1.21	6.15	*Slc23a2*	-1.12	3.73
			H2-Aa	-0.52	7.21	*Osm*	-1.20	2.73	*Dclk1*	-1.11	4.78
			Arid5b	-0.51	5.96	*Tubb6*	-1.18	3.78	*Enc1*	-1.09	4.30
			Nipsnap3b	-0.49	5.97	*Mir22hg*	-1.18	5.01	*Tubb6*	-1.08	3.78
			Sla	-0.46	7.23	*Fgf2*	-1.18	3.39	*Prg4*	-1.07	10.26
			Rsl1d1	-0.45	7.06	*Cpne8*	-1.18	3.99	*Kdelr3*	-1.07	3.87
			Mat2a	-0.44	7.92	*Il13ra1*	-1.16	4.42	*Ltbp2*	-1.07	4.20

Hnrnpdl	-0.42	8.26	*Lilr4b*	-1.16	5.21	*Angptl4*	-1.06	4.67
Eif3e	-0.36	8.02	*Il4ra*	-1.15	5.44	*Il13ra1*	-1.05	4.42
Xrn2	-0.33	8.05	*Rcan1*	-1.14	4.84	*Cacna1d*	-1.05	2.41
Sptbn1	0.32	8.73	*Tacc2*	-1.09	5.92	*Lox*	-1.03	7.68
H13	0.40	6.67	*Slc7a11*	-1.06	3.75	*Zfp512b*	-1.02	3.25
Zeb2	0.42	7.65	*Pmaip1*	-1.06	2.97	*Penk*	-1.01	4.72
Lima1	0.44	6.75	*Pus1*	-1.04	3.38	*Adamts1*	-1.01	5.66
Cbfa2t3	0.46	6.32	*Osmr*	-1.04	3.88	*Emp1*	-1.00	7.55
Ncbp2	0.47	6.00	*Hopx*	-1.04	3.13	*Tnfrsf11a*	-1.00	4.09
Ski	0.49	6.22	*Csf1*	-1.04	5.38	*Bhlhe40*	-0.99	5.16
Cx3cr1	0.56	6.21	*Gpr35*	-1.03	2.60	*Hopx*	-0.99	3.13
Crispld1	0.57	6.15	*Nt5e*	-1.01	5.13	*Asb5*	-0.98	5.30
Chordc1	0.59	7.15	*Fst*	-1.01	4.57	*Junb*	-0.98	6.50
Abca8a	0.69	5.62	*Bhlhe40*	-0.99	5.16	*Niban2*	-0.97	5.18
Syne2	0.69	6.55	*Slc23a2*	-0.99	3.73	*Rdh10*	-0.96	3.61
Hspa8	0.70	7.76	*Pde4b*	-0.98	6.36	*Yif1b*	-0.96	3.75
Ar	0.70	5.83	*Emp1*	-0.98	7.55	*Sfrp1*	-0.95	4.41
Banp	0.73	5.15	*Penk*	-0.96	4.72	*Pmepa1*	-0.95	7.02
Ptprf	0.77	5.37	*Ccr1*	-0.95	5.77	*Pkib*	-0.94	3.52
Morrbid	0.82	4.42	*Apold1*	-0.94	4.14	*Il4ra*	-0.93	5.44
Clec3b	0.90	4.43	*Ccr5*	-0.94	3.57	*Csgalnact1*	-0.92	4.62
Elovl7	0.93	4.19	*Thbd*	-0.93	5.98	*Mir100hg*	-0.92	4.06
Tmem100	1.03	4.20	*Clec4d*	-0.91	5.89	*Dab2*	-0.92	6.38
Slc25a10	1.06	3.44	*Uap1*	-0.89	6.64	*Bpnt1*	-0.89	4.07
Chst1	1.07	4.98	*Tnfrsf11b*	-0.89	4.58	*Tspan4*	-0.89	5.72
Gas1	1.09	5.73	*Il1rap*	-0.87	3.74	*Dse*	-0.88	4.75
Cdon	1.12	4.51	*Zfp36*	-0.86	5.40	*Cstb*	-0.87	6.40
Tmod2	1.13	3.56	*Ccl9*	-0.85	5.84	*Fads3*	-0.85	4.17
Dkk1	1.49	2.34	*Gk*	-0.83	4.93	*Ccr2*	-0.85	8.13
Hspa1b	1.56	3.42	*Niban2*	-0.82	5.18	*Fst*	-0.84	7.35
B3galt2	1.76	3.92	*Bmp2*	-0.81	5.46	*Epb41l1*	-0.84	4.32
Pck1	1.87	3.89	*Bst1*	-0.80	4.58	*Csf1*	-0.84	5.38
Acvr1c	2.07	2.88	*Tlr13*	-0.80	4.32	*Lrrc17*	-0.83	4.60
			Rars2	-0.79	4.03	*Rab7b*	-0.82	4.63
			Cebpb	-0.79	6.03	*Basp1*	-0.81	5.89
			Cd3eap	-0.78	4.72	*Ipo4*	-0.81	4.06
			Naaa	-0.77	4.91	*S100a4*	-0.79	8.01
			Il1r1	-0.75	5.22	*Mrpl27*	-0.79	4.14
			Fgl2	-0.75	6.54	*Fbxo32*	-0.78	6.90
			Gcnt2	-0.74	5.77	*Aebp1*	-0.77	4.82
			Tspan4	-0.74	5.72	*S100a16*	-0.77	4.65
			Pmepa1	-0.72	7.02	*Esm1*	-0.76	5.65
			H6pd	-0.72	4.24	*Plin2*	-0.76	6.24
			Rab10os	-0.72	4.12	*Thbs4*	-0.75	6.58
			Ugdh	-0.72	6.12	*Dsel*	-0.74	4.24
			Sbno2	-0.72	5.95	*Pno1*	-0.74	5.45
			Il1rn	-0.72	6.62	*Lgmn*	-0.74	6.31
			Pla2g7	-0.71	5.79	*Rcan1*	-0.74	4.84
			Srgn	-0.71	7.80	*Lsg1*	-0.73	5.03
			Eef1e1	-0.70	4.16	*Sfxn3*	-0.73	4.42
			Ttc39b	-0.70	5.39	*Ms4a6b*	-0.72	5.73
			Hilpda	-0.69	5.30	*Ttc39b*	-0.70	5.39
			Cd300lf	-0.69	6.18	*Arl4c*	-0.69	4.10
			Cd300ld	-0.69	4.98	*Ccl9*	-0.69	5.84
			Il1rl1	-0.68	4.89	*Pid1*	-0.69	5.92
			Rbm34	-0.67	4.87	*Tef*	-0.69	5.63
			Pim3	-0.67	5.92	*Rbm3*	-0.69	5.54
			Dab2	-0.67	6.38	*Apex1*	-0.67	5.00
			Hif1a	-0.66	7.29	*Sdc4*	-0.67	6.15
			Mmp13	-0.65	9.20	*Slc7a2*	-0.66	4.67
			Tmbim1	-0.65	5.20	*Smad7*	-0.66	4.66
			Ccr2	-0.64	8.13	*Lat2*	-0.65	5.70
			Acsl4	-0.64	6.77	*Snhg4*	-0.65	5.03
			Eps8	-0.63	5.05	*Gtf2ird1*	-0.64	4.20
			Lox	-0.61	7.68	*Ttc37*	-0.64	4.67
			Btg1	-0.60	5.64	*Myadm*	-0.63	5.12

			Prg4	-0.59	10.26	*Ccnd1*	-0.63	6.92
			Ext1	-0.58	5.42	*Smim4*	-0.61	5.96
			Srxn1	-0.57	5.49	*Vim*	-0.61	8.95
			Csf2rb	-0.57	6.50	*Tceal8*	-0.60	5.78
			Sf3b5	-0.56	5.89	*Snhg9*	-0.60	5.28
			Slc25a20	-0.56	4.73	*Hif1a*	-0.60	7.29
			Eif1a	-0.55	6.72	*Trmt6*	-0.59	6.38
			Lrrc59	-0.55	5.88	*Calu*	-0.58	7.61
			Myd88	-0.55	5.59	*Col6a3*	-0.58	7.12
			Tpd52	-0.54	6.85	*Uap1*	-0.58	6.64
			Ints2	-0.53	5.04	*Col3a1*	-0.57	8.18
			Cd44	-0.51	9.04	*Nt5e*	-0.57	5.13
			Chil3	-0.51	9.58	*Slc35b2*	-0.57	4.93
			Rnh1	-0.50	5.87	*Ugdh*	-0.57	6.12
			Tgm2	-0.49	6.35	*Slc6a6*	-0.56	8.16
			Spp1	-0.49	9.48	*Postn*	-0.56	6.99
			Tmed5	-0.48	6.78	*Ctsl*	-0.55	7.56
			Wdr75	-0.47	5.93	*Hmox1*	-0.55	7.34
			Tcof1	-0.46	6.12	*Mtap*	-0.55	5.03
			Sod2	-0.46	7.01	*Lrp1*	-0.55	6.70
			Ifrd1	-0.46	6.83	*Mgat4b*	-0.54	5.54
			Ms4a6c	-0.45	7.96	*Hnrnpdl*	-0.53	8.26
			Cct3	-0.44	6.80	*Nudcd2*	-0.52	6.50
			S100a10	-0.43	6.66	*Lmna*	-0.52	6.55
			Ppa1	-0.43	6.68	*Rnh1*	-0.52	5.87
			Glul	-0.41	8.57	*Otulinl*	-0.52	5.34
			Hspa9	-0.41	8.01	*Lgals1*	-0.52	7.47
			Ccl6	-0.41	8.83	*Lipa*	-0.47	6.48
			Adamts5	-0.41	6.83	*Srsf5*	-0.47	8.24
			Ctsl	-0.40	7.56	*Acsl4*	-0.47	6.77
			Psmd3	-0.39	7.18	*Spp1*	-0.45	9.48
			C1qbp	-0.39	7.75	*Tmem258*	-0.44	7.21
			Sell	-0.38	7.84	*Rbpj*	-0.43	6.00
			Stat3	-0.38	8.12	*Atp6v1g1*	-0.42	5.89
			Denr	-0.37	6.76	*Psmd3*	-0.41	7.18
			Runx1	-0.36	7.32	*Tuba1a*	-0.40	7.77
			Clic4	-0.35	8.76	*Rsl1d1*	-0.40	7.06
			Hnrnpdl	-0.33	8.26	*Nme1*	-0.38	7.15
			Timp2	0.39	9.60	*Prdx1*	-0.38	8.56
			Gsn	0.39	8.57	*Mbtd1*	-0.37	7.11
			Igfbp5	0.44	8.31	*Cd63*	-0.37	9.54
			Nfix	0.45	7.22	*Pak1ip1*	-0.36	6.87
			Dcn	0.46	10.29	*Psmd1*	-0.36	7.83
			Thra	0.47	6.77	*Ctss*	-0.35	9.24
			Mxra8	0.51	6.32	*Camkk2*	-0.34	7.23
			Utrn	0.52	7.49	*Xrn2*	-0.33	8.05
			Chd3	0.52	5.81	*Ssr3*	-0.33	8.27
			Ar	0.54	5.83	*Msn*	-0.31	8.80
			Sdc2	0.56	6.74	*Ssr1*	-0.31	8.37
			Zbtb20	0.57	8.38	*Ccnd2*	-0.26	8.91
			Syne2	0.57	6.55	*Nudt4*	0.26	8.34
			Myo6	0.59	6.05	*Tln1*	0.29	9.07
			Abca9	0.64	4.59	*Ncor1*	0.29	9.20
			Fkbp7	0.65	6.01	*Sfpq*	0.29	9.25
			Plac9a	0.66	5.76	*Ubr2*	0.31	7.41
			Adipoq	0.67	7.12	*Ccpg1*	0.36	6.15
			Enpp2	0.67	5.89	*Samd9l*	0.39	6.65
			Scd1	0.70	8.22	*Ppp2r5a*	0.40	8.10
			Plxdc2	0.71	5.48	*Aldh2*	0.41	8.39
			Dnaja4	0.72	4.98	*Treml1*	0.42	7.40
			Sparcl1	0.74	6.59	*Sptbn1*	0.43	8.73
			Fasn	0.75	5.90	*Timp2*	0.44	9.60
			Ddah2	0.75	5.24	*Ralgapa1*	0.44	6.44
			Tmem100	0.76	4.20	*Niban1*	0.44	6.64
			Itih5	0.76	6.74	*Igfbp5*	0.45	8.31
			Rarres2	0.78	4.67	*Irak4*	0.48	5.99

			Car3	0.82	9.20	*Abcc5*	0.48	5.78
			Clic5	0.82	5.01	*Treml2*	0.48	7.05
			Fndc1	0.84	4.59	*Ltf*	0.55	9.77
			Crispld1	0.85	6.15	*Syne2*	0.55	6.55
			Ptprz1	0.86	4.65	*Itih5*	0.56	6.74
			Gas1	0.86	5.73	*Kalrn*	0.57	5.38
			Clstn1	0.88	4.83	*Lcn2*	0.57	9.04
			Dpt	0.89	6.28	*Hspa4l*	0.57	6.80
			Cilp	0.91	7.16	*Mtrf1l*	0.57	4.92
			Cd34	0.95	6.04	*Cd226*	0.57	6.16
			Sema3c	0.95	4.94	*Fkbp4*	0.58	6.99
			Cyb5d2	0.95	3.34	*Tob1*	0.59	5.09
			Gdf10	0.98	4.45	*Mcpt8*	0.59	6.65
			Col14a1	1.02	5.18	*Chordc1*	0.60	7.15
			Cilp2	1.05	5.89	*Pou2af1*	0.60	5.80
			Pcsk6	1.06	5.57	*Mad2l1bp*	0.61	4.90
			Creb5	1.10	4.97	*Peg13*	0.62	4.90
			Boc	1.11	3.45	*Ar*	0.63	5.83
			Lyve1	1.11	5.04	*Gas1*	0.63	5.73
			Kera	1.16	3.89	*Hspa8*	0.65	7.76
			Abca8a	1.18	5.62	*Ppp1r42*	0.66	4.40
			Ogn	1.23	6.36	*Hdc*	0.66	7.49
			Sfrp2	1.40	4.65	*Prom1*	0.67	5.09
			Ostn	1.41	2.51	*Tsc22d3*	0.68	6.74
			Frzb	1.46	4.38	*C3*	0.68	7.69
			Aspn	1.46	6.57	*Arhgef18*	0.68	4.89
			Myoc	1.47	6.40	*Plac9a*	0.68	5.76
			Ecm2	1.48	4.92	*Ecrg4*	0.69	6.81
			Tmod2	1.53	3.56	*Vit*	0.71	5.24
			Piezo2	1.54	2.60	*Dio2*	0.72	5.80
			Cd209f	1.54	4.33	*Gsn*	0.73	8.57
			Clec3b	1.58	4.43	*Enpp2*	0.74	5.89
			Cdon	1.65	4.51	*AW011738*	0.75	4.51
			Nnat	1.69	5.36	*Abca9*	0.75	4.59
			Col8a2	1.69	3.20	*Aspn*	0.76	6.57
			Cyp2f2	1.74	4.61	*Car3*	0.77	9.20
			Ky	1.83	3.39	*Fndc1*	0.79	4.59
			Cd248	1.91	2.73	*C1s1*	0.79	4.17
			Abca8b	1.99	3.52	*Ccdc3*	0.80	5.65
			Vsig4	2.00	2.62	*Supt3*	0.80	3.95
			Lgals12	2.00	2.02	*Cilp*	0.84	7.16
			Naalad2	2.01	2.62	*Elovl7*	0.85	4.19
			Aoc3	2.01	4.74	*Adipoq*	0.86	7.12
			Emc9	2.08	1.74	*Dpt*	0.86	6.28
			B3galt2	2.10	3.92	*Pcsk6*	0.87	5.57
			Fam124a	2.20	2.32	*Tppp3*	0.93	5.49
			Tppp3	2.30	5.49	*Sparcl1*	0.94	6.59
			Plin1	2.35	5.19	*Clic5*	0.94	5.01
			Ppl	2.45	2.13	*Mgl2*	0.95	4.97
			Adig	2.59	1.14	*Omd*	0.95	5.16
			Dkk2	2.76	2.52	*Zfp866*	0.96	3.87
			Thrsp	2.80	3.86	*Sh3bgrl2*	0.97	3.77
			Cyp2e1	3.06	2.87	*Cytl1*	1.00	7.17
			Pck1	3.57	3.89	*Hps4*	1.00	3.31
			Acvr1c	3.69	2.88	*H4c4*	1.00	4.43
						Cdo1	1.00	5.28
						H2ac4	1.04	4.43
						Gstz1	1.05	4.42
						Fasn	1.11	5.90
						Dnah8	1.11	4.29
						Cidec	1.12	4.16
						Hrc	1.16	5.58
						Cilp2	1.16	5.89
						Sypl2	1.20	4.24
						Purg	1.22	2.09
						Abca8a	1.24	5.62

			Ccn3	1.27	3.46
			Itga11	1.28	2.73
			Mylk4	1.28	7.22
			Boc	1.30	3.45
			B3galt2	1.31	3.92
			Hsph1	1.33	6.48
			Htra4	1.38	3.81
			Dkk2	1.41	2.52
			Cfd	1.41	8.30
			Gm36738	1.45	2.33
			Aoc3	1.45	4.74
			Scd1	1.47	8.22
			Ecm2	1.47	4.92
			Igfbp6	1.51	4.24
			Abca8b	1.53	3.52
			Plin1	1.63	5.19
			Ky	1.71	3.39
			Abra	1.74	4.64
			Hspa1b	1.74	3.42
			Myoc	1.76	6.40
			Lgals12	1.77	2.02
			Cyp2f2	1.91	4.61
			Nr4a3	2.05	2.40
			Tspan15	2.16	2.14
			C7	2.21	1.86
			Pck1	2.25	3.89
			Ces1d	2.28	2.88
			Retn	2.38	2.91
			Clec3b	2.43	4.43
			Acvr1c	2.48	2.88
			Adig	2.56	1.14
			Mettl21c	2.69	3.00
			Thrsp	2.78	3.86
			Retnla	2.95	3.88
			Cyp2e1	3.20	2.87
			Nnat	3.36	5.36

Next, we performed ontology analysis on the AIR genes for each timepoint to determine the general pathways and functions of the AIR genes over time (Figure 2.1D,E,F). In the first hour, the upregulated genes are primarily involved in transcriptional regulation molecular functions. These functions include DNA binding and polymerase II recruitment and activating factors. Following four hours there was increases in cytokine and chemokine signaling which peaked at eight hours with some continuation at twenty-four hours. Many receptor and ligand associated genes were upregulated at hours four, eight, and twenty-four. At eight hours many genes associated with integrins, collagen, and ECM were downregulated. The ontology of biological processes in the AIR genes showed a strong response to stimulus at one and four hours. This was followed by cytokine response at four and eight hours. During this period responses to growth factors and TGFB were downregulated. At eight hours the biological

processes related to leukocyte chemotaxis were enriched. Finally at twenty-four hours processes related to angiogenesis and cell migration were enriched. When organized by pathways for ontological analysis, at one and four hours IL-17, Oncostatin M (part of the IL-6 family) and TNF, were highly enriched. At one hour AIR genes also showed in enrichment in the pathways identified in spinal cord injury. At the later timepoints of eight and twenty-four hours we observed an enrichment in Th2 type pathways including *Il4*, *Il13*, as well as *Il10* which inhibits Th1 responses. Several pathways related to fibrosis were also enriched in the later times. In the pathway analysis several ECM related pathways were downregulated at eight and twenty-four hours.

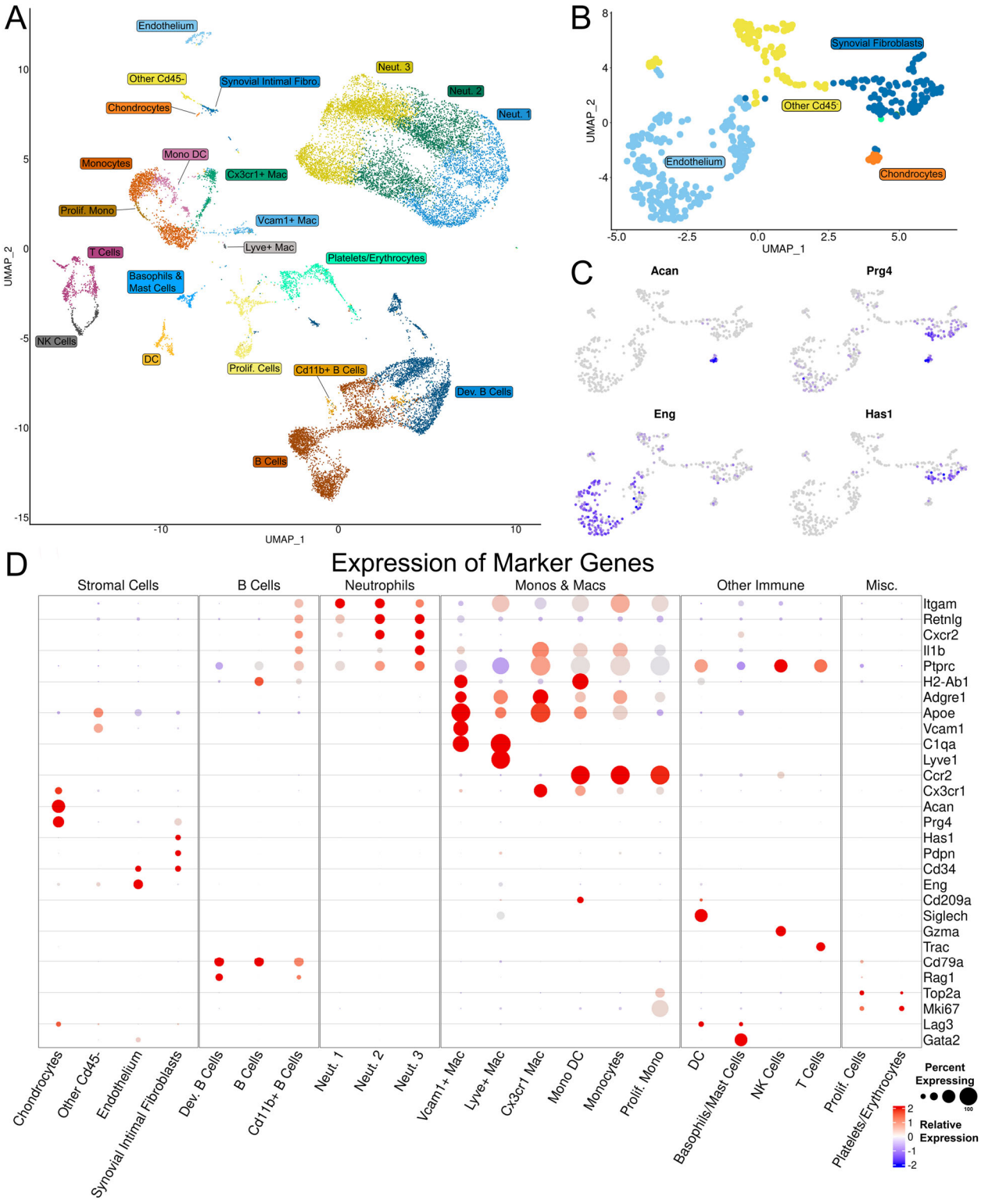

Figure 2.1: scRNA-seq of the whole knee captures a wide variety of cell-types. A) Uniform Manifold Approximation and Projection (UMAP) of single-cell RNA sequencing scRNA-seq data from the

mouse injured at three hours. Twenty-two different cell-types or subtypes were identified in the whole knee digest as shown here. B) UMAP of reclustered *Cd45* negative cells from the whole knee dataset. C) UMAPs of the *Cd45*- cells with selected aggrecan, lubricin, endoglin and hyaluronan synthase 1 expression highlighted. D) Dotplot showing the expression of selected marker genes of identified cell types. The dot size represents the percentage of cells within each column expressing the gene, and dot color indicated normalized average expression level of each gene.

To determine the potential cellular sources of AIR expression within the murine knee, we performed single-cell RNA seq of the whole knee digests from a mouse to first survey and identify the cell populations present. We found a larger population of *Cd45*$^{+}$ immune cells relative to *Cd45*$^{-}$ stromal cells, these populations were clearly delineated in the scRNA-seq data. We identified twenty-two distinct cell populations within the whole knee digest (Figure 2.2A).

Within the stromal cells we identified chondrocytes, endothelial cells, and synovial fibroblasts by subsetting the *Cd45*$^{-}$ cells (Figure 2.2B). The genes aggrecan, lubricin, endoglin and hyaluronan synthase 1 are shown within the stromal cell subset data in Figure 2.2C. Chondrocytes were identified by expression of *Acan* and *Prg4*[101]. Endothelial cells were identified by expression of *Eng*[102], and synovial fibroblasts were identified by expression of *Has1*, and *Prg4*[69, 103].

Many immune cells were identified within the knee digest, including many B cells, neutrophils and monocytes and macrophages, T cells and NK cells, as well as basophils, mast cells and dendritic cells (DCs). Figure 2.2D shows the chosen markers for each cell type and their expression. B cells were identified by expression of *Cd79a*[104] while developing B cells also expressed *Rag1* [105]. A Cd11b+ B cell subpopulation expressed *Cd11b* and appeared to express similar genes to that of neutrophils or other trafficking immunes cells. Neutrophils were identified by expression of *Cd11b*, *Retnlg*, and *Cxcr2*.Neutrophils are short lived cells that exist along a continual path of development and activation

which has been termed “neutrotime”, in this study we split the neutrophils into three clusters based on the expression of neutrotime markers[106], early (naïve) neutrophils (Neutrophil 1) express less *Il-1b* and *Cxcr1*, while later more activated neutrophils express greater levels.

Macrophages and Monocytes expressed *Apoe* and *Adrge1*[107]. Monocytes expressed *Ccr2* as well proliferating monocytes were identified by expression of *Top2a*[108, 109]. Monocyte dendritic cells were identified by expression of *Cd209a* and major histocompatibility complex (MHCII, the gene *H2-Ab1*)[110] while Macrophages lacked *Ccr2* relative to monocytes. Macrophages expressing *Vcam1*, as well as MHCII we designated *Vcam1*$^{+}$. *Cx3cr1*$^{+}$ macrophages expressed Cx3cr1, indicative of a more resident role and niche[111]. Lyve^{+} Macrophages expressed *Lyve1* and high levels of *Cd11b* [112].
Dendritic cells (DCs) expressed *Siglech*, *Cd209a* and *Lag3*[113]. The basophil and mast cell cluster was identified by expression of *Gata2*[114]. NK cells were identified by expression of granzyme a (*Gzma*)[115]. T Cells were identified by expression of the T cell receptor alpha constant (*Trac*). Proliferating cells were identified by expression of *Mki67* and *Top2a*[108].

In summary we identified a broad range of cells including large populations of immune cells.

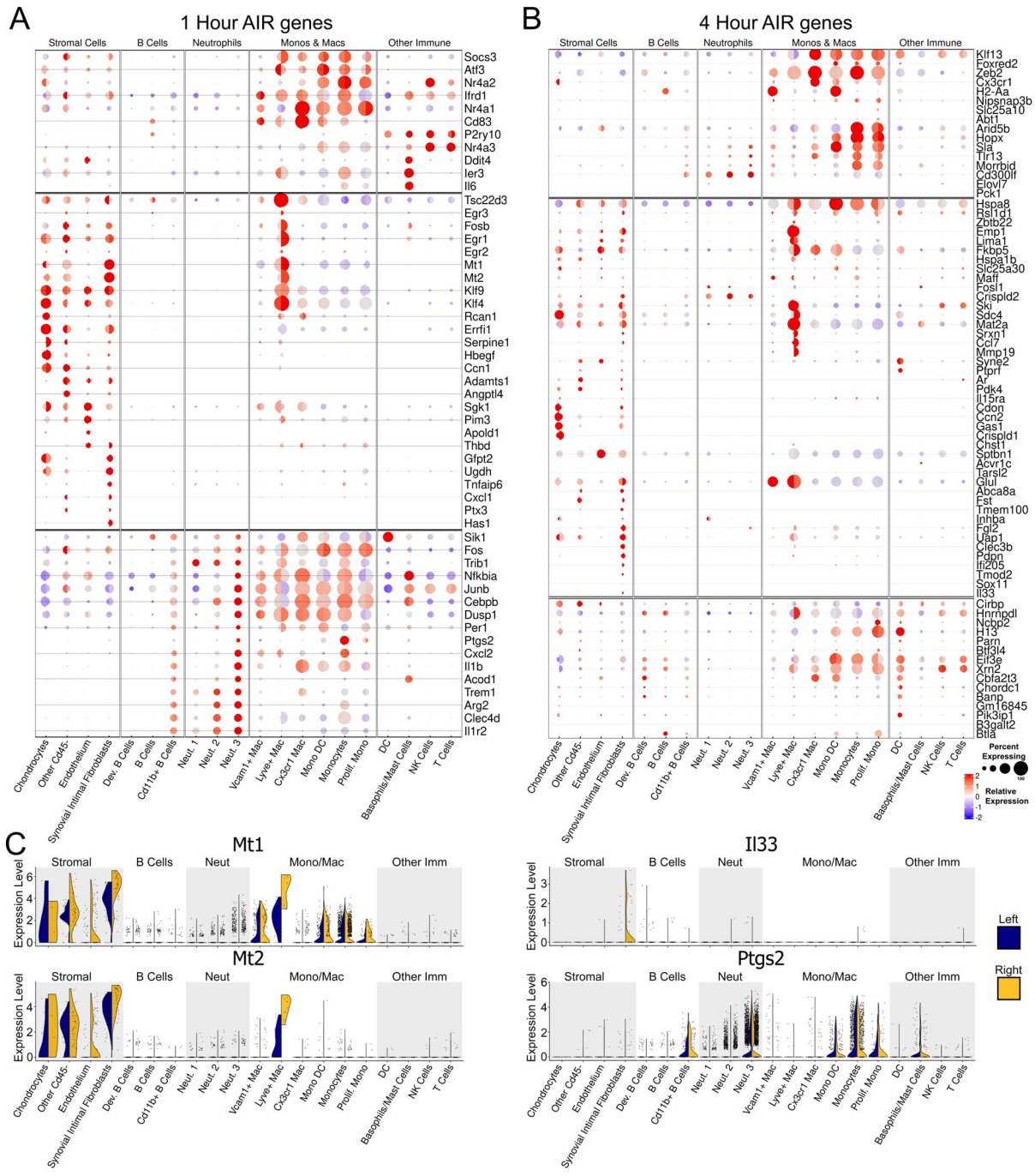

Figure 2.3: Three hours post injury, single-cell sequencing reveals differences in stromal and immune population's Acute Injury Responses. A-B) Dot plots showing expression of the unique 1 hour AIR gene list (A) or unique 4 hour AIR gene list (B) by single-cell seq at three hours post-injury. Left half of circles represeent uninjured limb cells, right half of circles represent injured limb cells. Circle size

show the percent of cells in each cluster expressing each gene, circle color shows relative expression levels of the gene in each cluster. Gene lists have been partitioned by K-means into groups of similarly expressed genes by clusters. C) Violinplots of selected AIR genes across knee cell populations. Expression of uninjured limb cells are on the left (blue) and cells from the injured limb on the right (yellow) for each cluster. Expression of *Mt1*, *Mt2*, *Il-33* and *Ptgs2* are displayed.

To ascertain the cellular origins of AIR genes identified via bulk sequencing, we compared AIR gene expression in control versus injured knees three hours post-injury using single-cell RNA sequencing data. By filtering the expression using the unique AIR genes at one and four hours, distinct AIR gene expression profiles were evident in immune cells and stromal cells (Figure 2.3A-B).

The 1-hour genes are arranged by K-means partitioning to visually organize similar gene expression patterns across the cell-type clusters (Figure 2.3A). The genes in middle partition are expressed predominately within the stromal cell clusters. These genes include many transcription factors including *Egr1, Egr2, Egr3, Klf4, Klf9*. Chondrocytes and SIF cells are the predominate expressors within this partition. Many genes related to the ECM are found within this partition including *Mt1, Mt2, Adamts1, Ccn1*, and *Has1*. In the bottom partition, neutrophils contribute to many of the 1 hour AIR genes, particularly the more activated neutrophils in the Neutrophil 3 cluster. *Il1r2, Clec4d, Trem1, Acod, Arg2* and *Il1b* were conspicuous in this pattern. Many genes are shared between neutrophils and monocytes and macrophages including *Nfkbia, Junb, Fos, Trib1*, and *Dusp1*. The genes in the top partition were expressed primarily in the monocyte and macrophage groups as well as T, NK and Basophil/Mast cells. Within the monocytes, *Nr4a2, Nr4a1* are highly expressed and have been previously shown to be elevated in chronic arthritis [116]. Expression of *Ifrd1*, a repressor of NF-KB, is generally increased after injury in stromal cells, but decreased in monocytes and macrophages.

Using the same 3-hour post injury scRNA-seq dataset we then partitioned and plotted the expression of the 4-hour AIR genes to assess which populations may be contributing to these genes (Figure 2.3B). In

the bottom partition, the overall expression pattern is mixed with B-Cells, monocytes and macrophages, and other immune cells contributing primarily. Many of these genes are related to mRNA processing and metabolism [117, 118] (*Ncbp2, Xrn2, Parn, Eif3e*) and are expressed across these groups with an increase in the dendritic cell and proliferating monocytes clusters.

In the middle partition we found expression primarily driven by the stromal cell groups. Using gene ontology analysis (Table 2.2) we found that many genes were associated with negative regulation of cell proliferation (*Ski, Acvr1c, Pdpn, Sox11, Inhba, Hspa1B*) and nervous system development (*Acvr1C, Tmod2, Sox11, Inhba, Sptbn1, Cdon*)[93]. The cytokines *Ccl7* and *Il33* are found within this partition and were expressed by synovial fibroblasts (*Ccl7, Il33*) as well as Vcam1^{+} and Lyve^{+} Macrophages (*Ccl7*). In the top partition we found the genes expressed most strongly within the neutrophils, monocytes, and macrophages. The *Cd11b*$^{+}$ B-cells also were represented within this partition, expressing a similar pattern to that of neutrophils. The genes within the partition don't share many pathways (Table 2.2) but represent a mix of genes from transcription factors (*Klf13, Zeb2, Arid5b*), immune related receptors (*Cd300lf, Cx3cr1, Tlr13*), mitochondrial related genes (*Foxred2, Slc25a10*) and others.

To further understand the differences and similarities between stromal and immune we have highlighted several AIR genes represented in differing populations in the knee three hours post injury. We found that *Mt1* is expressed within stromal cells as well as monocytes and macrophages within the knee, whereas *Mt2* is expressed within stromal cells and a subpopulation of macrophages (Figure 2.3C).

Metallothioneins are intracellular proteins which help maintain heavy metal ion balance in cells, protect against oxidative stresses, and are known to be induced by oxidative and inflammatory stressors[119]. We found that *Il-33*, an Il-1 family cytokine and alarmin with many pro-inflammatory and some anti-inflammatory effects[120], was expressed in synovial fibroblasts after injury. *Ptgs2* is expressed in monocytes, later neutrophils and *Cd11b*$^{+}$ B-cells, as well as basophils and Mast cells. *Ptgs2* is the gene

encoding Cyclooxygenase-2 (*Cox2*) , responsible for the production of prostaglandin E2, a potent inflammatory mediator and frequent target of inhibition in the treatment for OA pain[121].

Table 2.2: Gene Ontology of AIR Genes by scRNA-seq Clustering. Gene ontology analysis of AIR genes from one and four hours based on K-means partitioning of AIR expression my cluster from Figure 2.3.

1 Hour Top

Biological Processes

Term	P-value	Adjusted P-value	Odds Ratio	Combined Score	Genes
Regulation Of Type B Pancreatic Cell Proliferation (GO:0061469)	0.00	0.00	1480	18957	*NR4A1;NR4A3*
T-helper 17 Cell Lineage Commitment (GO:0072540)	0.00	0.00	888	10715	*SOCS3;IL6*
T-helper 17 Cell Differentiation (GO:0072539)	0.00	0.00	740	8716	*SOCS3;IL6*
T-helper Cell Lineage Commitment (GO:0002295)	0.00	0.00	555	6273	*SOCS3;IL6*
Positive Regulation Of Leukocyte Cell-Cell Adhesion (GO:1903039)	0.00	0.01	106	872	*IL6;NR4A3*
Positive Regulation Of Smooth Muscle Cell Proliferation (GO:0048661)	0.00	0.01	98	801	*IL6;NR4A3*
Regulation Of Receptor Signaling Pathway Via JAK-STAT (GO:0046425)	0.00	0.01	87	686	*SOCS3;IL6*
Regulation Of Smooth Muscle Cell Proliferation (GO:0048660)	0.00	0.01	85	669	*IL6;NR4A3*
Fat Cell Differentiation (GO:0045444)	0.00	0.01	74	559	*NR4A1;NR4A3*
Regulation Of Tyrosine Phosphorylation Of STAT Protein (GO:0042509)	0.00	0.01	70	526	*SOCS3;IL6*
Negative Regulation Of Programmed Cell Death (GO:0043069)	0.00	0.02	19	134	*SOCS3;IL6;IER3*
Cellular Response To Peptide Hormone Stimulus (GO:0071375)	0.00	0.02	51	349	*NR4A1;NR4A3*
Regulation Of Epithelial Cell Proliferation (GO:0050678)	0.00	0.02	50	339	*NR4A1;NR4A3*
Positive Regulation Of Transcription By RNA Polymerase II (GO:0045944)	0.00	0.02	12	78	*NR4A1;IL6;NR4A3;ATF3*
Negative Regulation Of Apoptotic Process (GO:0043066)	0.00	0.03	15	95	*SOCS3;IL6;IER3*
Positive Regulation Of Epithelial Cell Proliferation (GO:0050679)	0.00	0.03	36	227	*NR4A1;NR4A3*
Regulation Of Glucagon Secretion (GO:0070092)	0.00	0.03	500	2946	*IL6*
Regulation Of Interleukin-1-Mediated Signaling Pathway (GO:2000659)	0.00	0.03	500	2946	*IL6*
Response To Catecholamine (GO:0071869)	0.00	0.03	500	2946	*NR4A3*
Inflammatory Response To Wounding (GO:0090594)	0.00	0.03	500	2946	*IL6*
Response To Peptidoglycan (GO:0032494)	0.00	0.03	500	2946	*IL6*
Regulation Of Apoptotic DNA Fragmentation (GO:1902510)	0.00	0.03	500	2946	*IL6*
Leukocyte Apoptotic Process (GO:0071887)	0.00	0.03	500	2946	*IL6*
Defense Response To Symbiont (GO:0140546)	0.00	0.03	30	177	*IL6;DDIT4*

Positive Regulation Of Gliogenesis (GO:0014015)	0.00	0.03	400	2284	*IL6*
Positive Regulation Of Mast Cell Activation (GO:0033005)	0.00	0.03	400	2284	*NR4A3*
Negative Regulation Of miRNA Processing (GO:1903799)	0.00	0.03	400	2284	*IL6*
Cellular Response To Monoamine Stimulus (GO:0071868)	0.00	0.03	400	2284	*NR4A3*
Neurotrophin TRK Receptor Signaling Pathway (GO:0048011)	0.00	0.03	400	2284	*DDIT4*
Positive Regulation Of DNA-templated Transcription (GO:0045893)	0.00	0.03	9	49	*NR4A1;IL6;NR4A3;ATF3*
Cellular Response To Leptin Stimulus (GO:0044320)	0.00	0.03	333	1852	*NR4A3*
Positive Regulation Of T-helper 2 Cell Cytokine Production (GO:2000553)	0.00	0.03	333	1852	*IL6*
Myeloid Leukocyte Mediated Immunity (GO:0002444)	0.00	0.03	333	1852	*IL6*
Positive Regulation Of Vascular Associated Smooth Muscle Cell Migration (GO:1904754)	0.00	0.03	333	1852	*NR4A3*
Positive Regulation Of Extracellular Matrix Disassembly (GO:0090091)	0.00	0.03	333	1852	*IL6*
Regulation Of Glial Cell Proliferation (GO:0060251)	0.00	0.03	285	1549	*IL6*
Response To Leptin (GO:0044321)	0.00	0.03	285	1549	*NR4A3*
Endothelial Cell Chemotaxis (GO:0035767)	0.00	0.03	285	1549	*NR4A1*
Defense Response To Virus (GO:0051607)	0.00	0.03	24	127	*IL6;DDIT4*
Negative Regulation Of Lipid Localization (GO:1905953)	0.00	0.03	250	1326	*IL6*
Negative Regulation Of Tyrosine Phosphorylation Of STAT Protein (GO:0042532)	0.00	0.03	250	1326	*SOCS3*
Negative Regulation Of Bone Resorption (GO:0045779)	0.00	0.03	250	1326	*IL6*
Mast Cell Activation Involved In Immune Response (GO:0002279)	0.01	0.03	222	1156	*NR4A3*
Mast Cell Degranulation (GO:0043303)	0.01	0.03	222	1156	*NR4A3*
Response To Corticosteroid (GO:0031960)	0.01	0.03	222	1156	*IL6*
Regulation Of T-helper 2 Cell Cytokine Production (GO:2000551)	0.01	0.03	222	1156	*IL6*
Regulation Of Apoptotic Process (GO:0042981)	0.01	0.03	10	53	*SOCS3;IL6;IER3*
Mast Cell Mediated Immunity (GO:0002448)	0.01	0.03	200	1021	*NR4A3*
Positive Regulation Of Platelet Aggregation (GO:1901731)	0.01	0.03	200	1021	*IL6*
Positive Regulation Of Behavior (GO:0048520)	0.01	0.03	200	1021	*NR4A3*
Regulation Of Astrocyte Differentiation (GO:0048710)	0.01	0.03	200	1021	*IL6*
Negative Regulation Of Bone Remodeling (GO:0046851)	0.01	0.03	200	1021	*IL6*
Regulation Of Cell Activation (GO:0050865)	0.01	0.03	200	1021	*IL6*
Positive Regulation Of Neuroinflammatory Response (GO:0150078)	0.01	0.03	182	912	*IL6*
Regulation Of Vascular Associated Smooth Muscle Cell Migration (GO:1904752)	0.01	0.03	182	912	*NR4A3*
Regulation Of Leukocyte Adhesion To Vascular Endothelial Cell (GO:1904994)	0.01	0.03	182	912	*IL6*
Neutrophil Mediated Immunity (GO:0002446)	0.01	0.03	182	912	*IL6*
Positive Regulation Of Fatty Acid Oxidation (GO:0046321)	0.01	0.03	182	912	*NR4A3*
Apoptotic Process (GO:0006915)	0.01	0.03	19	97	*DDIT4;IER3*
Mature B Cell Differentiation Involved In Immune Response (GO:0002313)	0.01	0.03	166	823	*IL6*

Acute-Phase Response (GO:0006953)	0.01	0.03	166	823	*IL6*
Interleukin-6-Mediated Signaling Pathway (GO:0070102)	0.01	0.03	166	823	*IL6*
Positive Regulation Of Type 2 Immune Response (GO:0002830)	0.01	0.03	166	823	*IL6*
Regulation Of Extracellular Matrix Disassembly (GO:0010715)	0.01	0.03	154	748	*IL6*
Regulation Of Feeding Behavior (GO:0060259)	0.01	0.03	154	748	*NR4A3*
Negative Regulation Of Receptor Signaling Pathway Via STAT (GO:1904893)	0.01	0.03	154	748	*SOCS3*
Positive Regulation Of Acute Inflammatory Response (GO:0002675)	0.01	0.03	154	748	*IL6*
Regulation Of Microglial Cell Activation (GO:1903978)	0.01	0.03	154	748	*IL6*
Platelet-Derived Growth Factor Receptor Signaling Pathway (GO:0048008)	0.01	0.03	143	685	*NR4A3*
Positive Regulation Of Transmembrane Transport (GO:0034764)	0.01	0.03	143	685	*NR4A3*
Neurotrophin Signaling Pathway (GO:0038179)	0.01	0.03	143	685	*DDIT4*
Positive Regulation Of Homotypic Cell-Cell Adhesion (GO:0034112)	0.01	0.03	133	631	*IL6*
Regulation Of Fatty Acid Oxidation (GO:0046320)	0.01	0.03	133	631	*NR4A3*
Positive Regulation Of Muscle Hypertrophy (GO:0014742)	0.01	0.03	133	631	*NR4A3*
Positive Regulation Of Myeloid Leukocyte Cytokine Production Involved In Immune Response (GO:0061081)	0.01	0.03	133	631	*NR4A3*
Negative Regulation Of Receptor Signaling Pathway Via JAK-STAT (GO:0046426)	0.01	0.03	133	631	*SOCS3*
Positive Regulation Of Smooth Muscle Cell Migration (GO:0014911)	0.01	0.03	133	631	*NR4A3*
Negative Regulation Of Biosynthetic Process (GO:0009890)	0.01	0.03	133	631	*IL6*
Negative Regulation Of Chemokine Production (GO:0032682)	0.01	0.03	133	631	*IL6*
Regulation Of Receptor Signaling Pathway Via STAT (GO:1904892)	0.01	0.03	125	584	*IL6*
Cell Migration Involved In Sprouting Angiogenesis (GO:0002042)	0.01	0.03	125	584	*NR4A1*
Positive Regulation Of Leukocyte Adhesion To Vascular Endothelial Cell (GO:1904996)	0.01	0.03	125	584	*IL6*
Regulation Of Glucose Transmembrane Transport (GO:0010827)	0.01	0.03	125	584	*NR4A3*
Regulation Of Leukocyte Chemotaxis (GO:0002688)	0.01	0.03	125	584	*IL6*
Positive Regulation Of Cardiac Muscle Hypertrophy (GO:0010613)	0.01	0.03	125	584	*NR4A3*
Positive Regulation Of Fatty Acid Metabolic Process (GO:0045923)	0.01	0.03	125	584	*NR4A3*
Regulation Of Collagen Biosynthetic Process (GO:0032965)	0.01	0.03	117	543	*IL6*
Negative Regulation Of Lipid Storage (GO:0010888)	0.01	0.03	117	543	*IL6*
Negative Regulation Of Nervous System Development (GO:0051961)	0.01	0.03	117	543	*IL6*
T-helper Cell Differentiation (GO:0042093)	0.01	0.03	117	543	*IL6*
Positive Regulation Of Cytokine Production Involved In Inflammatory Response (GO:1900017)	0.01	0.03	117	543	*IL6*
Positive Regulation Of Extracellular Matrix Organization (GO:1903055)	0.01	0.03	117	543	*IL6*
Transmembrane Receptor Protein Tyrosine Kinase Signaling Pathway (GO:0007169)	0.01	0.03	16	71	*NR4A3;DDIT4*

Cellular Response To Catecholamine Stimulus (GO:0071870)	0.01	0.03	111	507	*NR4A3*
Gastrulation (GO:0007369)	0.01	0.03	111	507	*NR4A3*
Regulation Of Acute Inflammatory Response (GO:0002673)	0.01	0.03	111	507	*IL6*
Intrinsic Apoptotic Signaling Pathway In Response To DNA Damage By P53 Class Mediator (GO:0042771)	0.01	0.03	111	507	*DDIT4*
Regulation Of Neuroinflammatory Response (GO:0150077)	0.01	0.03	111	507	*IL6*
Response To Fibroblast Growth Factor (GO:0071774)	0.01	0.03	105	475	*NR4A1*
Positive Regulation Of Vascular Associated Smooth Muscle Cell Proliferation (GO:1904707)	0.01	0.03	105	475	*NR4A3*
Positive Regulation Of T Cell Cytokine Production (GO:0002726)	0.01	0.03	100	446	*IL6*
Regulation Of Lipid Storage (GO:0010883)	0.01	0.03	100	446	*IL6*
Fc Receptor Mediated Stimulatory Signaling Pathway (GO:0002431)	0.01	0.03	95	420	*NR4A3*
Fc-epsilon Receptor Signaling Pathway (GO:0038095)	0.01	0.03	95	420	*NR4A3*
Negative Regulation Of Cell Development (GO:0010721)	0.01	0.03	95	420	*IL6*
Blood Vessel Endothelial Cell Migration (GO:0043534)	0.01	0.03	95	420	*NR4A1*
Cellular Response To Interleukin-6 (GO:0071354)	0.01	0.03	91	397	*IL6*
Regulation Of Cardiac Muscle Hypertrophy (GO:0010611)	0.01	0.03	91	397	*NR4A3*
Positive Regulation Of Epithelial Cell Apoptotic Process (GO:1904037)	0.01	0.03	91	397	*IL6*
Positive Regulation Of Interleukin-17 Production (GO:0032740)	0.01	0.03	87	376	*IL6*
Positive Regulation Of Vascular Endothelial Growth Factor Production (GO:0010575)	0.01	0.03	87	376	*IL6*
Peptide Hormone Secretion (GO:0030072)	0.01	0.03	83	357	*IL6*
Regulation Of B Cell Activation (GO:0050864)	0.01	0.03	83	357	*IL6*
Regulation Of Platelet Aggregation (GO:0090330)	0.01	0.03	83	357	*IL6*
Regulation Of Vascular Endothelial Growth Factor Production (GO:0010574)	0.01	0.03	80	340	*IL6*
Acute Inflammatory Response (GO:0002526)	0.01	0.03	80	340	*IL6*
Response To Glucocorticoid (GO:0051384)	0.01	0.03	80	340	*IL6*
Negative Regulation Of Neurogenesis (GO:0050768)	0.01	0.03	77	324	*IL6*
Regulation Of Immunoglobulin Production (GO:0002637)	0.01	0.03	77	324	*IL6*
Positive Regulation Of Cytosolic Calcium Ion Concentration Involved In Phospholipase C-activating G Protein-Coupled Signaling Pathway (GO:0051482)	0.01	0.03	77	324	*P2RY10*
Regulation Of Bone Resorption (GO:0045124)	0.02	0.03	74	309	*IL6*
Maintenance Of Blood-Brain Barrier (GO:0035633)	0.02	0.03	71	296	*IL6*
Regulation Of DNA-templated Transcription (GO:0006355)	0.02	0.03	5	22	*NR4A1;IL6;NR4A3;ATF3*
Positive Regulation Of Interleukin-10 Production (GO:0032733)	0.02	0.03	69	283	*IL6*
Negative Regulation Of Peptidyl-Tyrosine Phosphorylation (GO:0050732)	0.02	0.03	69	283	*SOCS3*
Regulation Of Vasculature Development (GO:1901342)	0.02	0.03	69	283	*IL6*

Positive Regulation Of Glucose Transmembrane Transport (GO:0010828)	0.02	0.03	67	271	*NR4A3*
Positive Regulation Of Leukocyte Migration (GO:0002687)	0.02	0.03	67	271	*IL6*
Positive Regulation Of Rho Protein Signal Transduction (GO:0035025)	0.02	0.03	67	271	*P2RY10*
Regulation Of Macrophage Activation (GO:0043030)	0.02	0.03	67	271	*IL6*
Negative Regulation Of Fat Cell Differentiation (GO:0045599)	0.02	0.04	64	261	*IL6*
Positive Regulation Of Immunoglobulin Production (GO:0002639)	0.02	0.04	60	241	*IL6*
Cellular Response To Hydrogen Peroxide (GO:0070301)	0.02	0.04	60	241	*IL6*
Cellular Response To Vascular Endothelial Growth Factor Stimulus (GO:0035924)	0.02	0.04	60	241	*NR4A1*
Regulation Of Interleukin-17 Production (GO:0032660)	0.02	0.04	60	241	*IL6*
Intrinsic Apoptotic Signaling Pathway By P53 Class Mediator (GO:0072332)	0.02	0.04	59	232	*DDIT4*
Liver Development (GO:0001889)	0.02	0.04	59	232	*IL6*
Regulation Of Transcription By RNA Polymerase II (GO:0006357)	0.02	0.04	5	20	*NR4A1;IL6;NR4A3;ATF3*
Cellular Response To Oxygen-Containing Compound (GO:1901701)	0.02	0.04	11	42	*IL6;NR4A3*
Regulation Of Vascular Associated Smooth Muscle Cell Proliferation (GO:1904705)	0.02	0.04	55	216	*NR4A3*
Positive Regulation Of Receptor Signaling Pathway Via JAK-STAT (GO:0046427)	0.02	0.04	55	216	*IL6*
Positive Regulation Of Receptor Signaling Pathway Via STAT (GO:1904894)	0.02	0.04	55	216	*IL6*
Positive Regulation Of Production Of Molecular Mediator Of Immune Response (GO:0002702)	0.02	0.04	54	209	*IL6*
Endothelial Cell Migration (GO:0043542)	0.02	0.04	51	196	*NR4A1*
Regulation Of Chemokine Production (GO:0032642)	0.02	0.04	50	190	*IL6*
Lysosome Localization (GO:0032418)	0.02	0.04	49	184	*NR4A3*
Monocyte Chemotaxis (GO:0002548)	0.02	0.04	49	184	*IL6*
Energy Derivation By Oxidation Of Organic Compounds (GO:0015980)	0.02	0.04	47	178	*NR4A3*
Phosphatidylinositol Phosphate Biosynthetic Process (GO:0046854)	0.02	0.04	46	173	*SOCS3*
Positive Regulation Of Osteoblast Differentiation (GO:0045669)	0.02	0.04	46	173	*IL6*
Positive Regulation Of Chemotaxis (GO:0050921)	0.02	0.04	46	173	*IL6*
Regulation Of Cytokine Production Involved In Inflammatory Response (GO:1900015)	0.03	0.04	44	163	*IL6*
Regulation Of Interleukin-10 Production (GO:0032653)	0.03	0.04	44	163	*IL6*
Response To Hydrogen Peroxide (GO:0042542)	0.03	0.04	44	163	*IL6*
Positive Regulation Of Lymphocyte Activation (GO:0051251)	0.03	0.04	43	159	*IL6*
Response To Organonitrogen Compound (GO:0010243)	0.03	0.04	43	159	*IL6*
Positive Regulation Of Epithelial To Mesenchymal Transition (GO:0010718)	0.03	0.04	43	159	*IL6*
Intrinsic Apoptotic Signaling Pathway In Response To DNA Damage (GO:0008630)	0.03	0.04	42	151	*DDIT4*
Cell Chemotaxis (GO:0060326)	0.03	0.05	41	147	*NR4A1*
Pyruvate Metabolic Process (GO:0006090)	0.03	0.05	41	147	*NR4A3*
Positive Regulation Of Ras Protein Signal Transduction (GO:0046579)	0.03	0.05	40	143	*P2RY10*

Positive Regulation Of Cell Population Proliferation (GO:0008284)	0.03	0.05	9	32	*IL6;NR4A3*
Sprouting Angiogenesis (GO:0002040)	0.03	0.05	39	139	*NR4A1*
Positive Regulation Of B Cell Activation (GO:0050871)	0.03	0.05	39	139	*IL6*
Regulation Of Peptide Hormone Secretion (GO:0090276)	0.03	0.05	39	139	*IL6*
Positive Regulation Of Chemokine Production (GO:0032722)	0.03	0.05	38	136	*IL6*
Positive Regulation Of Leukocyte Chemotaxis (GO:0002690)	0.03	0.05	38	133	*IL6*
Negative Regulation Of TOR Signaling (GO:0032007)	0.03	0.05	38	133	*DDIT4*
Cellular Response To Fibroblast Growth Factor Stimulus (GO:0044344)	0.03	0.05	37	130	*NR4A1*
Neuron Migration (GO:0001764)	0.03	0.05	37	130	*DDIT4*
Positive Regulation Of Tyrosine Phosphorylation Of STAT Protein (GO:0042531)	0.03	0.05	37	130	*IL6*
Positive Regulation Of Interleukin-1 Beta Production (GO:0032731)	0.03	0.05	36	124	*IL6*
Negative Regulation Of Cytokine-Mediated Signaling Pathway (GO:0001960)	0.03	0.05	34	118	*IL6*

Molecular Functions

Term	P-value	Adjusted P-value	Odds Ratio	Combined Score	Genes
Nuclear Glucocorticoid Receptor Binding (GO:0035259)	0.00	0.00	740	8716	*NR4A1;NR4A3*
DNA-binding Transcription Activator Activity, RNA Polymerase II-specific (GO:0001228)	0.00	0.01	21	153	*NR4A1;NR4A3;ATF3*
Nuclear Receptor Binding (GO:0016922)	0.00	0.02	39	248	*NR4A1;NR4A3*
Protein Tyrosine Kinase Inhibitor Activity (GO:0030292)	0.00	0.02	400	2284	*SOCS3*
Interleukin-6 Receptor Binding (GO:0005138)	0.00	0.02	400	2284	*IL6*
Protein Heterodimerization Activity (GO:0046982)	0.00	0.02	23	126	*NR4A1;ATF3*
cAMP Response Element Binding (GO:0035497)	0.00	0.02	250	1326	*NR4A3*
1-Phosphatidylinositol-3-Kinase Regulator Activity (GO:0046935)	0.01	0.03	154	748	*SOCS3*
Phosphatidylinositol 3-Kinase Regulator Activity (GO:0035014)	0.01	0.03	125	584	*SOCS3*

1 Hour Middle

Biological Process

Term	P-value	Adjusted P-value	Odds Ratio	Combined Score	Genes
Negative Regulation Of Hemostasis (GO:1900047)	0.00	0.01	208	1982	*THBD;SERPINE1*
Negative Regulation Of Fibrinolysis (GO:0051918)	0.00	0.01	185	1725	*THBD;SERPINE1*
Negative Regulation Of Coagulation (GO:0050819)	0.00	0.01	166	1522	*THBD;SERPINE1*
Regulation Of Angiogenesis (GO:0045765)	0.00	0.01	18	159	*ADAMTS1;SERPINE1;ANGPTL4;KLF4*
Hyaluronan Metabolic Process (GO:0030212)	0.00	0.01	139	1224	*TNFAIP6;HAS1*
Nucleotide-Sugar Biosynthetic Process (GO:0009226)	0.00	0.01	128	1111	*UGDH;GFPT2*

Regulation Of Fibrinolysis (GO:0051917)	0.00	0.01	119	1016	*THBD;SERPINE1*
Positive Regulation Of Blood Coagulation (GO:0030194)	0.00	0.01	88	700	*THBD;SERPINE1*
Aminoglycan Biosynthetic Process (GO:0006023)	0.00	0.01	88	700	*UGDH;HAS1*
Positive Regulation Of Angiogenesis (GO:0045766)	0.00	0.02	22	170	*SERPINE1;ANGPTL4;KLF4*
Regulation Of Epidermal Growth Factor-Activated Receptor Activity (GO:0007176)	0.00	0.02	69	524	*ERRFI1;HBEGF*
Glycosaminoglycan Metabolic Process (GO:0030203)	0.00	0.02	64	474	*UGDH;HAS1*
Negative Regulation Of Wound Healing (GO:0061045)	0.00	0.02	64	474	*THBD;SERPINE1*
Regulation Of Blood Coagulation (GO:0030193)	0.00	0.02	62	452	*THBD;SERPINE1*
Negative Regulation Of Blood Coagulation (GO:0030195)	0.00	0.02	59	432	*THBD;SERPINE1*
Negative Regulation Of Response To External Stimulus (GO:0032102)	0.00	0.02	18	127	*TNFAIP6;SERPINE1;KLF4*
Cellular Response To Growth Factor Stimulus (GO:0071363)	0.00	0.02	17	117	*EGR3;HAS1;KLF4*
Positive Regulation Of Wound Healing (GO:0090303)	0.00	0.02	44	293	*SERPINE1;HBEGF*
Positive Regulation Of miRNA Transcription (GO:1902895)	0.00	0.03	41	266	*EGR1;KLF4*
Regulation Of Wound Healing (GO:0061041)	0.00	0.03	37	235	*SERPINE1;HBEGF*
Positive Regulation Of miRNA Metabolic Process (GO:2000630)	0.00	0.03	35	223	*EGR1;KLF4*
Regulation Of Apoptotic Process (GO:0042981)	0.00	0.03	7	41	*EGR1;EGR3;PIM3;ANGPTL4;SGK1*
Cell Chemotaxis (GO:0060326)	0.00	0.03	35	216	*EGR3;HBEGF*
Negative Regulation Of Response To Stimulus (GO:0048585)	0.00	0.03	33	205	*PIM3;KLF4*
Glycosaminoglycan Biosynthetic Process (GO:0006024)	0.00	0.03	30	177	*UGDH;HAS1*
Muscle Organ Development (GO:0007517)	0.00	0.03	30	177	*EGR3;HBEGF*
Regulation Of miRNA Transcription (GO:1902893)	0.00	0.03	29	173	*EGR1;KLF4*
Fat Cell Differentiation (GO:0045444)	0.00	0.04	28	161	*EGR2;KLF4*
Negative Regulation Of Apoptotic Process (GO:0043066)	0.00	0.04	7	42	*EGR3;PIM3;ANGPTL4;KLF4*
Regulation Of Inflammatory Response (GO:0050727)	0.00	0.04	11	61	*TNFAIP6;SERPINE1;KLF4*

Molecular Function

Term	P-value	Adjusted P-value	Odds Ratio	Combined Score	Genes
Double-Stranded DNA Binding (GO:0003690)	0.00	0.02	7	47	*EGR1;EGR2;EGR3;FOSB;KLF4*
Promoter-Specific Chromatin Binding (GO:1990841)	0.00	0.02	42	274	*EGR1;KLF4*
Sequence-Specific Double-Stranded DNA Binding (GO:1990837)	0.00	0.02	6	40	*EGR1;EGR2;EGR3;FOSB;KLF4*
Sequence-Specific DNA Binding (GO:0043565)	0.00	0.02	6	40	*EGR1;EGR2;EGR3;FOSB;KLF4*
Cis-Regulatory Region Sequence-Specific DNA Binding (GO:0000987)	0.00	0.02	5	31	*EGR1;EGR2;EGR3;KLF9;FOSB;KLF4*
RNA Polymerase II Cis-Regulatory Region Sequence-Specific DNA Binding (GO:0000978)	0.00	0.02	5	30	*EGR1;EGR2;EGR3;KLF9;FOSB;KLF4*
Transcription Regulatory Region Nucleic Acid Binding (GO:0001067)	0.00	0.02	12	68	*EGR1;EGR2;KLF4*
RNA Polymerase II Transcription Regulatory Region Sequence-Specific DNA Binding (GO:0000977)	0.00	0.03	5	25	*EGR1;EGR2;EGR3;KLF9;FOSB;KLF4*

Growth Factor Activity (GO:0008083)	0.01	0.03	20	104	*CXCL1;HBEGF*
Double-Stranded Methylated DNA Binding (GO:0010385)	0.01	0.03	200	1006	*EGR1*
DNA-binding Transcription Activator Activity, RNA Polymerase II-specific (GO:0001228)	0.01	0.05	7	34	*EGR1;EGR2;KLF4*

1 Hour Bottom

Biological Process

Term	P-value	Adjusted P-value	Odds Ratio	Combined Score	Genes
Integrated Stress Response Signaling (GO:0140467)	0.00	0.00	177	2374	*CEBPB;FOS;JUNB*
Regulation Of p38MAPK Cascade (GO:1900744)	0.00	0.00	135	1713	*PER1;DUSP1;IL1B*
Positive Regulation Of Unsaturated Fatty Acid Biosynthetic Process (GO:2001280)	0.00	0.00	714	8292	*IL1B;PTGS2*
Regulation Of Prostaglandin Biosynthetic Process (GO:0031392)	0.00	0.00	714	8292	*IL1B;PTGS2*
Response To Molecule Of Bacterial Origin (GO:0002237)	0.00	0.00	70	749	*IL1B;TRIB1;CXCL2*
Inflammatory Response (GO:0006954)	0.00	0.00	28	295	*CEBPB;IL1B;FOS;CXCL2*
Regulation Of Inflammatory Response (GO:0050727)	0.00	0.00	28	288	*NFKBIA;IL1B;ACOD1;PTGS2*
Positive Regulation Of Acute Inflammatory Response (GO:0002675)	0.00	0.00	238	2335	*IL1B;PTGS2*
Regulation Of MAP Kinase Activity (GO:0043405)	0.00	0.00	41	382	*DUSP1;IL1B;TRIB1*
Regulation Of Neuroinflammatory Response (GO:0150077)	0.00	0.00	168	1542	*IL1B;PTGS2*
Positive Regulation Of Defense Response (GO:0031349)	0.00	0.00	38	341	*NFKBIA;IL1B;ACOD1*
Entrainment Of Circadian Clock By Photoperiod (GO:0043153)	0.00	0.00	136	1195	*PER1;SIK1*
Positive Regulation Of Vascular Endothelial Growth Factor Production (GO:0010575)	0.00	0.00	130	1130	*IL1B;PTGS2*
Photoperiodism (GO:0009648)	0.00	0.00	130	1130	*PER1;SIK1*
Regulation Of Vascular Endothelial Growth Factor Production (GO:0010574)	0.00	0.00	119	1016	*IL1B;PTGS2*
Positive Regulation Of Nitric Oxide Biosynthetic Process (GO:0045429)	0.00	0.00	114	967	*IL1B;PTGS2*
Negative Regulation Of DNA-binding Transcription Factor Activity (GO:0043433)	0.00	0.00	31	265	*NFKBIA;SIK1;TRIB1*
Positive Regulation Of Nitric Oxide Metabolic Process (GO:1904407)	0.00	0.00	110	922	*IL1B;PTGS2*
Positive Regulation Of Response To External Stimulus (GO:0032103)	0.00	0.00	30	251	*NFKBIA;IL1B;ACOD1*
Cellular Response To Oxygen-Containing Compound (GO:1901701)	0.00	0.00	16	135	*IL1B;ACOD1;FOS;CXCL2*
Response To Lipopolysaccharide (GO:0032496)	0.00	0.00	29	243	*IL1B;TRIB1;CXCL2*
Positive Regulation Of DNA-templated Transcription (GO:0045893)	0.00	0.00	9	75	*NFKBIA;PER1;CEBPB;IL1B;FOS;JUNB*
Regulation Of Metal Ion Transport (GO:0010959)	0.00	0.01	89	714	*PER1;SIK1*
Regulation Of Sodium Ion Transport (GO:0002028)	0.00	0.01	86	687	*PER1;SIK1*
Negative Regulation Of Stress-Activated MAPK Cascade (GO:0032873)	0.00	0.01	81	638	*PER1;DUSP1*
Regulation Of Nitric Oxide Biosynthetic Process (GO:0045428)	0.00	0.01	77	596	*IL1B;PTGS2*
Positive Regulation Of Transcription By RNA Polymerase II (GO:0045944)	0.00	0.01	9	68	*NFKBIA;PER1;CEBPB;FOS;JUNB*

Positive Regulation Of Fat Cell Differentiation (GO:0045600)	0.00	0.01	59	429	*CEBPB;PTGS2*
Cellular Response To Lipid (GO:0071396)	0.00	0.01	20	146	*IL1B;ACOD1;CXCL2*
Negative Regulation Of MAP Kinase Activity (GO:0043407)	0.00	0.01	58	418	*DUSP1;IL1B*
Regulation Of Mitotic Nuclear Division (GO:0007088)	0.00	0.01	53	370	*DUSP1;IL1B*
Positive Regulation Of Cellular Metabolic Process (GO:0031325)	0.00	0.01	53	370	*ARG2;ACOD1*
Cellular Response To Chemokine (GO:1990869)	0.00	0.01	50	345	*DUSP1;CXCL2*
Cytokine-Mediated Signaling Pathway (GO:0019221)	0.00	0.01	18	123	*NFKBIA;IL1B;CXCL2*
Neutrophil Chemotaxis (GO:0030593)	0.00	0.02	42	275	*CXCL2;TREM1*
Granulocyte Chemotaxis (GO:0071621)	0.00	0.02	40	260	*CXCL2;TREM1*
Neutrophil Migration (GO:1990266)	0.00	0.02	38	242	*CXCL2;TREM1*
Regulation Of T Cell Proliferation (GO:0042129)	0.00	0.02	38	242	*CEBPB;IL1B*
Cellular Response To Cytokine Stimulus (GO:0071345)	0.00	0.02	15	95	*NFKBIA;DUSP1;IL1B*
Negative Regulation Of Protein Serine/Threonine Kinase Activity (GO:0071901)	0.00	0.02	36	230	*DUSP1;IL1B*
Positive Regulation Of Cytokine Production (GO:0001819)	0.00	0.02	14	89	*CEBPB;IL1B;PTGS2*
Regulation Of NIK/NF-kappaB Signaling (GO:1901222)	0.00	0.02	35	219	*NFKBIA;IL1B*
Positive Regulation Of Inflammatory Response (GO:0050729)	0.00	0.03	28	161	*NFKBIA;IL1B*
Negative Regulation Of MAPK Cascade (GO:0043409)	0.00	0.03	28	159	*DUSP1;IL1B*
Regulation Of JNK Cascade (GO:0046328)	0.00	0.03	26	149	*PER1;IL1B*
Response To Lipid (GO:0033993)	0.00	0.03	26	149	*IL1B;TRIB1*
Cellular Response To Molecule Of Bacterial Origin (GO:0071219)	0.00	0.03	25	137	*IL1B;CXCL2*
Negative Regulation Of Glucocorticoid Receptor Signaling Pathway (GO:2000323)	0.00	0.03	333	1839	*PER1*
Negative Regulation Of Meiotic Cell Cycle (GO:0051447)	0.00	0.03	333	1839	*DUSP1*
Negative Regulation Of Monocyte Chemotaxis (GO:0090027)	0.00	0.03	333	1839	*DUSP1*
Regulation Of Immature T Cell Proliferation In Thymus (GO:0033084)	0.00	0.03	333	1839	*IL1B*
Regulation Of Mitotic Spindle Checkpoint (GO:1903504)	0.00	0.03	333	1839	*DUSP1*
Cellular Response To Cold (GO:0070417)	0.00	0.03	333	1839	*NFKBIA*
Positive Regulation Of T-helper 1 Cell Cytokine Production (GO:2000556)	0.00	0.03	333	1839	*IL1B*
Regulation Of T-helper 1 Cell Cytokine Production (GO:2000554)	0.00	0.03	333	1839	*IL1B*
Regulation Of Calcidiol 1-Monooxygenase Activity (GO:0060558)	0.00	0.03	333	1839	*IL1B*
Positive Regulation Of Fever Generation (GO:0031622)	0.00	0.03	333	1839	*PTGS2*
Cellular Response To Lipopolysaccharide (GO:0071222)	0.00	0.03	23	127	*IL1B;CXCL2*
Positive Regulation Of Humoral Immune Response (GO:0002922)	0.00	0.03	266	1423	*IL1B*
Positive Regulation Of Icosanoid Secretion (GO:0032305)	0.00	0.03	266	1423	*IL1B*
Regulation Of Glucocorticoid Receptor Signaling Pathway (GO:2000322)	0.00	0.03	266	1423	*PER1*
Negative Regulation Of p38MAPK Cascade (GO:1903753)	0.00	0.03	266	1423	*DUSP1*

Hyaluronan Biosynthetic Process (GO:0030213)	0.00	0.03	266	1423	*IL1B*
Regulation Of Striated Muscle Cell Differentiation (GO:0051153)	0.00	0.03	266	1423	*SIK1*
Regulation Of T-helper Cell Differentiation (GO:0045622)	0.00	0.03	266	1423	*JUNB*
Regulation Of Adiponectin Secretion (GO:0070163)	0.00	0.03	266	1423	*IL1B*
Regulation Of Cell Adhesion Molecule Production (GO:0060353)	0.00	0.03	266	1423	*IL1B*
Regulation Of Myeloid Leukocyte Differentiation (GO:0002761)	0.01	0.03	222	1151	*CEBPB*
Arginine Catabolic Process (GO:0006527)	0.01	0.03	222	1151	*ARG2*
Leukocyte Aggregation (GO:0070486)	0.01	0.03	222	1151	*IL1B*
Cytoplasmic Sequestering Of NF-kappaB (GO:0007253)	0.01	0.03	222	1151	*NFKBIA*
Regulation Of Endothelial Cell Development (GO:1901550)	0.01	0.03	190	962	*IL1B*
Regulation Of Gap Junction Assembly (GO:1903596)	0.01	0.03	190	962	*IL1B*
Regulation Of Glial Cell Proliferation (GO:0060251)	0.01	0.03	190	962	*IL1B*
Positive Regulation Of Monocyte Chemotactic Protein-1 Production (GO:0071639)	0.01	0.03	190	962	*IL1B*
Negative Regulation Of Triglyceride Metabolic Process (GO:0090209)	0.01	0.03	190	962	*SIK1*
Regulation Of Mitotic Sister Chromatid Segregation (GO:0033047)	0.01	0.03	190	962	*DUSP1*
Regulation Of RNA Biosynthetic Process (GO:2001141)	0.01	0.03	190	962	*IL1B*
Cyclooxygenase Pathway (GO:0019371)	0.01	0.03	190	962	*PTGS2*
Regulation Of Complement Activation (GO:0030449)	0.01	0.03	166	822	*IL1B*
Negative Regulation Of Hormone Secretion (GO:0046888)	0.01	0.03	166	822	*IL1B*
Negative Regulation Of Lipid Localization (GO:1905953)	0.01	0.03	166	822	*NFKBIA*
Regulation Of Hair Cycle (GO:0042634)	0.01	0.03	166	822	*PER1*
Positive Regulation Of Vascular Endothelial Growth Factor Receptor Signaling Pathway (GO:0030949)	0.01	0.03	166	822	*IL1B*
Ornithine Metabolic Process (GO:0006591)	0.01	0.03	166	822	*ARG2*
Positive Regulation Of RNA Biosynthetic Process (GO:1902680)	0.01	0.03	166	822	*IL1B*
Negative Regulation Of Lipopolysaccharide-Mediated Signaling Pathway (GO:0031665)	0.01	0.03	148	715	*TRIB1*
Negative Regulation Of Transmembrane Transport (GO:0034763)	0.01	0.03	148	715	*IL1B*
Regulation Of Mitotic Sister Chromatid Separation (GO:0010965)	0.01	0.03	148	715	*DUSP1*
Positive Regulation Of Transcription From RNA Polymerase II Promoter In Response To Endoplasmic Reticulum Stress (GO:1990440)	0.01	0.03	148	715	*CEBPB*
Positive Regulation Of Transforming Growth Factor Beta Production (GO:0071636)	0.01	0.03	148	715	*PTGS2*
Positive Regulation Of Cellular Senescence (GO:2000774)	0.01	0.03	148	715	*ARG2*
Positive Regulation Of Cellular Biosynthetic Process (GO:0031328)	0.01	0.04	16	79	*IL1B;PTGS2*
Negative Regulation Of Glucose Transmembrane Transport (GO:0010829)	0.01	0.04	133	631	*IL1B*
Negative Regulation Of Leukocyte Chemotaxis (GO:0002689)	0.01	0.04	133	631	*DUSP1*
Regulation Of Monocyte Chemotactic Protein-1	0.01	0.04	133	631	*IL1B*

Production (GO:0071637)					
Regulation Of T Cell Mediated Immunity (GO:0002709)	0.01	0.04	133	631	*IL1B*
Regulation Of T-helper 17 Cell Differentiation (GO:2000319)	0.01	0.04	133	631	*JUNB*
Positive Regulation Of Nucleic Acid-Templated Transcription (GO:1903508)	0.01	0.04	8	38	*CEBPB;IL1B;FOS*
Negative Regulation Of Macrophage Derived Foam Cell Differentiation (GO:0010745)	0.01	0.04	121	563	*NFKBIA*
Negative Regulation Of Mononuclear Cell Migration (GO:0071676)	0.01	0.04	121	563	*DUSP1*
Positive Regulation Of Neuroinflammatory Response (GO:0150078)	0.01	0.04	121	563	*IL1B*
Positive Regulation Of Protein Export From Nucleus (GO:0046827)	0.01	0.04	121	563	*IL1B*
Regulation Of Monooxygenase Activity (GO:0032768)	0.01	0.04	121	563	*IL1B*
Positive Regulation Of T-helper 1 Type Immune Response (GO:0002827)	0.01	0.04	121	563	*IL1B*
Regulation Of Cell Differentiation (GO:0045595)	0.01	0.04	15	68	*CEBPB;SIK1*
Positive Regulation Of Granulocyte Macrophage Colony-Stimulating Factor Production (GO:0032725)	0.01	0.04	111	507	*IL1B*
Acute-Phase Response (GO:0006953)	0.01	0.04	111	507	*CEBPB*
Cardiocyte Differentiation (GO:0035051)	0.01	0.04	111	507	*SIK1*
Response To Chemokine (GO:1990868)	0.01	0.04	111	507	*DUSP1*
Positive Regulation Of Brown Fat Cell Differentiation (GO:0090336)	0.01	0.04	111	507	*PTGS2*
Cytoplasmic Sequestering Of Protein (GO:0051220)	0.01	0.04	111	507	*NFKBIA*
Cytoplasmic Sequestering Of Transcription Factor (GO:0042994)	0.01	0.04	111	507	*NFKBIA*
Regulation Of T-helper 17 Type Immune Response (GO:2000316)	0.01	0.04	111	507	*JUNB*
Response To Progesterone (GO:0032570)	0.01	0.04	111	507	*ACOD1*
Positive Regulation Of Protein Metabolic Process (GO:0051247)	0.01	0.04	15	66	*NFKBIA;IL1B*
Positive Regulation Of Heterotypic Cell-Cell Adhesion (GO:0034116)	0.01	0.04	102	461	*IL1B*
Positive Regulation Of Membrane Protein Ectodomain Proteolysis (GO:0051044)	0.01	0.04	102	461	*IL1B*
Hyaluronan Metabolic Process (GO:0030212)	0.01	0.04	102	461	*IL1B*
Negative Regulation Of Smooth Muscle Cell Migration (GO:0014912)	0.01	0.04	102	461	*TRIB1*
Prostanoid Biosynthetic Process (GO:0046457)	0.01	0.04	102	461	*PTGS2*
Positive Regulation Of Adaptive Immune Response Based On Somatic Recombination Of Immune Receptors Built From Immunoglobulin Superfamily Domains (GO:0002824)	0.01	0.04	102	461	*IL1B*
Endoderm Development (GO:0007492)	0.01	0.04	102	461	*DUSP1*
Regulation Of MAPK Cascade (GO:0043408)	0.01	0.04	14	63	*DUSP1;IL1B*
Defense Response To Bacterium (GO:0042742)	0.01	0.04	14	63	*CEBPB;IL1B*
DNA Alkylation (GO:0006305)	0.01	0.04	95	421	*FOS*
Negative Regulation Of Gluconeogenesis (GO:0045721)	0.01	0.04	95	421	*SIK1*
Regulation Of Granulocyte Macrophage Colony-Stimulating Factor Production (GO:0032645)	0.01	0.04	95	421	*IL1B*
Negative Regulation Of Synaptic Transmission (GO:0050805)	0.01	0.04	95	421	*IL1B*
Nitric Oxide Biosynthetic Process (GO:0006809)	0.01	0.04	95	421	*ARG2*

Regulation Of Establishment Of Endothelial Barrier (GO:1903140)	0.01	0.04	89	387	*IL1B*
Antifungal Innate Immune Response (GO:0061760)	0.01	0.04	89	387	*CLEC4D*
Nitric Oxide Metabolic Process (GO:0046209)	0.01	0.04	89	387	*ARG2*
Regulation Of Transforming Growth Factor Beta Production (GO:0071634)	0.01	0.04	89	387	*PTGS2*
Regulation Of Triglyceride Biosynthetic Process (GO:0010866)	0.01	0.04	89	387	*SIK1*
Positive Regulation Of Cell Migration Involved In Sprouting Angiogenesis (GO:0090050)	0.01	0.04	89	387	*PTGS2*
Regulation Of Glucose Transmembrane Transport (GO:0010827)	0.01	0.04	83	358	*IL1B*
Regulation Of Mitotic Cell Cycle Spindle Assembly Checkpoint (GO:0090266)	0.01	0.04	83	358	*DUSP1*
Positive Regulation Of Transcription From RNA Polymerase II Promoter In Response To Stress (GO:0036003)	0.01	0.04	83	358	*CEBPB*
Prostaglandin Biosynthetic Process (GO:0001516)	0.01	0.04	83	358	*PTGS2*
Regulation Of Brown Fat Cell Differentiation (GO:0090335)	0.01	0.04	83	358	*PTGS2*
Apoptotic Process (GO:0006915)	0.01	0.04	12	53	*NFKBIA;IL1B*
Positive Regulation Of Interleukin-4 Production (GO:0032753)	0.01	0.04	78	333	*CEBPB*
Negative Regulation Of Lipid Catabolic Process (GO:0050995)	0.01	0.04	78	333	*IL1B*
Regulation Of Epithelial Cell Differentiation (GO:0030856)	0.01	0.04	78	333	*CEBPB*
Negative Regulation Of Lipid Storage (GO:0010888)	0.01	0.04	78	333	*NFKBIA*
Negative Regulation Of Nervous System Development (GO:0051961)	0.01	0.04	78	333	*IL1B*
Negative Regulation Of Intracellular Signal Transduction (GO:1902532)	0.01	0.04	12	52	*PER1;DUSP1*
Regulation Of DNA-templated Transcription (GO:0006355)	0.01	0.04	4	18	*PER1;CEBPB;IL1B;FOS;JUNB*
Regulation Of I-kappaB kinase/NF-kappaB Signaling (GO:0043122)	0.01	0.04	12	52	*PER1;IL1B*
Interleukin-1-Mediated Signaling Pathway (GO:0070498)	0.02	0.04	74	310	*IL1B*
Regulation Of Smooth Muscle Cell Migration (GO:0014910)	0.02	0.04	74	310	*TRIB1*
Striated Muscle Cell Differentiation (GO:0051146)	0.02	0.04	70	290	*SIK1*
DNA Methylation (GO:0006306)	0.02	0.04	70	290	*FOS*
Positive Regulation Of Leukocyte Activation (GO:0002696)	0.02	0.04	70	290	*CLEC4D*
Positive Regulation Of Lipid Catabolic Process (GO:0050996)	0.02	0.04	70	290	*IL1B*
Negative Regulation Of Reproductive Process (GO:2000242)	0.02	0.04	70	290	*DUSP1*
Regulation Of Meiotic Cell Cycle (GO:0051445)	0.02	0.04	70	290	*DUSP1*
Lipopolysaccharide-Mediated Signaling Pathway (GO:0031663)	0.02	0.04	70	290	*IL1B*
Regulation Of Lipid Storage (GO:0010883)	0.02	0.04	67	272	*NFKBIA*
Regulation Of Lipopolysaccharide-Mediated Signaling Pathway (GO:0031664)	0.02	0.04	67	272	*TRIB1*
Regulation Of Membrane Protein Ectodomain Proteolysis (GO:0051043)	0.02	0.04	67	272	*IL1B*
Positive Regulation Of T Cell Cytokine Production (GO:0002726)	0.02	0.04	67	272	*IL1B*
Response To Cadmium Ion (GO:0046686)	0.02	0.04	67	272	*FOS*

Regulation Of Anoikis (GO:2000209)	0.02	0.04	67	272	*SIK1*
Negative Regulation Of Extrinsic Apoptotic Signaling Pathway In Absence Of Ligand (GO:2001240)	0.02	0.04	63	257	*IL1B*
Negative Regulation Of Signal Transduction In Absence Of Ligand (GO:1901099)	0.02	0.04	63	257	*IL1B*
Regulation Of Protein Export From Nucleus (GO:0046825)	0.02	0.04	63	257	*IL1B*
Cellular Response To Cadmium Ion (GO:0071276)	0.02	0.04	63	257	*FOS*
Regulation Of Vascular Endothelial Growth Factor Receptor Signaling Pathway (GO:0030947)	0.02	0.04	63	257	*IL1B*
Positive Regulation Of Cholesterol Efflux (GO:0010875)	0.02	0.04	63	257	*NFKBIA*
Negative Regulation Of Cell Communication (GO:0010648)	0.02	0.04	63	257	*IL1B*
Negative Regulation Of Cell Development (GO:0010721)	0.02	0.04	63	257	*IL1B*
Regulation Of Transcription By RNA Polymerase II (GO:0006357)	0.02	0.04	4	16	*NFKBIA;PER1;CEBPB;FOS;JUNB*
Regulation Of Interleukin-4 Production (GO:0032673)	0.02	0.04	60	242	*CEBPB*
Regulation Of Lipid Catabolic Process (GO:0050994)	0.02	0.04	60	242	*IL1B*
Regulation Of Myotube Differentiation (GO:0010830)	0.02	0.04	60	242	*SIK1*
Negative Regulation Of Signal Transduction (GO:0009968)	0.02	0.04	11	42	*IL1B;TRIB1*
Positive Regulation Of Lipid Metabolic Process (GO:0045834)	0.02	0.04	58	229	*IL1B*
Regulation Of Heterotypic Cell-Cell Adhesion (GO:0034114)	0.02	0.04	58	229	*IL1B*
Positive Regulation Of p38MAPK Cascade (GO:1900745)	0.02	0.04	58	229	*IL1B*
Protein Kinase B Signaling (GO:0043491)	0.02	0.04	58	229	*IL1B*
Negative Regulation Of Cell Junction Assembly (GO:1901889)	0.02	0.04	58	229	*IL1B*
Positive Regulation Of Interleukin-2 Production (GO:0032743)	0.02	0.04	55	217	*IL1B*
Negative Regulation Of Lipid Biosynthetic Process (GO:0051055)	0.02	0.04	55	217	*SIK1*
Regulation Of Monocyte Chemotaxis (GO:0090025)	0.02	0.04	55	217	*DUSP1*
Cellular Response To Steroid Hormone Stimulus (GO:0071383)	0.02	0.04	55	217	*ACOD1*
Regulation Of Biomineral Tissue Development (GO:0070167)	0.02	0.04	55	217	*CEBPB*
Negative Regulation Of Insulin Receptor Signaling Pathway (GO:0046627)	0.02	0.04	53	207	*IL1B*
Negative Regulation Of Lipid Metabolic Process (GO:0045833)	0.02	0.04	53	207	*IL1B*
Positive Regulation Of Monooxygenase Activity (GO:0032770)	0.02	0.04	53	207	*IL1B*
Positive Regulation Of Nuclear Division (GO:0051785)	0.02	0.04	53	207	*IL1B*
Acute Inflammatory Response (GO:0002526)	0.02	0.04	53	207	*CEBPB*
Cellular Response To Xenobiotic Stimulus (GO:0071466)	0.02	0.04	53	207	*IL1B*
Positive Regulation Of Cell Differentiation (GO:0045597)	0.02	0.04	10	39	*CEBPB;IL1B*
Regulation Of Extrinsic Apoptotic Signaling Pathway In Absence Of Ligand (GO:2001239)	0.02	0.04	51	197	*IL1B*
Negative Regulation Of Neurogenesis	0.02	0.04	51	197	*IL1B*

(GO:0050768)					
Cardiac Muscle Cell Differentiation (GO:0055007)	0.02	0.04	51	197	*SIK1*
Myeloid Cell Development (GO:0061515)	0.02	0.04	51	197	*CEBPB*
Negative Regulation Of Cellular Response To Insulin Stimulus (GO:1900077)	0.02	0.04	51	197	*IL1B*
Negative Regulation Of Signaling (GO:0023057)	0.02	0.04	49	188	*IL1B*
Regulation Of Nitric-Oxide Synthase Activity (GO:0050999)	0.02	0.04	49	188	*IL1B*
JNK Cascade (GO:0007254)	0.02	0.04	48	179	*TRIB1*
Peptidyl-Tyrosine Dephosphorylation (GO:0035335)	0.02	0.04	48	179	*DUSP1*
Negative Regulation Of DNA Binding (GO:0043392)	0.02	0.04	48	179	*NFKBIA*
Defense Response To Fungus (GO:0050832)	0.02	0.04	48	179	*CLEC4D*
Regulation Of Intracellular Signal Transduction (GO:1902531)	0.02	0.04	10	36	*NFKBIA;IL1B*
Regulation Of Cell Cycle (GO:0051726)	0.02	0.04	10	36	*SIK1;JUNB*
Regulation Of Macrophage Derived Foam Cell Differentiation (GO:0010743)	0.02	0.04	46	172	*NFKBIA*
Intrinsic Apoptotic Signaling Pathway In Response To Endoplasmic Reticulum Stress (GO:0070059)	0.02	0.04	46	172	*CEBPB*
Prostaglandin Metabolic Process (GO:0006693)	0.02	0.04	46	172	*PTGS2*
Negative Regulation Of Carbohydrate Metabolic Process (GO:0045912)	0.02	0.04	46	172	*SIK1*
Regulation Of Cell Migration Involved In Sprouting Angiogenesis (GO:0090049)	0.02	0.04	46	172	*PTGS2*
Negative Regulation Of Intracellular Steroid Hormone Receptor Signaling Pathway (GO:0033144)	0.02	0.05	44	164	*PER1*
Regulation Of Gluconeogenesis (GO:0006111)	0.02	0.05	44	164	*SIK1*
Positive Regulation Of Cholesterol Transport (GO:0032376)	0.02	0.05	44	164	*NFKBIA*
Regulation Of Cholesterol Efflux (GO:0010874)	0.03	0.05	43	158	*NFKBIA*
NIK/NF-kappaB Signaling (GO:0038061)	0.03	0.05	43	158	*NFKBIA*
Cellular Nitrogen Compound Biosynthetic Process (GO:0044271)	0.03	0.05	43	158	*ARG2*
Positive Regulation Of Nitrogen Compound Metabolic Process (GO:0051173)	0.03	0.05	42	152	*NFKBIA*
Negative Regulation Of Small Molecule Metabolic Process (GO:0062014)	0.03	0.05	42	152	*SIK1*
Positive Regulation Of RNA Metabolic Process (GO:0051254)	0.03	0.05	42	152	*IL1B*
Negative Regulation Of JNK Cascade (GO:0046329)	0.03	0.05	40	146	*PER1*
Regulation Of Cellular Senescence (GO:2000772)	0.03	0.05	39	140	*ARG2*
Positive Regulation Of Mitotic Nuclear Division (GO:0045840)	0.03	0.05	39	140	*IL1B*
Liver Development (GO:0001889)	0.03	0.05	39	140	*CEBPB*
Endoderm Formation (GO:0001706)	0.03	0.05	39	140	*DUSP1*

Cellular Compartment

Term	P-value	Adjusted P-value	Odds Ratio	Combined Score	Genes
Nucleus (GO:0005634)	0.01	0.14	3	15	*NFKBIA;PER1;CEBPB;DUSP1;SIK1;FOS;TRIB1;JUNB*
Nuclear Outer Membrane (GO:0005640)	0.02	0.14	74	310	*PTGS2*

Nuclear Inner Membrane (GO:0005637)	0.02	0.16	44	164	*PTGS2*
Intracellular Membrane-Bounded Organelle (GO:0043231)	0.03	0.16	3	10	*NFKBIA;PER1;CEBPB;DUSP1;SIK1;FOS;TRIB1;JUNB*
Ficolin-1-Rich Granule Membrane (GO:0101003)	0.05	0.18	23	69	*CLEC4D*
Tertiary Granule Membrane (GO:0070821)	0.06	0.18	19	54	*CLEC4D*

Molecular Function

Term	P-value	Adjusted P-value	Odds Ratio	Combined Score	Genes
Transcription Regulatory Region Nucleic Acid Binding (GO:0001067)	0.00	0.02	21	150	*PER1;CEBPB;FOS*
RNA Polymerase II-specific DNA-binding Transcription Factor Binding (GO:0061629)	0.00	0.02	20	146	*NFKBIA;FOS;TRIB1*
Ubiquitin Protein Ligase Binding (GO:0031625)	0.00	0.02	17	114	*NFKBIA;PER1;TRIB1*
DNA-binding Transcription Factor Binding (GO:0140297)	0.00	0.02	16	108	*SIK1;FOS;TRIB1*
Ubiquitin-Like Protein Ligase Binding (GO:0044389)	0.00	0.02	16	104	*NFKBIA;PER1;TRIB1*
Sequence-Specific Double-Stranded DNA Binding (GO:1990837)	0.00	0.02	9	56	*PER1;CEBPB;FOS;JUNB*
Transcription Coregulator Binding (GO:0001221)	0.00	0.02	29	172	*PER1;FOS*
Mitogen-Activated Protein Kinase Kinase Binding (GO:0031434)	0.00	0.03	266	1423	*TRIB1*
Transcription Cis-Regulatory Region Binding (GO:0000976)	0.01	0.03	10	49	*PER1;CEBPB;FOS*
cAMP Response Element Binding Protein Binding (GO:0008140)	0.01	0.03	190	962	*SIK1*
Hydrolase Activity, Acting On Carbon-Nitrogen (But Not Peptide) Bonds, In Linear Amidines (GO:0016813)	0.01	0.03	166	822	*ARG2*
Interleukin-1 Binding (GO:0019966)	0.01	0.03	166	822	*IL1R2*
Interleukin-1 Receptor Binding (GO:0005149)	0.01	0.03	166	822	*IL1B*
Protein Kinase Binding (GO:0019901)	0.01	0.03	9	44	*DUSP1;SIK1;TRIB1*
Cytokine Activity (GO:0005125)	0.01	0.03	16	76	*IL1B;CXCL2*
Cis-Regulatory Region Sequence-Specific DNA Binding (GO:0000987)	0.01	0.04	6	27	*PER1;CEBPB;FOS;JUNB*
RNA Polymerase II Cis-Regulatory Region Sequence-Specific DNA Binding (GO:0000978)	0.01	0.04	6	26	*PER1;CEBPB;FOS;JUNB*
CXCR Chemokine Receptor Binding (GO:0045236)	0.01	0.04	89	387	*CXCL2*
Double-Stranded DNA Binding (GO:0003690)	0.01	0.04	7	29	*CEBPB;FOS;JUNB*
RNA Polymerase II Transcription Regulatory Region Sequence-Specific DNA Binding (GO:0000977)	0.01	0.04	5	22	*PER1;CEBPB;FOS;JUNB*
Mannose Binding (GO:0005537)	0.01	0.04	78	333	*CLEC4D*
R-SMAD Binding (GO:0070412)	0.02	0.04	74	310	*FOS*
Oxidoreductase Activity, Acting On Single Donors With Incorporation Of Molecular Oxygen, Incorporation Of Two Atoms Of Oxygen (GO:0016702)	0.02	0.04	67	272	*PTGS2*
Sequence-Specific DNA Binding (GO:0043565)	0.02	0.04	6	25	*CEBPB;FOS;JUNB*
Mitogen-Activated Protein Kinase Binding (GO:0051019)	0.02	0.04	60	242	*DUSP1*
Nuclear Localization Sequence Binding (GO:0008139)	0.02	0.04	58	229	*NFKBIA*
ATP Binding (GO:0005524)	0.02	0.04	10	40	*SIK1;TRIB1*
NF-kappaB Binding (GO:0051059)	0.02	0.04	53	207	*NFKBIA*

Carboxy-Lyase Activity (GO:0016831)	0.02	0.04	51	197	*ACOD1*
Adenyl Ribonucleotide Binding (GO:0032559)	0.02	0.05	9	34	*SIK1;TRIB1*
Kinase Inhibitor Activity (GO:0019210)	0.03	0.05	40	146	*TRIB1*
Core Promoter Sequence-Specific DNA Binding (GO:0001046)	0.03	0.05	39	140	*FOS*
DNA Binding (GO:0003677)	0.03	0.05	5	19	*PER1;CEBPB;JUNB*

4 Hour Top

Biological Process

Term	P-value	Adjusted P-value	Odds Ratio	Combined Score	Genes
Gluconeogenesis (GO:0006094)	0.00	0.02	95	773	*SLC25A10;PCK1*
Hexose Biosynthetic Process (GO:0019319)	0.00	0.02	86	687	*SLC25A10;PCK1*
Liver Development (GO:0001889)	0.00	0.02	86	687	*ARID5B;PCK1*
Glucose Metabolic Process (GO:0006006)	0.00	0.04	50	345	*SLC25A10;PCK1*
Succinate Transport (GO:0015744)	0.00	0.04	333	1839	*SLC25A10*
Cell Junction Disassembly (GO:0150146)	0.00	0.04	333	1839	*CX3CR1*
His-Purkinje System Development (GO:0003164)	0.00	0.04	333	1839	*HOPX*
Negative Regulation Of Mast Cell Activation (GO:0033004)	0.00	0.04	333	1839	*CD300LF*
Negative Regulation Of Myeloid Leukocyte Mediated Immunity (GO:0002887)	0.00	0.04	333	1839	*CX3CR1*
Autocrine Signaling (GO:0035425)	0.00	0.04	333	1839	*CX3CR1*
Short-Chain Fatty Acid Catabolic Process (GO:0019626)	0.00	0.04	333	1839	*PCK1*
Positive Regulation Of I-kappaB Phosphorylation (GO:1903721)	0.00	0.04	333	1839	*CX3CR1*
Hepatocyte Differentiation (GO:0070365)	0.00	0.04	333	1839	*PCK1*
Regulation Of I-kappaB Phosphorylation (GO:1903719)	0.00	0.04	266	1423	*CX3CR1*
Host-Mediated Regulation Of Intestinal Microbiota Composition (GO:0048874)	0.00	0.04	266	1423	*CX3CR1*
Regulation Of Microglial Cell Migration (GO:1904139)	0.00	0.04	266	1423	*CX3CR1*
Fatty Acid Elongation, Monounsaturated Fatty Acid (GO:0034625)	0.00	0.04	266	1423	*ELOVL7*
Fatty Acid Elongation, Polyunsaturated Fatty Acid (GO:0034626)	0.00	0.04	266	1423	*ELOVL7*
Fatty Acid Elongation, Saturated Fatty Acid (GO:0019367)	0.00	0.04	266	1423	*ELOVL7*
Fatty Acid Elongation, Unsaturated Fatty Acid (GO:0019368)	0.00	0.04	266	1423	*ELOVL7*
Positive Regulation Of Apoptotic Cell Clearance (GO:2000427)	0.01	0.04	222	1151	*CD300LF*
Positive Regulation Of Secondary Metabolite Biosynthetic Process (GO:1900378)	0.01	0.04	222	1151	*ZEB2*
Positive Regulation Of Melanin Biosynthetic Process (GO:0048023)	0.01	0.04	222	1151	*ZEB2*
Regulation Of Apoptotic Cell Clearance (GO:2000425)	0.01	0.04	222	1151	*CD300LF*
Regulation Of Nitric Oxide Metabolic Process (GO:0080164)	0.01	0.04	222	1151	*CX3CR1*
Regulation Of Macrophage Migration (GO:1905521)	0.01	0.04	190	962	*CX3CR1*
Synapse Pruning (GO:0098883)	0.01	0.04	190	962	*CX3CR1*

Positive Regulation Of Memory T Cell Differentiation (GO:0043382)	0.01	0.04	190	962	*PCK1*
Tricarboxylic Acid Metabolic Process (GO:0072350)	0.01	0.04	190	962	*PCK1*
Regulation Of Tumor Necrosis Factor Superfamily Cytokine Production (GO:1903555)	0.01	0.04	190	962	*CX3CR1*
Regulation Of Mast Cell Activation (GO:0033003)	0.01	0.04	166	822	*CD300LF*
Regulation Of Memory T Cell Differentiation (GO:0043380)	0.01	0.04	166	822	*PCK1*
Regulation Of Melanin Biosynthetic Process (GO:0048021)	0.01	0.04	148	715	*ZEB2*
Phosphate Ion Transmembrane Transport (GO:0035435)	0.01	0.04	148	715	*SLC25A10*
Regulation Of Biosynthetic Process (GO:0009889)	0.01	0.04	148	715	*PCK1*
Sulfate Transport (GO:0008272)	0.01	0.04	133	631	*SLC25A10*
C4-dicarboxylate Transport (GO:0015740)	0.01	0.04	121	563	*SLC25A10*
Fatty Acid Elongation (GO:0030497)	0.01	0.04	121	563	*ELOVL7*
Very Long-Chain Fatty Acid Biosynthetic Process (GO:0042761)	0.01	0.04	121	563	*ELOVL7*
Negative Regulation Of Toll-Like Receptor Signaling Pathway (GO:0034122)	0.01	0.04	111	507	*CD300LF*
Negative Regulation Of Leukocyte Mediated Cytotoxicity (GO:0001911)	0.01	0.05	102	461	*CX3CR1*
Negative Regulation Of Phagocytosis (GO:0050765)	0.01	0.05	95	421	*CD300LF*
Antifungal Innate Immune Response (GO:0061760)	0.01	0.05	89	387	*CX3CR1*
Negative Regulation Of Leukocyte Activation (GO:0002695)	0.01	0.05	83	358	*CD300LF*
Cellular Response To Glucocorticoid Stimulus (GO:0071385)	0.01	0.05	83	358	*PCK1*
Triglyceride Biosynthetic Process (GO:0019432)	0.01	0.05	83	358	*PCK1*
Leukocyte Tethering Or Rolling (GO:0050901)	0.01	0.05	83	358	*CX3CR1*
Long-Chain fatty-acyl-CoA Biosynthetic Process (GO:0035338)	0.01	0.05	83	358	*ELOVL7*
Positive Regulation Of Neuroblast Proliferation (GO:0002052)	0.01	0.05	78	333	*CX3CR1*

4 Hour Middle

Biological Process

Term	P-value	Adjusted P-value	Odds Ratio	Combined Score	Genes
Negative Regulation Of Glial Cell Proliferation (GO:0060253)	0.00	0.02	324	3248	*SKI;SOX11*
Negative Regulation Of Cell Population Proliferation (GO:0008285)	0.00	0.03	9	75	*SKI;ACVR1C;PDPN;SOX11;INHBA;HSPA1B*
Transmembrane Receptor Protein Serine/Threonine Kinase Signaling Pathway (GO:0007178)	0.00	0.03	16	140	*TMEM100;SKI;ACVR1C;INHBA*
Negative Regulation Of Activin Receptor Signaling Pathway (GO:0032926)	0.00	0.03	122	1035	*SKI;FST*
Nervous System Development (GO:0007399)	0.00	0.03	7	60	*ACVR1C;TMOD2;SOX11;INHBA;SPTBN1;CDON*
Cellular Response To Growth Factor Stimulus (GO:0071363)	0.00	0.03	13	108	*TMEM100;CLEC3B;ACVR1C;GAS1*
Regulation Of Activin Receptor Signaling Pathway (GO:0032925)	0.00	0.03	75	574	*SKI;FST*
Activin Receptor Signaling Pathway (GO:0032924)	0.00	0.03	69	524	*ACVR1C;INHBA*

Regulation Of BMP Signaling Pathway (GO:0030510)	0.00	0.03	21	155	*SKI;FST;SOX11*

Cellular Compartment

Term	P-value	Adjusted P-value	Odds Ratio	Combined Score	Genes
Ficolin-1-Rich Granule Lumen (GO:1904813)	0.00	0.01	17	152	*HSPA8;CRISPLD2;FGL2;HSPA1B*
Filopodium Membrane (GO:0031527)	0.00	0.01	108	899	*PDPN;SYNE2*
Ficolin-1-Rich Granule (GO:0101002)	0.00	0.01	11	83	*HSPA8;CRISPLD2;FGL2;HSPA1B*
Cell Projection Membrane (GO:0031253)	0.00	0.02	15	95	*LIMA1;PDPN;SYNE2*
Intracellular Organelle Lumen (GO:0070013)	0.00	0.02	4	27	*HSPA8;SDC4;CRISPLD2;FGL2;PDK4;SYNE2;HSPA1B*

Molecular Function

Term	P-value	Adjusted P-value	Odds Ratio	Combined Score	Genes
C3HC4-type RING Finger Domain Binding (GO:0055131)	0.00	0.00	324	3248	*HSPA8;HSPA1B*
Cadherin Binding (GO:0045296)	0.00	0.11	6	34	*LIMA1;HSPA8;RSL1D1;SPTBN1*
Cytokine Activity (GO:0005125)	0.01	0.11	8	43	*IL33;CCL7;INHBA*
Actin Binding (GO:0003779)	0.01	0.11	8	41	*LIMA1;SYNE2;SPTBN1*

4 Hour Bottom

Biological Process

Term	P-value	Adjusted P-value	Odds Ratio	Combined Score	Genes
Nuclear-Transcribed mRNA Catabolic Process (GO:0000956)	0.00	0.00	89	1316	*NCBP2;XRN2;PARN;EIF3E*
Positive Regulation Of mRNA Processing (GO:0050685)	0.00	0.01	118	1008	*NCBP2;CIRBP*
Nuclear-Transcribed mRNA Catabolic Process, Nonsense-Mediated Decay (GO:0000184)	0.00	0.01	118	1008	*NCBP2;EIF3E*
Cytoplasmic Translational Initiation (GO:0002183)	0.00	0.01	110	921	*NCBP2;EIF3E*
RNA Stabilization (GO:0043489)	0.00	0.01	88	699	*CIRBP;PARN*
Regulation Of Translation (GO:0006417)	0.00	0.01	25	193	*NCBP2;CIRBP;EIF3E*
Regulation Of Translational Initiation (GO:0006446)	0.00	0.02	49	333	*NCBP2;EIF3E*
Negative Regulation Of Catabolic Process (GO:0009895)	0.00	0.02	44	291	*CBFA2T3;BANP*
Positive Regulation Of Amide Metabolic Process (GO:0034250)	0.00	0.03	37	233	*CIRBP;EIF3E*
Positive Regulation Of Translation (GO:0045727)	0.00	0.03	29	169	*CIRBP;EIF3E*
RNA Metabolic Process (GO:0016070)	0.00	0.03	28	162	*XRN2;PARN*
Positive Regulation Of Macromolecule Biosynthetic Process (GO:0010557)	0.00	0.03	25	143	*CIRBP;EIF3E*
Cap-Dependent Translational Initiation (GO:0002191)	0.00	0.03	357	1994	*NCBP2*
Regulation Of mRNA Binding (GO:1902415)	0.00	0.03	357	1994	*EIF3E*
Galactolipid Biosynthetic Process (GO:0019375)	0.00	0.03	357	1994	*B3GALT2*
Galactosylceramide Biosynthetic Process (GO:0006682)	0.00	0.03	357	1994	*B3GALT2*
Positive Regulation Of RNA Binding (GO:1905216)	0.00	0.03	285	1543	*EIF3E*

Positive Regulation Of mRNA Binding (GO:1902416)	0.00	0.03	285	1543	*EIF3E*
Polyadenylation-Dependent snoRNA 3'-End Processing (GO:0071051)	0.00	0.03	285	1543	*PARN*
Glycosylceramide Biosynthetic Process (GO:0046476)	0.00	0.03	285	1543	*B3GALT2*
Negative Regulation Of Lipid Kinase Activity (GO:0090219)	0.01	0.03	238	1249	*PIK3IP1*
Termination Of RNA Polymerase II Transcription (GO:0006369)	0.01	0.03	238	1249	*XRN2*
Galactosylceramide Metabolic Process (GO:0006681)	0.01	0.03	238	1249	*B3GALT2*
ncRNA Export From Nucleus (GO:0097064)	0.01	0.03	204	1043	*NCBP2*
Positive Regulation Of mRNA 3'-End Processing (GO:0031442)	0.01	0.03	178	892	*NCBP2*
Negative Regulation Of Phosphatidylinositol 3-Kinase Signaling (GO:0014067)	0.01	0.03	178	892	*PIK3IP1*
Positive Regulation Of Cellular Biosynthetic Process (GO:0031328)	0.01	0.03	18	87	*CIRBP;EIF3E*
Negative Regulation Of Glycolytic Process (GO:0045820)	0.01	0.03	159	776	*CBFA2T3*
Regulation Of mRNA Polyadenylation (GO:1900363)	0.01	0.03	159	776	*NCBP2*
miRNA Catabolic Process (GO:0010587)	0.01	0.03	159	776	*PARN*
RNA Processing (GO:0006396)	0.01	0.03	17	81	*NCBP2;XRN2*
Regulation Of mRNA 3'-End Processing (GO:0031440)	0.01	0.03	143	685	*NCBP2*
Regulation Of RNA Export From Nucleus (GO:0046831)	0.01	0.03	143	685	*NCBP2*
pre-mRNA Cleavage Required For Polyadenylation (GO:0098789)	0.01	0.03	143	685	*NCBP2*
sno(s)RNA 3'-End Processing (GO:0031126)	0.01	0.03	143	685	*PARN*
Transcription By RNA Polymerase II (GO:0006366)	0.01	0.03	16	76	*NCBP2;XRN2*
mRNA Cleavage Involved In mRNA Processing (GO:0098787)	0.01	0.03	130	611	*NCBP2*
Primary miRNA Processing (GO:0031053)	0.01	0.03	130	611	*NCBP2*
Positive Regulation Of Protein Metabolic Process (GO:0051247)	0.01	0.03	16	74	*CIRBP;EIF3E*
Immune Response-Regulating Cell Surface Receptor Signaling Pathway (GO:0002768)	0.01	0.03	119	551	*BTLA*
Negative Regulation Of Translational Initiation (GO:0045947)	0.01	0.03	119	551	*EIF3E*
Formation Of Cytoplasmic Translation Initiation Complex (GO:0001732)	0.01	0.04	110	501	*EIF3E*
Regulation Of Cellular Response To Heat (GO:1900034)	0.01	0.04	102	458	*CHORDC1*
miRNA Metabolic Process (GO:0010586)	0.01	0.04	102	458	*PARN*
Alternative mRNA Splicing, Via Spliceosome (GO:0000380)	0.01	0.04	95	421	*NCBP2*
DNA-templated Transcription Termination (GO:0006353)	0.01	0.04	95	421	*XRN2*
Regulation Of Cellular Respiration (GO:0043457)	0.01	0.04	89	389	*CBFA2T3*
mRNA Cis Splicing, Via Spliceosome (GO:0045292)	0.01	0.04	89	389	*NCBP2*
ncRNA Metabolic Process (GO:0034660)	0.01	0.04	89	389	*PARN*
Regulation Of Aerobic Respiration (GO:1903715)	0.01	0.04	89	389	*CBFA2T3*
Regulation Of Telomerase RNA Localization To Cajal Body (GO:1904872)	0.01	0.04	89	389	*PARN*
ncRNA-mediated Post-Transcriptional Gene Silencing (GO:0035194)	0.01	0.04	84	362	*NCBP2*

Nuclear-Transcribed mRNA poly(A) Tail Shortening (GO:0000289)	0.01	0.04	75	316	*PARN*
Oligosaccharide Biosynthetic Process (GO:0009312)	0.02	0.04	68	279	*B3GALT2*
Histone mRNA Metabolic Process (GO:0008334)	0.02	0.04	65	264	*NCBP2*
Positive Regulation Of mRNA Splicing, Via Spliceosome (GO:0048026)	0.02	0.04	65	264	*CIRBP*
Stress Granule Assembly (GO:0034063)	0.02	0.04	62	250	*CIRBP*
Carbohydrate Biosynthetic Process (GO:0016051)	0.02	0.05	59	237	*B3GALT2*
miRNA-mediated Gene Silencing (GO:0035195)	0.02	0.05	57	225	*NCBP2*
Gene Expression (GO:0010467)	0.02	0.05	10	40	*NCBP2;XRN2*
RNA Phosphodiester Bond Hydrolysis (GO:0090501)	0.02	0.05	53	204	*PARN*

Molecular Function

Term	P-value	Adjusted P-value	Odds Ratio	Combined Score	Genes
3'-5'-RNA Exonuclease Activity (GO:0000175)	0.00	0.01	96	781	*XRN2;PARN*
RNA Binding (GO:0003723)	0.00	0.01	9	70	*HNRNPDL;NCBP2;XRN2;CIRBP;PARN;EIF3E*
Nuclease Activity (GO:0004518)	0.00	0.01	55	387	*XRN2;PARN*
mRNA Binding (GO:0003729)	0.00	0.01	18	120	*NCBP2;CIRBP;PARN*
mRNA 3'-UTR Binding (GO:0003730)	0.00	0.01	34	206	*CIRBP;PARN*
poly(G) Binding (GO:0034046)	0.01	0.03	238	1249	*HNRNPDL*
UDP-galactose:beta-N-acetylglucosamine Beta-1,3-Galactosyltransferase Activity (GO:0008499)	0.01	0.03	143	685	*B3GALT2*
poly(A)-specific Ribonuclease Activity (GO:0004535)	0.01	0.03	130	611	*PARN*
RNA 7-Methylguanosine Cap Binding (GO:0000340)	0.01	0.03	130	611	*NCBP2*
5'-3' Exonuclease Activity (GO:0008409)	0.01	0.03	119	551	*XRN2*
Beta-1,3-Galactosyltransferase Activity (GO:0048531)	0.01	0.03	110	501	*B3GALT2*
RNA Cap Binding (GO:0000339)	0.01	0.03	79	337	*NCBP2*
UDP-galactosyltransferase Activity (GO:0035250)	0.01	0.03	79	337	*B3GALT2*
Telomerase RNA Binding (GO:0070034)	0.02	0.03	71	296	*PARN*
poly(A) Binding (GO:0008143)	0.02	0.04	59	237	*HNRNPDL*
RNA Exonuclease Activity, Producing 5'-Phosphomonoesters (GO:0016896)	0.02	0.04	49	187	*XRN2*
Poly-Purine Tract Binding (GO:0070717)	0.02	0.04	48	179	*HNRNPDL*
Hsp90 Protein Binding (GO:0051879)	0.03	0.04	42	153	*CHORDC1*
Translation Initiation Factor Activity (GO:0003743)	0.03	0.05	36	125	*EIF3E*
3'-5' Exonuclease Activity (GO:0008408)	0.03	0.05	35	121	*XRN2*
snRNA Binding (GO:0017069)	0.03	0.05	34	117	*NCBP2*
rRNA Binding (GO:0019843)	0.03	0.05	32	107	*CIRBP*
Exonuclease Activity (GO:0004527)	0.03	0.05	32	107	*XRN2*

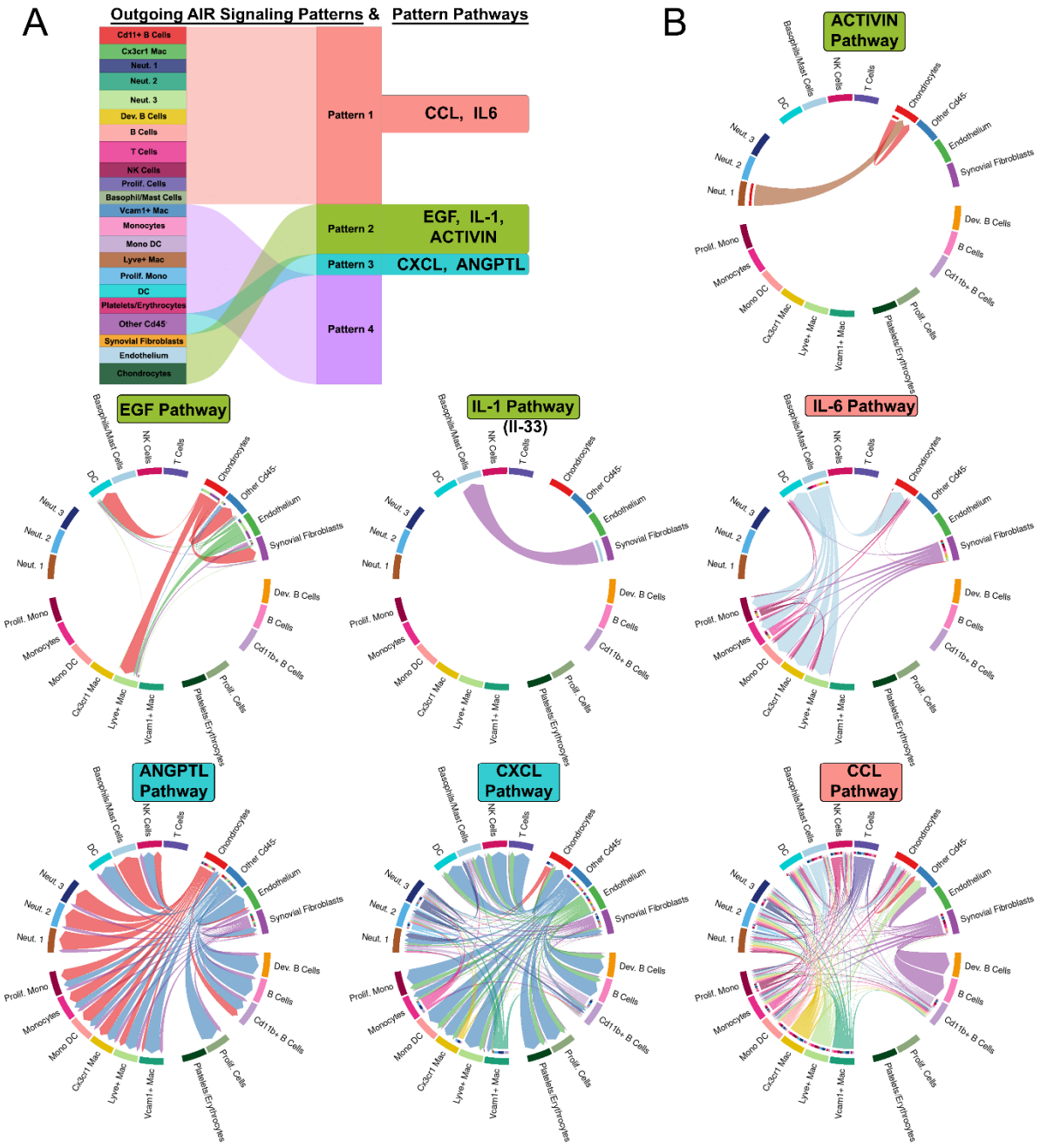

Figure 2.4: AIR signaling involves crosstalk between stromal and immune cell populations. A) River plot from filtered CellChat analysis shows outgoing AIR signaling patterns by knee cell populations and the pathways that comprise each pattern. B) Chord plots showing AIR gene pathways between cell-types, Flat end of chords indicate the origin of signaling/ligand expression, while the wedge end of chords indicates cells receiving signaling/receptor expression.

To determine intracellular signaling patterns in the AIR we used the CellChat tool to analyze the three-hour single-cell populations. CellChat infers potential cell communications by comparison of ligands and receptors expressed within a dataset. This analysis was restricted to pathways which included genes found in the one or four hour AIR gene lists. Outgoing communication patterns for each cell type were inferred based on expression of ligand-receptor interactions displayed as river plots in Figure 2.4A. The first pattern of signaling was primarily through *Il6* and *CCL* and was found predominately in neutrophils and other immune cells, including Basophils/Mast cells, B, T, and NK cells. *Il6* in the joint was expressed in Synovial Fibroblasts and Basophils/Mast cells and acting upon macrophages and monocytes (Figure 2.4B). CCL signaling was more complex, signaling originated from Synovial Fibroblasts as well as many Macrophages, Monocytes, and other immune cells and was broadly received across stromal cells, DCs, monocytes and neutrophils.

The second pattern of outgoing AIR signaling involved the EGF, Il-1, and Activin pathways, these pathways predominately originated from stromal cells. EGF ligands were expressed in chondrocytes and endothelium signaling to other stromal cells DCs and Lyve^{+} Macrophages. We found *Il33* an Il-1 family cytokine expressed in Synovial Fibroblasts while the receptor St2 (*Il1rl1*) was expressed in Basophil/Mast Cells. Activin signaling ligands were expressed in Chondrocytes and less activated Neutrophils (Neutrophil 1) while only chondrocytes expressed receptors.

The third pattern of outgoing signal consisted of the CXCL and Angiopoietin-Like Proteins. These signals were expressed primarily in stromal cells and were received broadly by immune cells within the joint.

Nh|	V|qryldo Ileureodvw jhqhv Xs	orjIF	V|qryldo Ileureodvw jhqhv Grzq	orjIF	O|yh. P df jhqhv Xs	orjIF	O|yh. P df jhqhv Grzq	orjIF	Ghy1E Fhov jhqhv Grzq	orjIF	Hqgrwkhdxp jhqhv Xs	orjIF	Hqgrwkhdxp jhqhv Grzq	orjIF	Sodwhohw) Hu|wkurf|whv jhqhv Xs	orjIF	Sodwhohw) Hu|wkurf|whv jhqhv Grzq	orjIF	Edvrskbv) P dvw Fhov jhqhv Grzq	orjIF
4 KrxuDIU	*P w4*	61k7	]ewe49	05 15<	*P w4*	915<	*Sp hsd4*	051k8	V433d;	0414;	Dnds45	4157	V433d<	0416;	K lvw4k5ds	4154	V433d<	04179	V433d;	04149
7 KrxuDIU	*P w5*	615<	*Wvf55g6*	05145	*P w5*	81k3	Vhvq4	05179			*P w4*	414<	Fdylq5	04156			V433d;	04173		
; KrxuDIU	*Ijd5*	5164	Q ild	05138	*Kp r{4*	7193	Ksjg	05147			*P w5*	414;	V433d;	0414;			[sr:	04153		
57 KrxuDIU	Dfwj4	5134	Urud	05134	*Vgf7*	61;8	Wsujo	041;:												
	Vgf7	41;4	Kwd6	041k5	*Gde5*	6186	R skq4	041:<												
	Fg77	41;3	W{qls	041;7	*Uesm*	6168	R dp o6	041:9												
	Vrfv6	41;3	Dogk4d4	041;6	*Hju4*	6153	G |qo6	04193												
	Wkeg	419;	Q ile	041;4	Iwq4	517<	Wqiuvi54	04179												
	Vdf58d8	4179	Z zr{	041:9	Grn5	5133	S fp wg5	04178												
	H li5v5	4177	Vvk5	041:7	Z qn4	41k:	Furw	04166												
	Qrs8;	4175	Wjieu6	04199	Udq	41;8	Grn4	0414<												
	Uso69do	4175	*Defd;d*	04193	Syw4	41;4														
	Gg{54	4173	Sog4	0418;	Kquqsde	419<														
	Sdn5	4163	Vhvq4	0417;	Fg6;	4197														
	Udq	415;	U lq5	0417:	P froq5	418<														
	Vp dufd8	414<	J de4	04179	Vdf:d4	4186														
	Vxe4	414;	Wquf9e	04175	Uswru	417;														
	Wxee9	414;	Uhuh	04174	Oweu	4163														
	Kvsd<	414:	Fuheui	04163	Xvs69	415<														
	W{qug4	4145	*Defd;e*	0415:																
			Ep shu	04158																
			Qryd4	04154																
			J ue43	04154																
			Q ilf	04153																
			Qfdp 4	04148																
			Djp r	04147																
			]ffkf57	04145																
			P jd	04144																
			Vwp 4	04144																

Table 2.3. Differentially Expressed Genes from Injury by Cluster. LogFC (base 2) of DEGs based on comparison of single cell seq data between injured knee relative to control knee in one mouse three hours after injury, cluster by cluster analysis. Positive values indicate increased expression in injured knee. AIR genes identified by bulk sequencing are highlighted by colors representing the first timepoint they appeared differentially regulated from bulk-seq data.

To determine cell-type specific changes due to injury, cells from the injured and uninjured knees were compared on a cluster-by-cluster basis to identify DEGs in the three hour scRNA-seq data. When these genes were then cross-referenced with the AIR genes identified by bulk-seq, the Synovial Fibroblast and Lyve+ Macrophage clusters contained the most DEGs, both positive and negative. *Mt1*, *Mt2, Fgl2, Sdc4*, *Thbd, Tubb6* and *Hspa9* were AIR genes upregulated in the injured limbs cells within the Synovial Fibroblast cluster, while *Tsc22d3, Abca8a, Abca8b* are downregulated. *Mt1* and *Mt2* are also upregulated with injury in the endothelial cluster. In the Lyve+ cluster *Mt1, Mt2, Hmox1, Sdc4, Dab2, Rbpj,* and *Egr1* are upregulated while *Pmepa1* is downregulated.

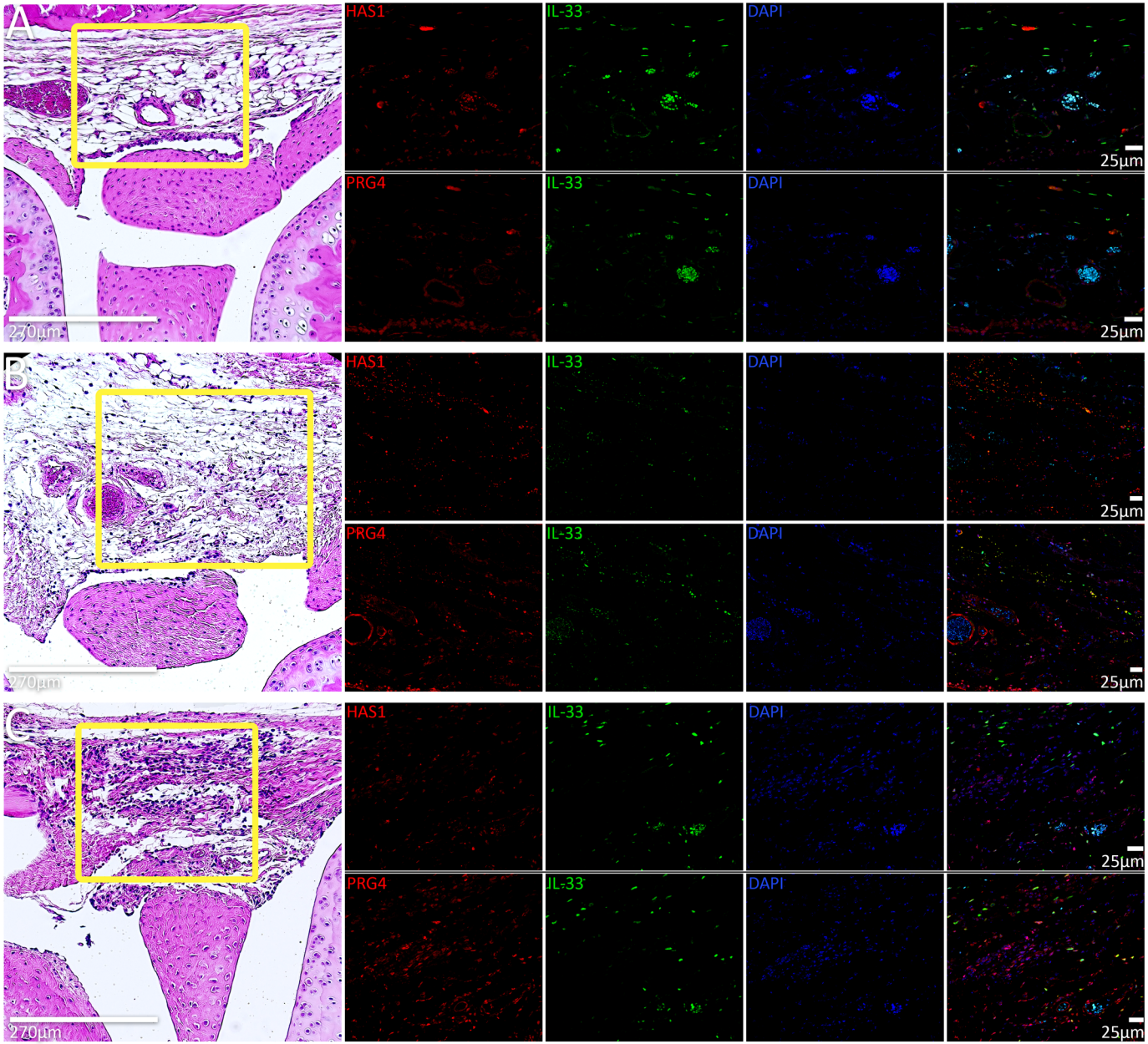
A
HAS1
IL-33
DAPI
25μm
PRG4
IL-33
DAPI
25μm
270μm
B
HAS1
IL-33
DAPI
25μm
PRG4
IL-33
DAPI
25μm
270μm
C
HAS1
IL-33
DAPI
25μm
PRG4
IL-33
DAPI
25μm
270μm

71

Figure 2.5: AIR Products Il-33, Prg4 and Has1 are expressed in the synovium in-vivo. IHC showing expression of HAS1, PRG4, and IL33 in (A) uninjured, (B) one-hour post injury, and (C) four-hour post injury in mouse knees. H&E (10x magnification) shows region of the joint and gross histology, IHC showing selected regions at higher magnification of the AIR genes: HAS1, PRG4, and IL33. IL33 is expressed in some synovial intimal lining cells but is prominent in the sublining cells distal from the joint interior.

To verify expression of AIR genes in-vivo, IHC for IL33, HAS1, and PRG4 was performed on mouse knees before injury, and one and hour hours post-injury (Figure 2.5). HAS1 and PRG4 were both expressed in synovial cells, with higher expression in the lining of the synovium. Before injury (Figure 2.5A) IL33 was primarily localized in sublining fibroblast cells distal to the joint interior, with some cells proximal to the joint lining expressing IL33. Beginning at one hour after injury (Figure 2.5B) there was a notable increase in cellularity within the synovium, this increase was even more pronounced at four hours (Figurer 2.5C). The mass of infiltrating cells did not express IL33, but many did express HAS1 and PRG4 at one and four hours. Many of these infiltrating cells contained lobular nuclei indicative of neutrophils.

This visualization confirmed the expression of selected AIR genes in-vivo and supports the cluster based expression profile of synovial fibroblasts determined by scRNA-seq.

Figure 2.6: Subsets of synovial Intimal fibroblasts identified correlate to larger populations of cells in other scRNA-seq datasets. A. fibroblasts clusters are isolated from the whole datasets, identified by expression of *Col1a1, Thbs4, Pdgfra* and *Prg4*. B. Within the reclustered synovial subsets synovial Intimal fibroblasts are identified by expression of *Tspan15, Has1, Prg4*^{Hi}, and *Col22a1*.

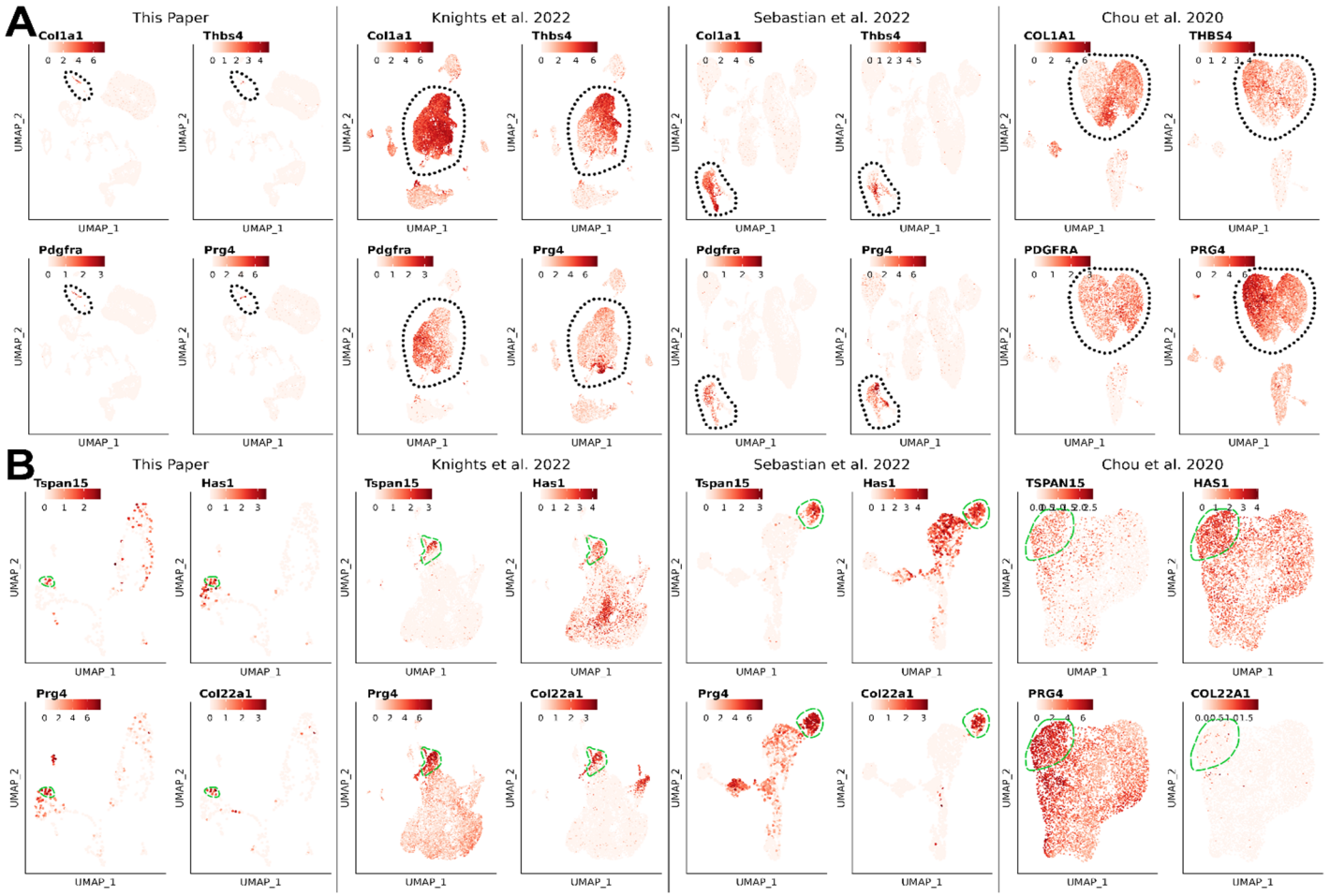

To assess a sub-population identified as synovial intimal fibroblasts we analyzed published and publicly available single-cell databases from murine and human knees for comparison. After selecting clusters expressing marker genes for fibroblasts, comparable cell populations were identifed in two datasets from murine knee tisues, and one from human OA synovium. These cells expressed high levels of *Prg4*, *Col22a1*, *Tspan15* and *Has1*.

DISCUSSION

In this study we provide a new perspective into the acute changes occurring after joint injury. While previous research has documented global transcriptional changes in animal models after injury, the timescale of these studies is typically days, weeks, or months[122-127]. To our knowledge this is the first study that has sequenced knee tissues across the first twenty-four hours after injury, characterizing the global transcriptional changes constituting the Acute Injury Response in the murine knee.

Utilizing a combination of a non-invasive injury model, whole joint bulk-RNA sequencing and scRNA-seq, we show that the Acute Injury Response in mouse joints is a dynamic event, beginning with only 54 genes in the first hour and expanding to 311 genes at twenty-four hours. At three hours there was a diverse response in AIR expression from immune and stromal cells. This work has generated a targetable list of AIR genes for further investigation, in combination with a snapshot of the cell populations expressing them within the joint post-injury.

One notable observation within the first hour after injury was the substantial expression of AIR genes in neutrophils (Figure 2.3A). Examples of these proinflammatory AIR genes include *Il1b,* a major inflammatory and catabolic cytokine[128], *Cxcl2* a potent chemokine and promoter of osteoclastogenesis[129], and *Trem1* which is overexpressed in OA tissues and may promote more inflammatory apoptosis over autophagy[130-132]. It is well known that neutrophils swiftly migrate to injury sites and accumulate within minutes of damage[133], the presence of many neutrophil specific

genes in the one-hour AIR genes is likely explained by the quantity of neutrophils active in the tissue at that time. Only 3 hours later most of the neutrophil associated genes have gone back to insignificant levels, although *Cxcl2* remains upregulated, likely due to infiltrating monocytes.

A large amount of AIR genes were expressed in synovial fibroblasts (Figure 2.3), the high expression of *Prg4* and *Has1* pointed to Synovial Intimal Fibroblasts, and indeed a subcluster of the fibroblasts expressed the unique fingerprint of *Prg4, Has1, Col22a1,* and *Tsnap15* (Figure 2.6) that matches synovial fibroblasts in other datasets[34, 69, 99]. Given their close vicinity to the synovial fluid and potential exposure to alarmins and Damage Associated Molecular Patterns (DAMPS) during ACL injury, these cells, and the synovial fibroblast cluster as a whole display a robust reaction to the injury, as indicated by the notable expression of multiple AIR genes.

Many AIR genes showed differential expression patters between immune and stromal cells, one example of this was the metallothionein proteins (*Mt1, Mt2* genes). *Mt1* has been shown to have a protective effect against reactive oxidative stress and inflammation, however *Mt2* overexpression in the joint caused increases in many matrix degrading enzymes and promoted PTOA development[134]. Metallothionein expression in the joint was increased from the first hour after injury through twenty-four hours, however using single scRNA-seq we found expression is split along stromal and immune lines at three hours. *Mt1* was expressed in immune and stromal cells, while *Mt2* was expressed in stromal cells and $Lyve^{+}$ macrophages. Metallothionein expression and presence has been shown in OA chondrocytes (*Mt2*)[135], synovial lining cells of patients with osteoarthritis, rheumatoid arthritis, ankylosing spondylitis (especially during periods of disease activity[136]), and psoriatic arthritis[137, 138]. Our finding suggest *Mt2* is produced within chondrocytes and $Cd45^{-}$ cells within the synovium.

Another AIR gene that had narrow expression within this study was *Il-33*, an Il-1 family pro-inflammatory cytokine that binds to *Il1rl1* (ST2), that has been shown to be upregulated at twenty-four hours post

injury or later [139-141]. Addition of IL-33 to the knee of PTOA model mice has shown an increase in cartilage damage, synovitis, pain, and osteophyte formation and promoted M1 macrophage polarization[142, 143]. We identified synovial fibroblast as the primary expressor of *Il33* at three hours post-injury (Figure 2.3). IL-33 has a role in other pathologies such as early tendinopathy where it disrupts homeostatic collagen expression[144]. One study however showed that synovial fibroblast-specific deletion of *Il33* decreased synovitis but did not impact disease outcomes, whilst cartilage-specific deletion of *Il33* (which expression was not detected in this study), as well as antibodies specific to IL-33 improved disease outcomes in vivo[143].

Looking at crosstalk within the knee through the lens of identified AIR genes identified several major patterns (Figure 2.4). IL-33 is an IL-1β family cytokine and was expressed in synovial fibroblasts and mast cells. IL-33 may act on mast cells expressing its' receptor, ST2 (*Il1rl1*), within the joint which has been shown to induce many proinflammatory genes and cytokines in mast cells[145], inducing IL-6 production. Interestingly one study found synovial levels of *Il6* expression to be elevated in end-stage knee OA relative to knees recently injured[146]. CCL signaling, which promotes monocyte infiltration, chemotaxis as well as degenerative joint changes[147] Macrophages, synovial fibroblasts, and T/NK cells expressed CCL pathway ligands acting broadly on monocytes and other cells within the joint to. Angiopoietin-Like Protein 4 (*Angptl4*) was highly expressed in stromal cells acting on a wide variety of stromal and immune cells. Recent work has shown that it exacerbates apoptosis and matrix degradation in chondrocytes and *Angptl4* lentiviral knockdown ameliorates OA development in a DMM mouse model[148]. *Cxcl* was highly expressed in stromal cells, as well as some immune cells, acting broadly on immune cells.

While the AIR genes defined in this paper provide a reasonable assessment of the bulk transcriptional shifts in the knee in the first twenty-four hours after injury, we acknowledge the limitations of the scRNA-seq data presented here, as the dataset was from a singular mouse and timepoint. First, gene

expression is dynamic, especially after injury, and we cannot extrapolate our three-hour post injury data to other timepoints. Second, this methodology does not necessarily capture enough cells of all cell-types to fully represent every present cell subset. However, the limited number of cells within this dataset of certain populations provide meaningful direction for future study and are mappable to larger datasets that target specific tissues and cell populations. This is evident within the synovial fibroblast cluster, where a substantial expression of AIR genes, including *Il33*, is observed. This aligns with findings from other datasets that specifically target synovial cells, further emphasizing the significance of this observation. Here we identified synovial intimal fibroblasts expressing many AIR genes. These cells are found in other scRNA-seq datasets (Figure 2.6) some of which specifically targeted the synovium for digestion and sequencing[34, 99, 149]. This study was able to identify these cells as significant expressors of AIR genes from the limited population present and provides justification for more targeted investigation, which have been shown to expand one and four weeks after injury[99]. Third, the stress of digestion is another concern for the use of single-cell sequencing, especially when dealing with joint tissues encompassing very soft and sensitive tissues alongside cells embedded in much more resilient extracellular matrix, the use of a two-stage digest helps reduce this stress response.

Significant injury to a joint may only happen once during a lifetime yet permanently alters the joints trajectory toward OA. This study has identified the first responses to injury within the knee that lay the path to PTOA development. We identified several trends in the expression of AIR genes, and the cells that may be responsible. We found a general trend of early transcription factor expression cascading into cytokine and chemokine signaling, followed by chemotaxis, cell infiltration and angiogenesis. Immune and stromal cells expressed different outgoing AIR signals after injury, with many AIR pathways potentially originating from stromal cells. Identifying the early pathways and cell populations involved in the acute injury response provides targets for further study or potential intervention.

CONTRIBUTIONS

Dustin M Leale – Conception of study, design, bioinformatics protocol designs, execution of IHC & scRNA-seq data, injury models, drafting of the article, interpretation of data, revising intellectual content.

Jasper Yik – Conception of study, wet protocol design (bulk RNA-Seq), execution of bulk-seq data, injury models, interpretation of data, revising intellectual content, administrative, technical, or logistic support

Dominik Haudenschild – Conception of study, design, interpretation of data, revising intellectual content. Obtaining of funding, administrative, technical, or logistic support.

CHAPTER III: A Review of Surgical Models for Knee Post-Traumatic Osteoarthritis in Sheep

Yang Song, Dustin M. Leale, Scott A. Katzman, Yik HN Jasper, Dominik R. Haudenschild

This work will be submitted to the journal:

Veterinary Surgery

Pending Co-author Approval

ABSTRACT

Post-traumatic osteoarthritis (PTOA) of the knee is a disease characterized by articular cartilage injury caused by trauma to joint. The etiology and pathogenesis of PTOA have not been fully elucidated, highlighting the need to for animal models to better define its pathological mechanism and develop effective diagnostic and treatment strategies. The knee joint of sheep displays kinematics similar to that of a human knee, making it a suitable model of PTOA. Several surgical models for the induction of PTOA in sheep have been developed, and each technique has its advantages and limitations. This review draws on published literature to summarize sheep PTOA surgical models, their prior use, and discuss their strengths. This will provide a reference for the most appropriate surgical models of PTOA in this species. The surgical methods we review include transection (ACL-T), partial ACL transection (p-ACL-T), ACL transection and subsequent repair (ACL-R), meniscectomy, partial meniscectomy, modified Hulth method, and the chondral defect method.

Keywords: Surgical model; Post-traumatic osteoarthritis; Sheep; Animal models, osteoarthritis, large animal models

INTRODUCTION

Post-traumatic osteoarthritis (PTOA) is a common type of osteoarthritis (OA) initiated by trauma to the knee joint tissues[150, 151]. Prior research has highlighted the complex disease mechanisms, irreversible progression, and current lack of clinical treatment options of PTOA[76, 152]. With the gradually increasing incidence of knee OA, the average annual medical expenditure aimed at diagnosis and treatment in the United States is approximately $265.4 billion [153]. The high morbidity and medical burden associated with knee OA – along with the current gap in understanding the disease pathogenesis – highlight the need for further study. Due to obvious ethical limitations, traumatic invasive biological and biomechanical analysis of PTOA are restricted in humans [154]. The establishment of animal models

remains the preferred method for studying PTOA pathology and treatment development. The ideal animal model should be able to simulate and mimic the pathophysiological process of PTOA and allow for the investigation of its mechanical mechanism and biochemistry under controlled conditions. Many species, both small and large, have been used to develop PTOA models. In this review we will discuss sheep as a surgical animal model for PTOA.

Species used for small animal models include mice, rats, rabbits, and guinea pigs. While species used for large animal models include dogs, pigs, mini pigs, goats, sheep, horses and nonhuman primates. Compared with large animal models, small animals mature faster, are less expensive, and are easier to manipulate. However, due to the differences in anatomy, biomechanics, and physiology between small animals and humans, the results obtained from small animal research during drug development may not consistently translate to humans with equal effectiveness[155]. Compared to small animal models, large animal models have the advantages of similar anatomical structure and biomechanics to humans; the ability to simulate human injury conditions and more readily available tissue for analysis [156]. However, ethical concerns and higher costs associated with the use of large animals has limited their widespread use as models of PTOA.

Sheep provide an excellent large animal model since human and sheep knees share a similar kinematic pattern [157] and anatomical size [158]. Primary similarities include the surface area and thickness of articular cartilage along with the firmness of subchondral bone [159]. Relative to other large animal models, sheep are easy to handle, like to live in groups, are easy to raise, and can be purchased in large numbers. Further, representative samples of the synovial membrane, cartilage, subchondral bone, and synovial joint fluid are plentiful and easy to harvest. Induction of PTOA in this species can be performed through minimally invasive arthroscopic techniques [160]. Therefore, the sheep model can simulate the kinematic characteristics of human knee joint[161, 162] and it has been widely used to study human PTOA disease[163, 164].

Among animal induced PTOA models, a variety of surgical methods to study PTOA and joint recovery have been established (Table 3.1, Figure 3.1). The main purpose of this review is to describe the pathophysiologic features, general severity, and time-course of PTOA observed with the different methods for inducing PTOA in a sheep model of knee OA. This information can subsequently be used by investigators to select the most appropriate model and tailor it to their individual needs.

Table 3.1. Overview of Ovine surgical models of PTOA

Methods	Specific Operation	Timeframe of Observed Results
ACL-T	Complete ACL transection	● 2-4 weeks: Degeneration of cartilage, onset of OA[165] ● 8 weeks: early OA manifestations[166]
p-ACL-T	Partial ACL transection	● 20 weeks: osteophyte formation, cartilage damage[167] ● 40 weeks: obvious gross and histological damage[168]
ACL-R	Complete ACL transection, followed by reconstruction	● 2 weeks: Significant inflammation with return to baseline levels 20 weeks[169] ● 20 weeks: early PTOA [169, 170]
Meniscectomy	Complete removal of the medial or lateral meniscus	● 3 months: cartilage surface fibrillated and osteophyte formation[171]; ● 6 months: local articular cartilage degeneration[172]
Partial meniscectomy	Partial defect in meniscus	● 6 months: visible cartilage damage [173, 174]
Modified Hulth methods	1. ACL-T with meniscectomy	● 12 weeks: cartilage defect formation[175];
	2. ACL-T with MCL-T	● 20 weeks: cartilage surface fibrillation, rupture, and small cartilage loss[176, 177]
Chondral Defects method	Direct induction of cartilage damage	● 2-3 months: Irregular chondral organization, tide line broken, and cartilage matrix lost Col-II [178].

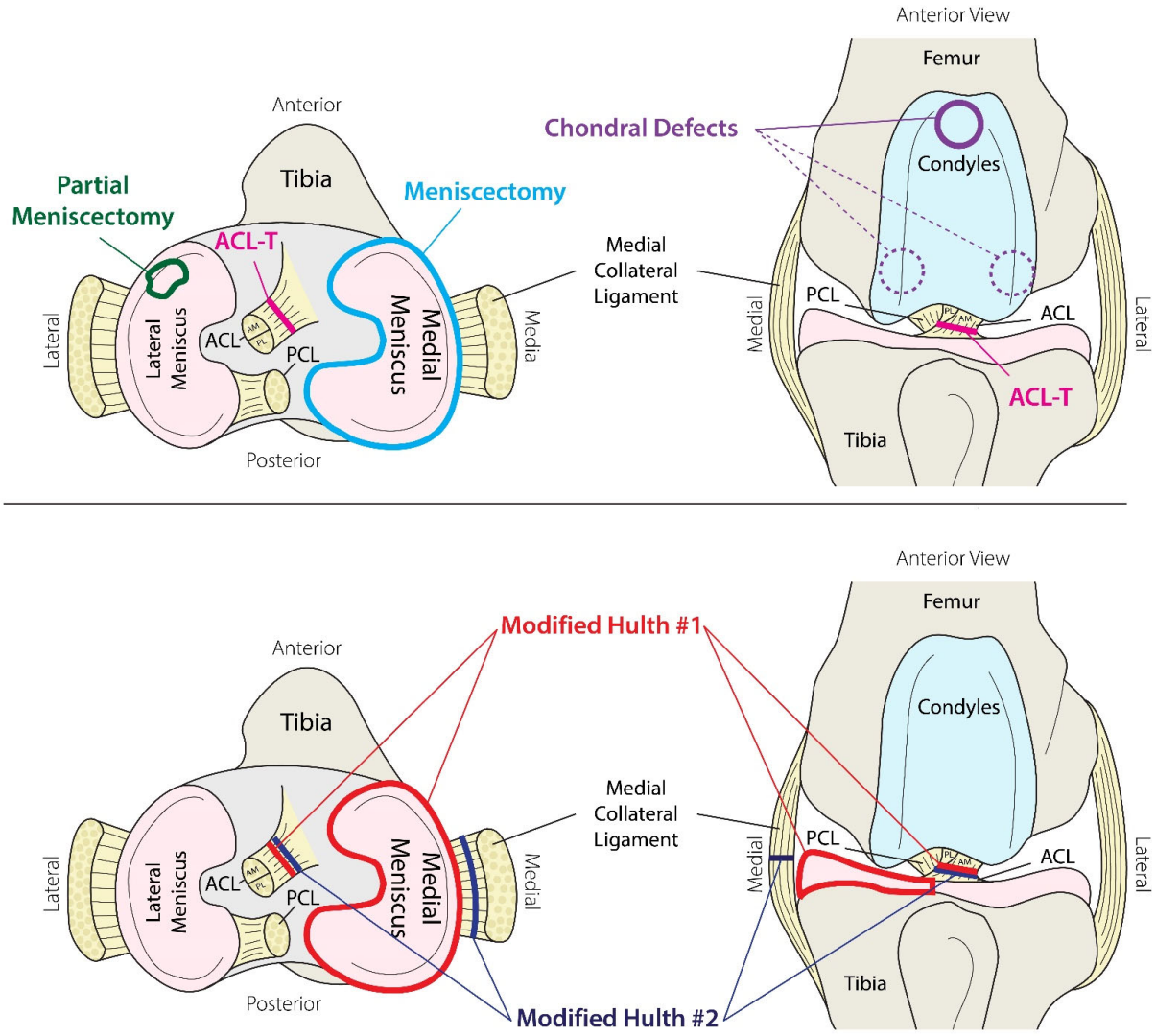

Figure 3.1: Visual overview of surgical sites in selected Ovine PTOA models. Highlighted areas and lines indicate surgical locations targeted in each PTOA Model.

SURGICAL METHODS

1. ACL-T

Anterior cruciate ligament transection (ACL-T) is a low complexity surgical method for inducing PTOA in animal models. ACL-T can be used to surgically simulate traumatic ACL rupture that can occur via injury.

This results in joint instability and weight bearing concentration, which causes cartilage damage in the areas of this concentration, and finally leads to PTOA [78, 179].

M. Atarod et al. found that in the sheep ACL-T model, proteoglycan-4 concentration was significantly increased two to four weeks after modeling, while hyaluronic acid (HA) concentration was significantly reduced, and the molecular weight distribution of HA also shifted to a lower – more fragmented – range. Due to changes in the composition of the synovial fluid and reduction of cartilage boundary lubricant, degenerative changes in the articular cartilage develop. Consequently OA may begin in two to four weeks after ACL-T [165]. In another study, J. Moya-Angeler demonstrated that the knee joint begins to show osteophyte formation and cartilage lesions within the femoro-tibial joint at week eight post ACL-T in sheep, a manifestation of early OA[166]. It is of note that in the interval between induction of PTOA using ACL-T and twenty weeks post induction, some abnormal movements of the knee joint were increased which is indicative of progressive joint instability. In the ACL-T model, the most obvious changes in kinematics are an increase in anterior and posterior translation of the tibia. Also noticed were slight increases in internal and external rotation, as well as abduction and adduction of the joint[180].

The ACL-T method results in a rapid, stable, and repeatable sheep PTOA model inducing synovial and bone changes similar to that seen in humans [181]. This model can be used to study the changes of cartilage and synovial fluid associated with early OA, as well as the changes associated with menisci [182], collateral ligaments and posterior cruciate ligament (PCL) load after ACL-T [183]. Overall, this model is reliable, surgically accessible, and generates PTOA degeneration within four to eight weeks.

2. Partial anterior cruciate ligament transection (p-ACL-T)

Anatomically, the ACL has two functional regions: the anterior medial bundle (AMB) and posterior-lateral bundle (PLB)[184], shown in Figure 1. These two components counteract, but complement one another

functionally, and each bundle is under tension under opposite circumstances. The PLB is tense when the knee is extended, and AMB is tense when the knee is flexed, and these differences reflect the anatomical basis of ACL partial rupture[185]. P-ACL rupture of AMB or PLB is common and accounts for about 10% to 28% of all ACL injuries[186].

Surgically, this injury can be simulated by a partial transection of the ACL. This compromises the integrity of the joint, resulting in instability, and leads to PTOA. M. Shekarforoush et al. reported that cartilage damage and osteophyte formation have been found after p-ACL(AMB) rupture at forty weeks[167]. I. Barton established a sheep model of p-ACL-T and found that although the progress of PTOA was not obvious at twenty weeks, compared with the control group, osteophytes had begun to develop and the articular cartilage had begun to degenerate. At fourty weeks, p-ACL-T had obvious gross and histological lesions, and these abnormalities gradually increased over time[168].

Compared to the ACL-T model, the p-ACL-T model induces a similar disease outcomes and joint degeneration, however it involves a longer time course with slower disease progression measured in months versus days or weeks. This milder model may more accurately simulate the longer disease progression in humans. Therefore, this may be a suitable model for investigators who want to study the development and progression of PTOA over a longer time-period.

3.ACL reconstruction (ACL-R)

It is widely accepted that mechanical joint instability can cause PTOA in both human[187] and animal[169] models. ACL-R is the gold standard for treating patients with ACL rupture, and the purpose of surgery is to restore the stability of the knee joint[188]. In the United States, it is estimated that as many as 200,000 patients undergo ACL-R surgery each year[189]. Repair techniques include: Single-bundle reconstruction[190], double-bundle reconstruction[191] among others [192]. Surgical reconstructions generally succeed in restoring the mechanical stability of the joint, but most patients

with ACL-R will eventually develop PTOA [193-199], possibly caused by trauma induced inflammation and catabolism [200, 201]. Due to the prevalence of ACL-R in clinical practice and the ultimate development of PTOA, ACL-R studies are included in this review alongside dedicated PTOA induction models.

Modeling the progression of PTOA in the reconstructed joint allows study of underlying pathologies combined with the ability to test possible interventions. Using sheep, J. Heard et al. found that after ACL-R surgery in sheep, there was no significant progress in joint damage assessed by the average morphological score from two to twenty weeks after surgery. However, beginning two weeks after surgery, mRNA expression of inflammatory and catabolic molecules was significantly increased in synovium and cartilage. By twenty weeks, these inflammatory and catabolic molecules returned to normal levels[169]. ACL-R model have developed morphological manifestations of early PTOA after twenty weeks [169, 170]. To test a potential treatment, A. T. Hexter et al. used an ACL-R model for the assessment of decellularized porcine derived xenografts while comparing two surgical methods of fixation for ACL reconstruction. Gait analysis, range of motion (ROM) assessment and histology after twelve weeks showed successful remodeling of xenografted tissues and a return of biomechanical function as determined by ground force reaction[202].

The ACL-R model may be most useful for studying the inflammatory factors and early catabolic mechanisms, pathogenesis, and ultimately the effects of interventions on the development of PTOA, especially in the absence of mechanical instability. Finally, this model is valuable as it is highly applicable to the current clinical treatment of ACL injuries in humans.

4. Complete meniscectomy

Meniscal injury is one of the most frequently occurring injuries affecting human athletes[203, 204]. One recognized treatment for meniscal injuries is meniscectomy. However, meniscectomy can increase the

risk of knee OA by approximately sixfold [205, 206]. Nonetheless, in the United States, more than 350,000 patients over the age of thirty-five undergo meniscectomy each year[207] largely because – if the primary meniscal injury is left untreated – it will lead to more serious consequences[208].

Sheep meniscectomy can reliably induce local cartilage, bone, and synovial disorders, which is very similar to human PTOA secondary to meniscectomy[164, 209]. A. Young, established a model of PTOA by performing a complete lateral meniscectomy on sheep and found that three months after surgery, cartilage surface fibrillation, and osteophytosis was observed on histologic and gross morphologic examination[210]. These findings are consistent with the development of early OA. R.C. Appleyard established a model of bilateral lateral meniscectomy in sheep and found that three months after meniscectomy, there was increased fibrosis, and within the articular cartilage: increased thickness and loss of proteoglycan indicative of hypertrophy[172]. These are typical pathological indicators of early OA[171]. In another experiment using a model of lateral meniscectomy in sheep, significant local articular cartilage degeneration and compensatory changes occurred across the lateral femorotibial compartment six months after the induction of PTOA[172]. Lubis et al used a lateral meniscectomy model to induce OA to assess injectable treatments[211], four weeks post injury knees showed signs of early OA radiologically before treatment.

Meniscectomy provides an effective model of PTOA particularly in modeling PTOA stemming from meniscal injury. This model reliably recreates early structural degradation and tissue level damage in the one to four month time-span following surgery.

5. Partial meniscectomy

A partial meniscectomy is another treatment option available following meniscal injury. However, similar to ACL-R, long-term cartilage protection has not been achieved using this treatment method, and it has been of limited value in clinical practice [212].

Due to the homology of the menisci, as well as viscoelastic similarities [213, 214], partial meniscectomy in sheep provides a useful simulation of human knee joint changes after partial meniscectomy. K. Gruchenberg, et al. compared the traditional treatment of partial medial meniscectomy to newer surgical scaffolds observed over three to six months. They found significant cartilage damage occurred in the partial meniscectomy group relative to sham and scaffold treated knees [173, 174]. A. Gigout applied medial meniscus transection in sheep to study the effects of a modified growth factor treatment in a PTOA model [215]. Treated animals exhibited minor improvement on weightbearing in the fourteen weeks following injury, with improved gross morphology. D.G. Cojocaru, used a partial medial meniscectomy model in sheep to evaluate meniscal transplantation and found the meniscus had collagen type I-rich repair tissue formation in the transplanted group 6 months after surgery[214, 216].

The partial meniscectomy PTOA model is suited for investigation into meniscal injury and allows for further study of meniscus transplantation on articular cartilage as well as additional factors that may influence meniscus healing. This model requires a longer time-span of several months to study post-surgical changes and for the longer-term assessment of surgical repair methods.

6. Hulth method (Modified)

The traditional Hulth method is a classic option for the surgical modeling of PTOA. Consisting of the removal of the ACL, PCL, medial collateral ligament (MCL), and the medial meniscus by surgery, it causes extreme instability of the joint causing acute severe synovial inflammation, resulting in rapid destruction of cartilage and subchondral bone. Although severe and rapid, the overall degenerative process is similar to that of the previously described models of PTOA, so this method has been widely used in rabbits[217] and mice[218]. However, due to the extreme trauma it causes with a high risk of infection, it is not appropriate for a sheep model of PTOA. In sheep, modifications are made to lessen invasiveness. This

modified version involves removal of the ACL with disruption of either the medial meniscus or MCL and has been widely used in sheep models of PTOA.

Modified Hulth: ACL-T and complete medial meniscectomy (CMM)

The first modification of the Hulth method involves the combination of ACL-T and a complete medial meniscectomy.

One study incorporated this method in combination with exercise programs of walking 100 meters per day at weeks four and six [219]. In the control group, osteophytes had developed in the anterior area of the medial tibial plateau, indicative of early OA[219, 220]. Al Faqeh, H. et al. also used the ACL-T and CMM model in sheep – at six weeks post-surgery – they found cartilage defects in the weight bearing regions of the medial tibial plateau and medial femoral condyle indicated the development of PTOA in the control group [175].

The ACL-T and CMM surgical model is useful to study the pathogenesis of PTOA, especially to observe whether a treatment can prevent cartilage damage or induce cartilage regeneration. Due to multiple surgical sites and disruptions, this is a faster model for PTOA development in the one to two month range.

Modified Hulth: ACL / MCL transection

Another, less severe, version of the Hulth method consists of combined ACL and MCL transection (ACL/MCL Tx). Frank CB used this method to induce a sheep PTOA model and found abnormal movement, cartilage surface fibrillation/fragmentation, and cartilage loss twenty weeks post-injury [221]. Also, at twenty weeks post ACL/MCL Tx, Tapper JE et al. observed cartilage degeneration, early evidence of cartilage surface destruction, osteophyte formation, and chondrocyte hyperplasia. The most

affected areas were the femoral groove, anterior medial and lateral tibial, patella and femoral surfaces, with OARSI scores increasing by approximately 50-70% [176, 177].

ACL / MCL transection is simpler and less invasive than the traditional Hulth method, and it results in a certain degree of knee stability being maintained. This is a slower model relative to ACL-T and CMM. Therefore, it is a suitable model for studying possible pathogenesis, structural outcomes, and potential interventions for moderately severe PTOA.

7. Chondral and osteochondral defect methods

Chondral or osteochondral defects methods involve articular cartilage being directly damaged surgically, resulting in the development of OA without joint destabilization. Since the damage is directly induced at a targeted location, this model is often used to evaluate the efficacy of cartilage repair strategies on focal defects, but the affected knee also does develop PTOA given time.

Márcio de Oliveira Carneiro as well as Kitamura, N.et al tested repair options using six to eight mm osteochondral defects. Twelve weeks after surgery control limbs showed cartilage erosion adjacent to the surgical site [222] and general cartilage degeneration [223]. Two months after induction of a six mm osteochondral defect, Manunta, A. F. histologically observed irregular chondrocytes organization, broken cell tide lines, and a loss of proteoglycans in articular cartilage [178]. M Schinhan created seven mm defects in cartilage on the weightbearing area of the medial femoral condyle, and the sheep performed a weightbearing regimen for twelve weeks to allow PTOA development after which they were operated on with or without treatment [224]. At four months and one year post injury the untreated sheep had developed severe cartilaginous damage histologically. This model is also frequently employed with more severe osteochondral defects to assess treatments of regenerating cartilage, but that is outside the scope of this review.

Chondral defect induced cartilage degeneration mimics human conditions and can simulate cartilage damage in different anatomical sites within the human knee. Superficial cartilage defects allow for a longer-term study of cartilage pathology and progression of degradation, while more critical defects are best suited for assessment of cartilage regenerative and repair methods. The chondral defect model is one of the most effective models for observing the early pathologic cartilage manifestations and evaluating treatment efficacy for cases of PTOA. This is a suitable model for observing the slower manifestations of OA, the protective or reparative effects of drugs and engineered constructs on cartilage when a more severe osteochondral defect is induced [225, 226].

Arthrotomy versus Arthroscopy

At present, the main surgical methods for inducing PTOA in sheep include arthroscopy and arthrotomy. In clinical human medicine, arthroscopic surgery is typical for the diagnosis and treatment joint diseases [227], this has the advantages of less trauma, faster recovery, and less bleeding than arthrotomy [228, 229]. However, at present, there is no clear evidence that arthroscopic surgery is better than arthrotomy in establishing a PTOA model for sheep. Previous studies have shown that pure arthrotomy has no relation to the occurrence and development of PTOA [169, 221]. No morphological differences were found between the arthrotomy surgical and non-surgical joints [230]. Therefore, both arthroscopy and arthrotomy are valid techniques for establishing a sheep PTOA model.

Table 3.2. Characteristics of surgical PTOA models in sheep

Methods		Advantages	Limitations	Examples of Measurement	Examples of Treatments
ACL Trauma	ACL-T p-ACL-T ACL-R	● Stable and reproducible ● Minimal surgical trauma [231] ● Models human synovial and bone changes well	● Longer development time of PTOA ● Surgery alone may cause traumatic synovial inflammation and affect the biochemical metabolism of synovium and cartilage [230] ● There is no standard ACL-R, different surgical methods may affect the results [190, 192]	● Study changes of cartilage and synovial fluid [165] ● Study changes in the load of the other ligaments of the knee[184] ● Study pathological process of cartilage degeneration[231] ● Assess mRNA expression levels for inflammatory, degradative, and structural molecules[168] ● Conduct biological and biomechanical analysis[232] ● Conduct gait and joint kinematics analysis[170] ● Evaluate PTOA's inflammatory factors and early catabolic mechanisms[201] ● Observe the pathology and occurrence of PTOA [164]	Observe drug treatments on PTOA development [168]: ● Methylprednisolone a cetate Compare Surgical reconstructive methods [169]
Meniscectomy	Meniscectomy Partial Meniscectomy	● Meniscal injuries are stable ● Minimal disruption within the joint environment [233]	● More technical surgery which requires a larger incision and careful hemostasis [209] ● The surgery takes a longer time than ACL-T to develop into PTOA [234] Sheep have to bear weight immediately post-operation, this may affect the observation of meniscus healing [237]	● Evaluate the clinical and pathological outcomes of cartilage and subchondral degradation ● Evaluate the biomechanical properties of meniscus tissue [213] ● Evaluate biomechanics of cartilage[160] ● Evaluate the inflammatory factors in the early stage of PTOA [235]	Observe the effects of different meniscus transplantation [235-238], repair [208] and immobilization [239]
Modified Hulth method	ACL-T+CMM ACL/MCL Tx	● While less traumatic that the Hulth Method, these provide multi-trauma models of PTOA modeling more severe injury and subsequent PTOA	● Large trauma may influence the joint responses to neuromuscular control systems [221] ● Greater surgical manipulation of the joint increases secondary inflammatory mediators may affect the experimental data.	● Evaluate joint kinematics and biomechanical research [240] ● Observe pathological characteristics of PTOA	Study the effect of intra-articular injection of different drugs on the effect of PTOA[220] ● TGF-β3 ● BMP-6 ● Stem cells (ADSCs or BMSCs)
Chondral Defects		● Joint inflammation is more mild than other models ● The operation is simple ● It can accurately model clinical cartilage damage ● Allows for the selection of defect location for precise studies [225, 241]	● The windows of observation for different severities may be highly variable [223] ● This model of PTOA may be undesirably slow [225, 241, 242]	● Evaluate cartilage repair and PTOA development by macroscopic, histological, immunohistochemical, and biochemical analyses [243]	Observe the effect of cartilage transplantation and local drug treatment on cartilage protection and repair. ● PRP gel [222] ● DN gel [244] ● ESL cells [178] ● Chitosan-blood implants [245] ● Chitosan-glycerol phosphate/blood implant [246] ● Drilling [247] ● Microfracture [248] ● OP-1 / BMP-7 [249]

CONCLUSIONS

Deciding on the proper model of PTOA is vital to ensure appropriate severity, outcomes and pathology for each induvial study and surgeon. The relative advantages (along with disadvantages) of the previously discussed four models are summarized in Table 2 along with. Overall, ACL-based models provide the advantages of simpler surgeries, easier reproducibility, and close similarity to human PTOA progression given ACL trauma or removal. Meniscal-based models were found to be less traumatic to the overall joint but involve a more complex surgical setup. It is important to note that sheep will immediately bear weight on the knee after surgery, which means these models may not represent human injury as accurately. The modified Hulth methods represent more severe multi-trauma injuries; however, this model creates an extremely potent response, which may make observing biochemical and cytokine changes in the joint difficult to observe. As such this model may be better suited for biomechanical or structural level studies. Chondral defect models allow longer term study of inflammatory development of PTOA; however, this model takes longer to develop into wider OA and may not represent larger injuries well within shorter study timelines.

There are several commonly used methods for surgically establishing a PTOA model in sheep. The ovine model can simulate most of the histopathological, and biomechanical features of human PTOA. Choice of model should be informed by the goals of the study, resources, and skill available. Considerations specific to the mode of action of the intervention strategy should be evaluated to most align the outcomes with the progression of the PTOA model.

CONTRIBUTIONS

Yang Song – Conception of study, design, drafting of the article

Dustin M Leale – Drafting of the article, interpretation of data, revising intellectual content.

Scott Katzman - Revising intellectual content, technical support

Jasper Yik – Interpretation of data, revising intellectual content, administrative, technical, or logistic support

Dominik Haudenschild – Conception of study, design, interpretation of data, revising intellectual content. Obtaining of funding, administrative, technical, or logistic support.

CHAPTER IV: Pharmacokinetics of an extended release flavopiridol formulation following intra-articular administration in equine middle carpal joints

Scott A. Katzman DVM DACVS-LA, Mark D. Hall MVB, Marcos Perez-Nogues LV MSc DACVS-LA, Grace Bloom, Briana Hamamoto, Dustin M. Leale, Derek Cissell VMD PhD DACVR, Chun-Yi Wu PhD, Anne K. Haudenschild PhD, Gang-yu Liu PhD, Jasper H.N. Yik PhD, Dominik R. Haudenschild PhD

This work is undergoing review in the journal:

Veterinary Surgery

ABSTRACT

Objective:

To establish the pharmacokinetics of the cyclin-dependent kinase-9 (CDK9) inhibitor flavopiridol in equine middle carpal joints, using an extended-release poly lactic-co-glycolic acid (PLGA) microparticle formulation.

Study Design:

A 6-week longitudinal pharmacokinetic study was conducted in two phases (6 weeks each) in 4 healthy horses.

Animals:

Four healthy horses without evidence of forelimb lameness.

Methods:

PLGA microparticles containing 122ug flavopiridol in 3ml saline were administered by intra-articular injection into one middle carpal joint, with empty PLGA microparticles injected into the contralateral joint as a control. Synovial fluid and plasma were collected at timepoints out to 6 weeks, and drug concentration in synovial fluid and plasma were determined using validated protocols. Additionally, synovial fluid total protein (TP), total nucleated cell count (TNCC) and differential, CBC, serum biochemistry and lameness exams performed at each of these timepoints.

Results:

Synovial fluid flavopiridol averaged 19nMol at week 1, gradually reduced to 1.4nMol by 4 weeks, and was generally below the detection limit at 5 and 6 weeks. There was no detectable flavopiridol in the plasma samples, and no adverse effects were observed at any timepoint.

Conclusion:

Intra-articular injection of PLGA microparticle-encapsulated flavopiridol was well tolerated in horses, with detectable levels of flavopiridol in the synovial fluid out to 4 weeks and negligible systemic exposure.

Clinical Significance:

Flavopiridol is a CDK-9 inhibitor with potent anti-inflammatory and analgesic activity. The extended release microparticle formulation promotes intra-articular retention of the drug and it may be an alternative to other intra-articular medications for treatment of joint disease.

INTRODUCTION

Joint disease leading to osteoarthritis (OA) is a common clinical problem in the horse.[250, 251] Surveys estimate that up to 60% of lameness is related to OA.[251, 252] Despite advances in the treatment and rehabilitation of horses with joint injuries, damage to the articular cartilage often results in the development of OA.[253] The subsequent lameness becomes limiting to a horse's long-term soundness and return to athletic performance. Inflammation and pain are common features of OA, and therapeutic interventions typically include anti-inflammatory treatments such as administration of intra-articular (IA) medications. While a variety of IA therapies are available including biologic products (autologous conditioned serum, platelet rich plasma, stem cells) polyacrylamide hydrogels, hyaluronic acid and polysulfated glycosaminoglycans among others, injection of corticosteroids remains the most commonly employed IA treatment.[254, 255] However, use of IA corticosteroids such as triamcinolone acetate and methylprednisolone acetate have been shown to have detrimental effects in addition to their potent anti-inflammatory activity. IA corticosteroid use in horses has been associated with the development of laminitis, joint flares, and loss of articular cartilage volume among other negative consequences, particularly with repeated administration.[256] Due to the adverse effects OA can have on the individual

horse, and the overarching negative impact OA has on the equine industry as a whole, there is an ongoing clinical need to develop new therapeutic strategies aimed at the prevention and treatment of OA.

Recent research demonstrates the role of cyclin-dependent kinase-9 (CDK9) in the development of OA following joint injury[87, 257-259]. CDK9 is a rate-limiting step for the transcriptional elongation of primary response genes[260-263] that include many inflammatory genes and mediators of pathways involved in OA pathogenesis.[87, 257, 258, 264] Pharmacological inhibition of CDK9 protected against the catabolic effects of pro-inflammatory cytokines in-vitro,[259] and prevented mechanical injury-induced inflammatory cytokine production, apoptosis, and the subsequent degradation of cartilage matrix in bovine explant cultures.[258] Pharmacological inhibition of CDK9 also reduced the severity of post-traumatic osteoarthritis (PTOA) in a mouse ACL rupture model of PTOA.[87, 257]

A number of small-molecule CDK9 inhibitors are being developed that either inhibit its kinase activity or target the protein for degradation.[265] The CDK9 inhibitors are primarily being developed for use as chemotherapeutics to target CDK9 in certain malignancies,[266] with the best-studied CDK9 inhibitor being flavopiridol (alvocidib). Flavopiridol is a semi-synthetic small-molecule CDK9 inhibitor that has been evaluated in 67 clinical trials currently listed on clinicaltrials.gov.[266-268] Most of the clinical trials using flavopiridol target CDK9 in the context of leukemia, which requires systemic intravenous administration of flavopiridol at high doses. These systemic studies determined that the maximum tolerated flavopiridol dose in humans and dogs is approximately 50mg/m2/day.[269, 270] Studies in rats suggest that flavopiridol is metabolized by glucuronidation in the liver and excreted in the bile,[271] and has a plasma elimination half-life of about 2 hours.[270]

In the diarthrodial joint, the synovial membrane provides a relatively impermeable barrier to the IA environment. This results in IA administration of medications being the preferred route of delivery to

achieve therapeutic concentrations. Additionally, IA delivery of medications allows for local therapeutic concentrations with low systemic burdens. However, small-molecule drugs such as corticosteroids diffuse out of the IA environment rapidly, limiting their duration of activity.[272] Newer generation IA small-molecule therapeutics are formulated using extended-release drug delivery strategies. Drug encapsulation in polylactic-*co*-glycolic acid (PLGA) is one of the most common approaches, as it serves to extend the duration of drug release as the PLGA is resorbed, and the PLGA particle size helps retain the drug within the joint space.[273]

The aim of this study was to establish the tolerability and pharmacokinetics of a sustained-release PLGA formulation of flavopiridol administered by IA injection into equine middle carpal joints. We hypothesized that IA administration of a therapeutic concentration of flavopiridol would result in detectable levels of flavopiridol in the synovial fluid, with minimal systemic exposure as measured by plasma flavopiridol levels. Further, we hypothesized that IA flavopiridol would result in no difference in lameness, joint effusion, swelling or synovial fluid parameters compared to administration of a placebo.

MATERIALS AND METHODS

Study Design

For phase 1 of the study, flavopiridol-PLGA microparticles, or blank-PLGA microparticles, were injected into the left and right middle carpal joints of four healthy horses. Synovial fluid was collected at weeks 0, 2, 4, and 6, with weekly plasma collections and lameness assessments. After a 5-week washout period, phase 2 of the study was conducted in a similar fashion to phase 1, however, the opposite joint received Flavopiridol-PLGA and the contralateral joint received blank-PLGA, and synovial fluid collection was performed at weeks 0, 1, 3, and 5.

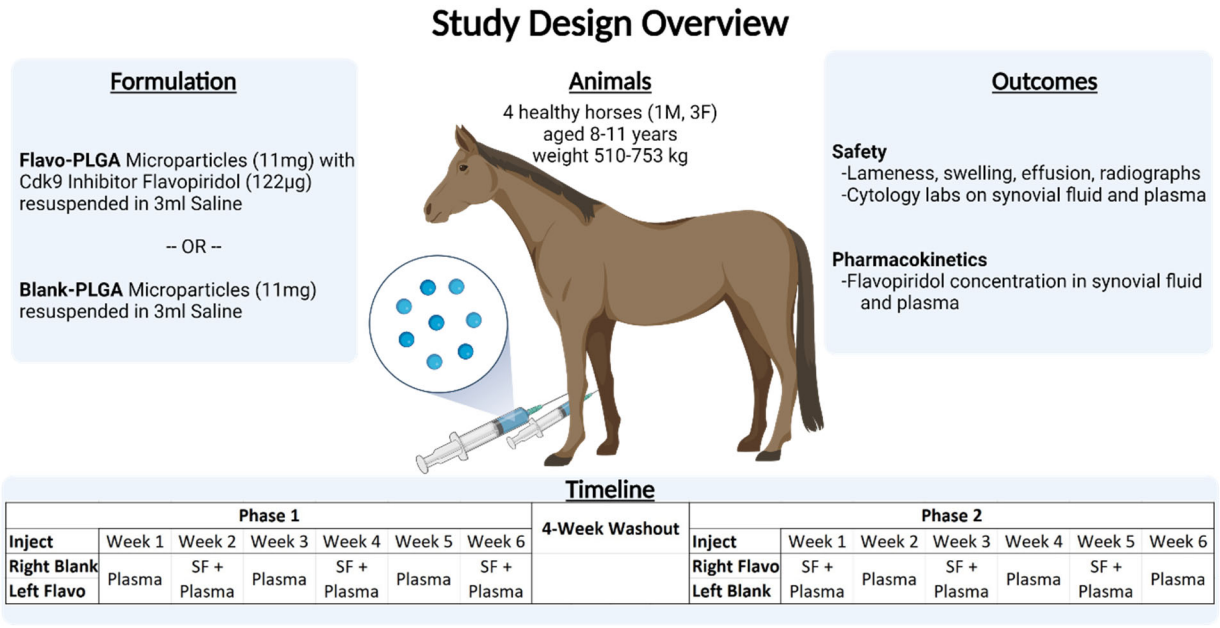

Figure 4.1: Study Design Overview **PLGA Microparticles**The formulation, manufacture, and initial characterization of the PLGA microparticles was outsourced to Phosphorex, Inc (Hopkinton, MA). At Phosphorex, the microparticles were filled as a suspension into glass vials under sterile conditions, then lyophilized and sealed. Each vial contained 122ug flavopiridol in a total of 11.29mg PLGA microparticles. The average particle size was 16.0 +/- 8.4 microns. Sterility and endotoxin testing were performed by Cambrex (East Rutherford, NJ) using industry-standard tests. The total bioburden was <12 CFU/SIP, and endotoxin levels were <0.05EU/ml. *In-vitro* release studies performed by Phosphorex indicated linear flavopiridol release out to 4 weeks, corresponding to approximately 4µg/day. Preparation of blank PLGA microparticles was the same but without the incorporation of flavopiridol into the microparticles. At the time of IA administration, 3ml sterile saline was added to each glass vial, which was then partially immersed in an ultrasonic cleaner bath (Model FS20 Fisher Scientific, Pittsburgh, PA) for 3-5 minutes to resuspend the particles fully.

Equine Inclusion Criteria

Four horses were selected from the teaching herd maintained by the UC Davis Center for Equine Health, and all procedures were approved by the Institutional Animal Care and Use Committee. All horses had physical and lameness examination performed by one author (SAK) prior to enrollment in the study. Static lameness examination included palpation and manipulation of the forelimbs with special attention paid to the carpi. Dynamic lameness examination included observation of the horses at the trot in a straight line and on a circle in both directions. Following initial observation, upper and lower forelimb flexions were performed. All horses were deemed to be free of forelimb lameness arising from the carpi and bilateral carpal radiographs were performed prior to inclusion in the study. Dorsopalmar, lateromedial, dorsolateral-palmaromedial, dorsomedial-palmarolateral and flexed lateromedial projections were obtained with no appreciable pathologic changes observed. Follow-up carpal radiographs were obtained 4 and 14 months after completion of the study. Animals were housed on dry lots with water and food *ad libitum* for the duration of the study.

Primary Cell Isolation and Culture

Primary equine chondrocytes and synoviocytes were isolated ex-vivo from animals that died of unrelated ailments (n=3 horses). Chondrocytes were digested from minced equine cartilage from the stifle joint in Trypsin-EDTA (0.25%, Gibco) for 20 minutes at 37^{o}c, followed by an overnight digestion in collagenase IV on a shaker at 37^{o}c (2mg/mL, Worthington Biochemical), in DMEM containing 5% FBS, cells were then washed, pelleted, and strained via 70um cell strainer. Synoviocytes were enzymatically isolated from minced equine synovium first by Trypsin-EDTA (0.25%, Gibco) for 30 minutes at 37^{o}c, followed by a two-hour digestion using Collagenase P (0.1%, Sigma-Aldrich) in DMEM with 10% FBS, cells were then washed, pelleted, and strained via 70um cell strainer[274]. All cells were cultured in DMEM containing 10% FBS. All assays were performed within two to three passages.

***In-vitro* Bioactivity and Toxicity**

Primary equine chondrocytes or synoviocytes (n=3 donors) were seeded in 96-well plates at 40-50% confluency by cell growth surface area. After overnight incubation, cells were treated with recombinant equine IL-1b (10 ng/ml, R&D Systems), in the presence of increasing concentration of flavopiridol (5 mg/ml stock dissolved in DMSO, diluted in growth media, Santa Cruz Biotech) for 3 hours. Cells were then washed with cold PBS and directly lyzed in wells to generate cDNA using the Cells-to-CT kit (Invitrogen) following the manufacturer's protocol. Expression of *Il6* and *18s* was quantified by qPCR in triplicates using the QuantStudio 6 instrument (Applied Biosystems) with custom made FAM probes against the equine *Il6* gene (Integrated DNA Technologies) and probes against eukaryotic *18s* (Applied Biosystems). Fold-change in *Il6* expression was calculated by the $2^{-\Delta\Delta Ct}$ method and normalized to 18S. Bioactivity of flavopiridol was calculated as the percentage of *Il6* expression in drug treated samples relative to untreated control. *Il6* probes (Forward primer: CACAACAACTCACCTCATCCT, Reverse primer: GAGGAAGGAATGCCCATGAA, FAM Probe: TCGAAGCCTTGAGGATTTCCTGCA).

Cytotoxicity was determined by quantifying the release of the mitochondrial enzyme (LDH) after 24 and 48 hours of drug exposure, measured in triplicates using the CyQuant cytotoxicity kit (Thermo Fisher). Chondrocytes or synoviocytes were seeded in 96-well plates at 40-50% confluency in triplicate wells. After overnight incubation, cells were treated with increasing concentration of flavopiridol for 24 or 48 hours. The levels of the mitochondrial enzyme LDH in the media were then measured using the CyQuant cytotoxicity kit (Thermo Fisher) according to the manufacturer's protocol.

Outlier analysis was performed on sequencing data using the Inter Quartile Range method and one bioactivity datapoint (One horse at one flavopiridol concentration) was excluded for exceeding Q3 + 1.5 IQR. To test for significant differences in cytotoxicity and bioactivity between equine chondrocytes and synoviocytes a Benjamini-Hochberg adjusted, 2 tailed, paired t-test was used at each concentration of flavopiridol.

Intra-articular Injection and Arthrocentesis

Each horse was sedated with 3-5mg Detomidine hydrochloride (Zoetis, Parsippany, NJ) administered intravenously and appropriately restrained. The dorsal aspect of each carpus underwent aseptic preparation centered over the middle carpal joint using betadine and isopropyl alcohol. Arthrocentesis was performed using a 21-gauge needle, and approximately 3mL of synovial fluid was collected for cytologic analysis. Without removing the needle, either 3.0mL of saline containing PLGA-flavopiridol microparticles, or 3.0ml of saline containing blank-PLGA microparticles was injected into the joint. All injections and all subsequent synovial fluid collections analyses were performed by one author (SAK) who was blinded to which joint (left or right) received the flavopiridol or blank microparticles. For phase 1 of the study, bilateral middle carpal joint arthrocentesis was performed at weeks 0, 2, 4, and 6. For phase 2, arthrocentesis was performed on weeks 0, 1, 3, and 5. The joint receiving flavopiridol microparticles in phase 1 received blank microparticles in phase 2, and *vice-versa*, and there was a 5-week washout period between phases 1 and 2 (Figure 4.1).

Plasma Pharmacokinetics

Plasma was collected weekly for both phase 1 and 2. For full plasma pharmacokinetics analysis, in phase 2 we collected plasma at 30-min, 1-hr, 2-hr, 4-hr, 8-hr, 24-hr, 2-day, 3-day, 4-day, and 5-day timepoints.

Lameness Grading

At each timepoint and prior to arthrocentesis, each horse was observed, and video recorded while walking and trotting in a straight line. 12 months after completion of data collection, the videos were randomized and independently evaluated by 3 equine veterinarians (SAK, MPN, MDH) experienced in lameness evaluation. Lameness was graded using the 5-point scale described by the American Association of Equine Practitioners.[275] In addition, range of motion was assessed weekly, and carpi

were examined for signs of periarticular swelling, effusion, or other signs of discomfort upon palpation or manipulation.

Flavopiridol Quantification in Plasma and Synovial Fluid

Flavopiridol was quantified in dipotassium-EDTA plasma and synovial fluid using LC-MS/MS with validated methods on a Waters Acquity I-Class UPLC and Xevo TQ-S Mass Spectrometer IVD system (Waters, Milford, MA). The lower limit of quantification in plasma and synovial fluid were 500pg/ml (1.25nM) and 50pg/ml (0.125nM), respectively, and both assays were linear to 1000ng/ml. For comparison, flavopiridol is typically active at 10-300nM concentrations. Additionally, CBC and serum biochemistry as well as routine synovial fluid analysis including TP, TNCC and TNCC differential, were performed at each timepoint.

Statistical Analysis and Blinding

A Huber robust outlier test was performed on all outcome measurements.[276] To determine which experimental factors had a significant effect on pharmacokinetic properties, multivariable linear regression modeling was performed using multiple independent variables (drug formulation, post-injection time point, animal, experimental phase, and side of injected leg) against each single dependent outcome measurement. All data is reported as mean ± standard deviation. To evaluate flavopiridol concentration in the synovial fluid and synovial fluid cytology over time, matched-pair t-test with Tukey's post-hoc analysis was performed at each time point with significant differences ($p < 0.05$) indicated by an asterisk. All statistics were performed using JMP v15 (SAS, Cary, NC).

RESULTS

Four mature horses aged 8-11 years with weights ranging from 500-700 kg were enrolled in the study. There were three geldings and one mare, and breeds included three Warmbloods and one Lusitano. A

target therapeutic concentration of 20-100nM (0.8-40 ng/ml) flavopiridol was estimated from the in-vitro bioactivity and toxicity analyses (Figure 4.2).

Bioactivity assay indicated that flavopiridol inhibited Il-6 expression at a EC50 of approximately 20 and 30 nM in IL-1β-treated chondrocytes and synoviocytes, respectively. Moreover, at concentrations of 100 nM or above, flavopiridol completely suppressed Il-6 expression (Figure 4.2). In contrast, cytotoxicity was not detected across all samples, even at 300 mM of flavopiridol, which is 4 orders of magnitude greater than the EC50. No significant differences were detected in cytotoxicity or bioactivity between chondrocytes and synoviocytes.

Based on the linear 4-week in-vitro release profile of our flavopiridol-PLGA microparticle formulation, we decided on an initial dose of 11mg microparticles containing 120ug of flavopiridol for the study.

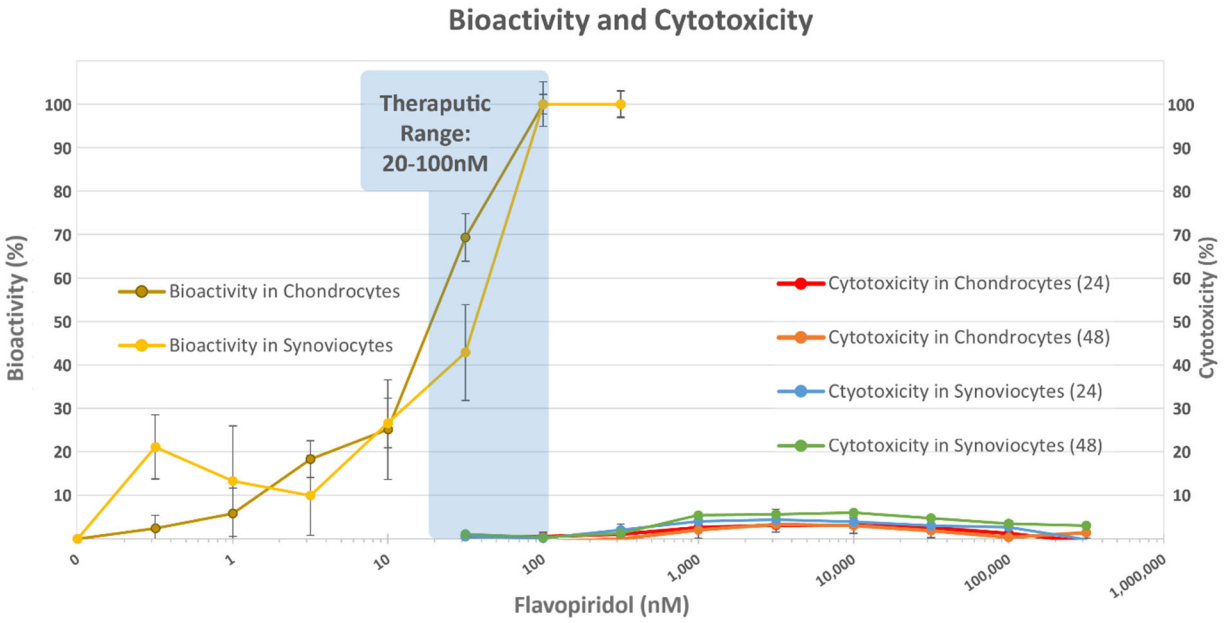

Figure 4.2: Flavopiridol has no detectable toxicity at therapeutic doses. Bioactivity was determined by the ability of flavopiridol to inhibit inflammatory stimuli (IL-1b). Toxicity was determined by quantifying LDH release from dying cells.

Safety and tolerability

All eight injections of PLGA-flavopiridol microparticles and all eight injections of PLGA-blank microparticles were well tolerated by the four horses enrolled in the study. There were no adverse effects noted at any time point. We did not observe decreased range of motion, swelling, effusion, or other signs of discomfort upon palpation or manipulation of the carpi at any timepoint. Mild and transient lameness was observed at some timepoints, but not significantly correlated with either the flavopiridol-PLGA or the blank-PLGA injections.

Synovial fluid flavopiridol concentrations

Flavopiridol remained detectable in the synovial fluid for at least four weeks. Huber outlier test identified 1 outlier in the flavopiridol concentration and the total nucleated cell measurements that were excluded from further analysis. Multivariable linear regression modeling indicated that the study phase was not a significant effect (p=0.9912), so data from phase 1 and 2 were combined into one data set for further analysis. Peak synovial flavopiridol concentrations of approximately 19nM were observed after 1 week, with gradually reducing amounts detected in weeks 2-4 (Figure 4.3). By 5 weeks the synovial fluid concentrations were below the lower limit of detection. A full pharmacokinetic analysis of plasma flavopiridol (C_{max}, C_{min}, t_{max}, AUC, etc.) was not possible because flavopiridol was not detected or fell below the lower limit of quantification of 500pg/ml at all time points.

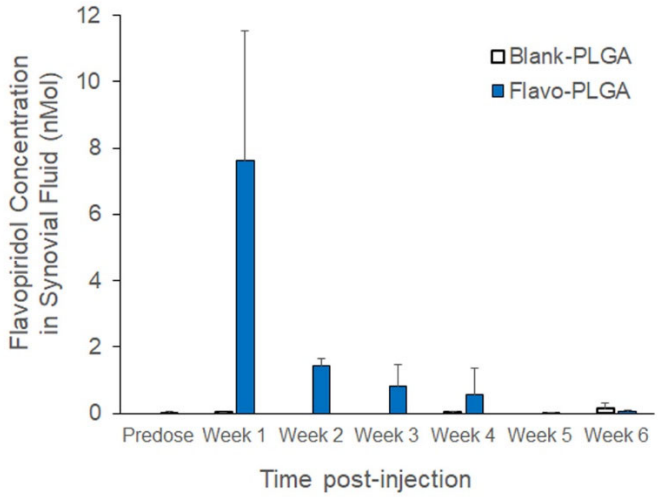

Figure 4.3: Flavopiridol concentrations in the synovial fluid over time

Synovial fluid cytology

Clinical analysis of the synovial fluid indicated a statistically significant difference in TNCC at some timepoints, with no statistically significant differences for TP, or TNCC differential. Furthermore, there was no statistically significant differences between joints receiving flavopiridol-PLGA or blank-PLGA microparticles, aside from the differences in TNCC (Figure 4.4). Importantly, although increases in TNCC were observed, values were within the normal reference range[277] (<500 cells//ml) at all timepoints.

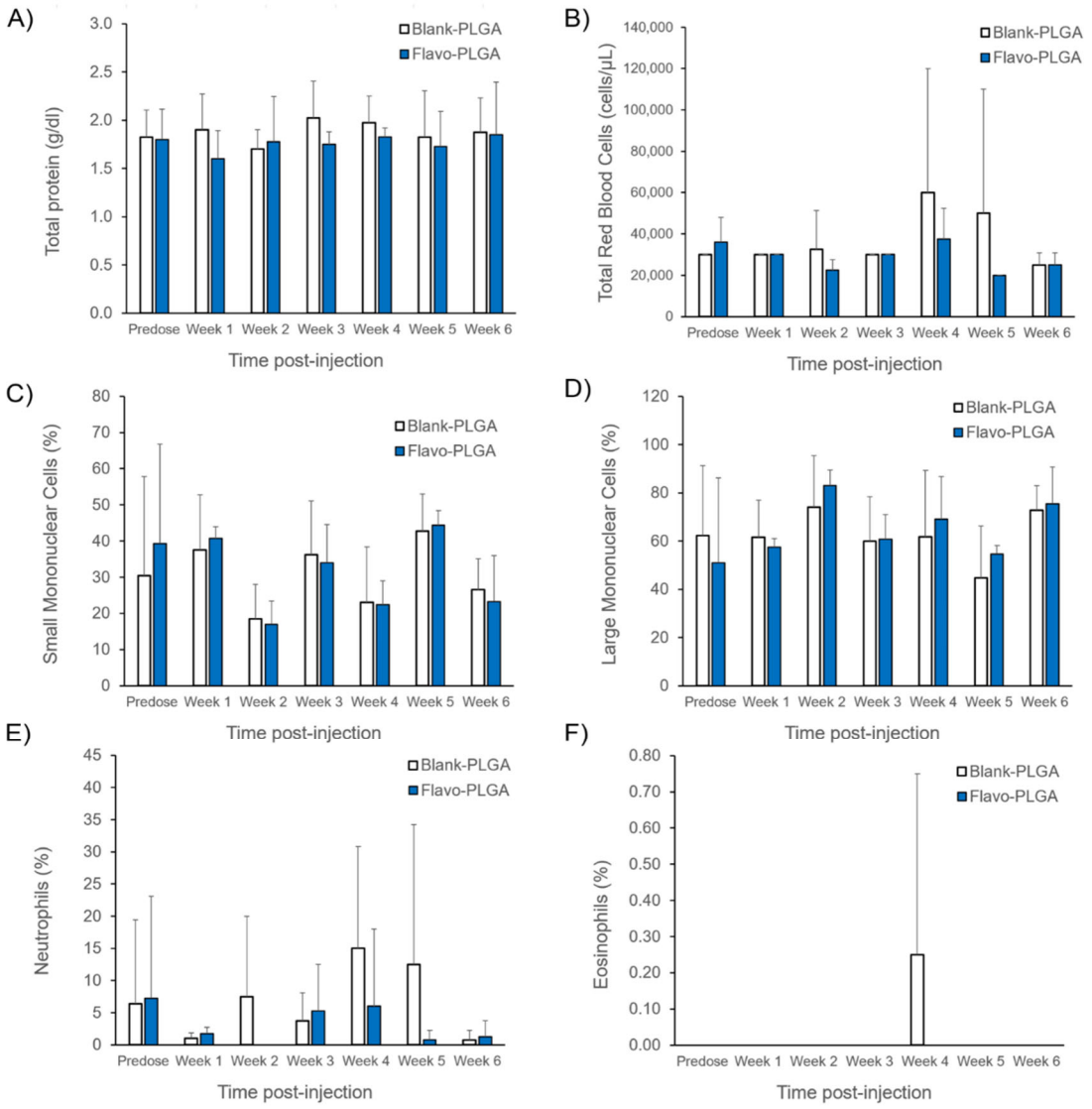

Figure 4.4: Synovial Fluid Clinical Analysis demonstrates all values are in the normal range at all time points, with no negative consequences upon administration of blank-PLGA or flavopiridol-PLGA.At baseline, the total nucleated cell counts averaged 60 cells/ml (Figure 4.5). We observed statistically significant increases ($p < 0.04$) in mean TNCC at all subsequent timepoints, ranging from approximately 100-325 cells/ml. Moreover, the mean TNCC was always higher in joints injected with blank-PLGA microparticles than in joints injected with flavopiridol-PLGA microparticles, and this difference was statistically significant ($p<0.05$) at the 1-week and 5-week time points.

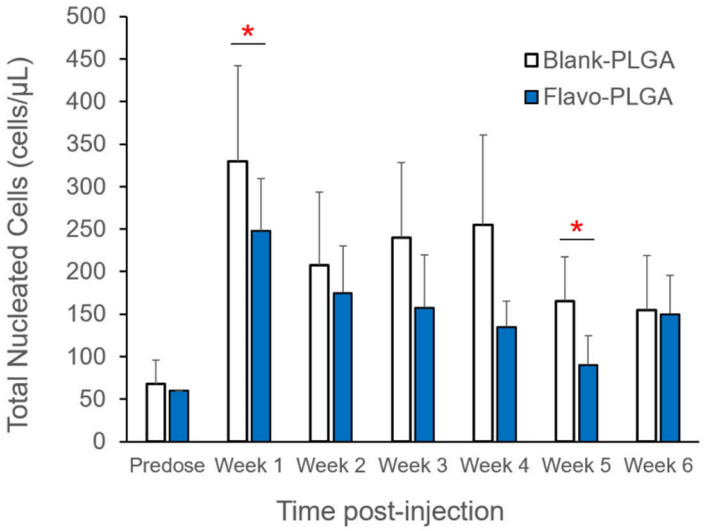

Figure 4.5: Total Nucleated Cell Count in Synovial Fluid. TNCC fall within the normal range at all time points, although elevated compared to the pre-dose values. Asterisk indicates significant difference ($p<0.05$) between blank-PLGA and flavopiridol-PLGA, with flavopiridol-PLGA consistently lower.

Radiographic Findings

There was no radiographic evidence of joint pathology prior to the start of the study, or at the follow-up timepoints of 4- and 14-monhts after study completion.

DISCUSSION

The aim of this study was to establish tolerability and pharmacokinetics of intra-articular injection of an extended release PLGA formulation of flavopiridol in equine middle carpal joints.

Main Findings

The main findings of this study are first, that intra-articular administration of an extended-release flavopiridol-PLGA microparticle formulation is well-tolerated in healthy horses, and second, that the formulation produces detectable levels of flavopiridol in the synovial fluid for approximately 4-weeks

post administration with negligible systemic exposure. Additionally, no adverse effects were observed during the entire study period. We did observe a slight, statistically significant increase in the synovial fluid TNCC, which remained within the normal range (<500 cells/ml) for all joints, and at all time points. It remains unclear whether the increased cellularity was a result of repeated arthrocentesis or a reaction to the PLGA microparticles, though it is well established that repeated arthrocentesis can result in an increase in synovial fluid parameters,[277] and that PLGA itself can be a mild inflammatory stimulus locally.[278, 279] The increased cellularity was less pronounced for joints injected with flavopiridol PGLA-microparticles than blank-PLGA-microparticles, which was anticipated given the anti-inflammatory activity of flavopiridol.

Comparisons to Steroids

Corticosteroids are among the most common intra-articular injections given to treat painful arthritic joints. Relatively high doses are typical, as soluble formulations of small-molecule drugs such as corticosteroids are rapidly lost from the joint into the general circulation, with serum peak levels typically within the first 12 hours and complete clearance within the first week.[280] Because of the relatively high doses, systemic side-effects from intra-articular corticosteroids occur frequently, and these side-effects have been thoroughly documented (reviewed in [280]). Briefly, endocrine side effects include reversible suppression of adrenocorticotropic hormone and serum cortisol levels through the hypothalamic-pituitary-adrenal axis. Metabolic effects include transiently increased blood glucose levels (especially in diabetics), decreases in markers of bone turnover and formation but not bone resorption, and growth suppression in children. Hematological effects include reductions in blood mononuclear cells and increases in polymorphonuclear leukocytes. Additional local effects of intra-articular corticosteroid injections can include loss of joint proteoglycans and changes to the mechanical integrity of cartilage,[254, 255] chondrocyte cell death (especially in combination with lidocaine),[281] and osteoporosis with long-term or repeated use.[282] Because these systemic side effects of soluble

corticosteroids can be quite severe, there is an ongoing effort to reduce the systemic exposure through formulations that remain in the joint capsule upon intra-articular injection. Common approaches include microcrystalline suspensions that dissolve slowly,[283] and extended-release formulations of steroids in bioresorbable polymers such as PLGA.[284] In these formulations, local corticosteroid concentrations remain therapeutically effective, with lower total doses, and reduced systemic exposure, and correspondingly fewer systemic side effects. However, a significant loss of joint proteoglycan content was still observed in dogs even with a locally administered extended-release formulation of triamcinolone-acetonide.[285] Cdk9 inhibitors such as flavopiridol can prevent the transcriptional activation of inflammatory genes, and as such, act through a different molecular mechanism to reduce inflammation than corticosteroids.[87, 257-259, 262, 264, 286, 287]

Safety and tolerability of flavopiridol from oncology studies

The Cdk9 inhibitor flavopiridol was the first CDK inhibitor primarily developed as a chemotherapeutic agent against certain leukemias.[277] As such, a high systemic dose of flavopiridol (at approximately 1-2 uM plasma concentration) is required to show efficacy in treating leukemia, by inducing cell cycle arrest and apoptosis of cancer cells in human patients. In contrast, our data showed that a markedly reduced flavopiridol concentration (order of magnitude lower) is sufficient to effectively inhibit the expression of inflammatory genes, without significant cytotoxicity (Figure 1.2). In addition, local delivery of flavopiridol into the joint space will only require a fraction of the total body dose and further reduce systemic drug exposure and side effects.

Limitations of the study

Limitations of this study are that it was performed in only four horses, and that it was not a terminal study, and no tissue biopsies were taken, thus, we could not histologically assess the joint tissues for signs of local toxicity due to prolonged exposure to flavopiridol. However, we would not expect

significant local toxicity at the low concentrations of flavopiridol, and there is evidence that flavopiridol can even be anti-apoptotic in bovine cartilage explants subjected to mechanical injury.[258] Additionally, no evidence of detrimental effects to the joints were observed clinically or radiographically. Lameness was subjectively graded, future studies may include objective measures.

An additional limitation is that in order to obtain weekly data points of synovial fluid flavopiridol concentrations, a two-phase study design was deemed necessary by the IACUC to avoid weekly repeated arthrocentesis. Phase 1 provided data at the 2, 4, and 6-week timepoints, while phase 2 provided data at the1, 3, and 5-week time points. To avoid possible confounding effects from repeated flavopiridol injections in the same joint, the opposite joint received the flavopiridol-PLGA microparticles in phase 2.

A further limitation is that we were unable to detect systemic plasma flavopiridol given the 500pg/ml lower limit of quantification of our HPLC/MS method. Thus, a full pharmacokinetic analysis was not possible in this study. The advantage of a locally administered extended-release formulation is that it achieves locally therapeutic concentrations of drug, with low systemic burden. We believe that an intra-articular dose high enough to produce detectable levels of plasma flavopiridol would result in local toxicity within the joint. Future studies might include a 2x and 5x dose escalation, but even at these higher doses we do not expect to detect plasma flavopiridol in 500-700kg animals.

Summary

In summary, we demonstrate that an intra-articular injection of extended-release flavopiridol-PLGA is well tolerated in healthy equine middle carpal joints. The pharmacokinetics show flavopiridol in the synovial fluid for at least four weeks, and no detectable systemic exposure. Future studies will test the beneficial effects of flavopiridol in joint disease and reinforce its potential as an intra-articular medication in horses.

CONTRIBUTIONS

Scott A Katzman – Conception and design, Analysis and interpretation of the data, Drafting of the article, Critical revision of the article for important intellectual content, Final approval of the article, Provision of study materials or patients, Statistical expertise, Obtaining of funding, Administrative, technical, or logistic support, Collection and assembly of data

Mark D Hall – Final approval of the article, Collection and assembly of data

Marcos Perez-Nogues – Final approval of the article, Collection and assembly of data

Grace Bloom – Final approval of the article, Collection and assembly of data

Briana Hamamoto – Final approval of the article, Collection and assembly of data

Dustin M Leale – Analysis and interpretation of the data, Drafting of the article, Critical revision of the article for important intellectual content, Final approval of the article, Statistical expertise, Administrative, technical, or logistic support, Collection and assembly of data, execution/design of toxicity & activity assays, cell cultures and isolation

Derek Cissell – Conception and design, Final approval of the article, Obtaining of funding

Chun-Yi Wu – Analysis and interpretation of the data, Final approval of the article, Administrative, technical, or logistic support

Anne K. Haudenschild – Analysis and interpretation of the data, Final approval of the article, Statistical expertise

Gang-yu Liu – Analysis and interpretation of the data, Final approval of the article, Administrative, technical, or logistic support

Jasper HN Yik – Conception and design, Analysis and interpretation of the data, Drafting of the article, Critical revision of the article for important intellectual content, Final approval of the article, Provision of

study materials or patients, Statistical expertise, Obtaining of funding, Administrative, technical, or logistic support, Collection and assembly of data

Dominik R Haudenschild – Conception and design, Analysis and interpretation of the data, Drafting of the article, Critical revision of the article for important intellectual content, Final approval of the article, Provision of study materials or patients, Statistical expertise, Obtaining of funding, Administrative, technical, or logistic support, Collection and assembly of data

CHAPTER V: CONCLUSION

It's well known that injury to a joint causes inflammation in the days and weeks that follow, and it is increasingly understood that inflammation drives OA development. The focus of my work has been to increase our understanding of this injury process and identify early processes that may translate into longer term inflammation. This period of AIR may provide windows and targets for therapeutic interventions and provide insight on how the initial joint trauma translates into longer-term inflammation and ultimately OA.

To study these early changes, I developed a method for applying single-cell RNA sequencing to joint tissues as a whole. It was important to include all the cells of the knee to acquire a full view of the cross-talk that is occurring in the joint during the AIR. The transcriptome measured with this method originates from the same tissue previously pulverized and sequenced in bulk, potentially allowing the comparison of whole-joint scRNA-seq with previous bulk RNA-seq data. Future studies could use this methodology to compare single cell expression with prior bulk data, as well as investigating the amount of stromal versus immune cells within this knee region.

Applying this methodology to study the AIR in mouse knees improves our understanding of the injury processes in joints. The identified AIR genes in combination with the snapshot of the cell populations expressing them, are targetable for further investigation. The combination of potential gene, pathway, and cellular sources provides a rich resource for guiding future studies. For example, synovial fibroblasts were prominent in AIR expression, and stromal cells—as a group—expressed a large amount of the AIR genes overall. Future work could focus on this tissue, or possibly the Angiopoietin-like protein pathway or Il-6, in the early timepoints after injury. Merely fifty-four genes exhibited notable upregulation at the one-hour mark, representing a relatively small and specific set for future targeting.

The knees of a human are very different from that of a mouse, but large animal models remain a reasonable steppingstone. Moving along this translational spectrum from mice to sheep, we reviewed and summarized the use of ovine surgical PTOA models establishing a convenient reference for researchers and surgeons who are planning PTOA studies in large animal models. Methods vary with the severity of injury they simulate. Thus, the scope of response within the joint ranging from the rapid and severe multi-trauma modified Hulth methods to milder chondral defect inductions. Future studies will benefit from this review as it conveniently summarizes prior uses of these models, timelines, and the benefits and complexities of these models.

Further along the translation medicine spectrum, we conducted pharmacokinetic and tolerability trials of a potential OA therapy in horses. OA is a frequent contributor to lameness in horses, with poor treatment options available currently. The treatment was well-tolerated, non-toxic, and released over time in the joint. With this data, established future work can assess the beneficial effects of Cdk9 inhibition therapy in horses, potentially creating new therapy options.

Altogether, the work presented in this thesis expands our knowledge of joint injury and supports future research into PTOA. First, by establishing protocols for digesting difficult knee tissues for sequencing. Second, by providing new insight into the AIR in the knee, providing a manageable list of genes for future research, as well as possible cell and tissue type to target them in. Third, by providing tools for investigators planning large animal model studies. Finally, by establishing the safety and viability of a potential treatment in horses.

REFERENCES

1. Findlay DM, Kuliwaba JS. Bone–cartilage crosstalk: a conversation for understanding osteoarthritis. Bone research. 2016;4(1):1-12.
2. Loeser RF, Goldring SR, Scanzello CR, Goldring MB. Osteoarthritis: a disease of the joint as an organ. Arthritis and rheumatism. 2012;64(6):1697-707. Epub 2012/03/07. doi: 10.1002/art.34453. PubMed PMID: 22392533; PubMed Central PMCID: PMCPMC3366018.
3. Scanzello CR. Role of low-grade inflammation in osteoarthritis. Curr Opin Rheumatol. 2017;29(1):79-85. doi: 10.1097/BOR.0000000000000353. PubMed PMID: 27755180; PubMed Central PMCID: PMCPMC5565735.
4. Robinson WH, Lepus CM, Wang Q, Raghu H, Mao R, Lindstrom TM, et al. Low-grade inflammation as a key mediator of the pathogenesis of osteoarthritis. Nat Rev Rheumatol. 2016;12(10):580-92. doi: 10.1038/nrrheum.2016.136. PubMed PMID: 27539668; PubMed Central PMCID: PMCPMC5500215.
5. van den Bosch MHJ. Inflammation in osteoarthritis: is it time to dampen the alarm(in) in this debilitating disease? Clinical and experimental immunology. 2019;195(2):153-66. Epub 2018/11/14. doi: 10.1111/cei.13237. PubMed PMID: 30421798; PubMed Central PMCID: PMCPMC6330652.
6. van den Bosch MHJ, van Lent PLEM, van der Kraan PM. Identifying effector molecules, cells, and cytokines of innate immunity in OA. Osteoarthritis and Cartilage. 2020;28(5):532-43. doi: https://doi.org/10.1016/j.joca.2020.01.016.
7. Krausgruber T, Fortelny N, Fife-Gernedl V, Senekowitsch M, Schuster LC, Lercher A, et al. Structural cells are key regulators of organ-specific immune responses. Nature. 2020;583(7815):296-302. doi: 10.1038/s41586-020-2424-4.
8. Prideaux M, Schutz C, Wijenayaka AR, Findlay DM, Campbell DG, Solomon LB, et al. Isolation of osteocytes from human trabecular bone. Bone. 2016;88:64-72. doi: https://doi.org/10.1016/j.bone.2016.04.017.
9. Chia LY, Walsh NC, Martin TJ, Sims NA. Isolation and gene expression of haematopoietic-cell-free preparations of highly purified murine osteocytes. Bone. 2015;72:34-42.
10. Rosengren S, Boyle DL, Firestein GS. Acquisition, culture, and phenotyping of synovial fibroblasts. Arthritis Research: Springer; 2007. p. 365-75.
11. Scialdone A, Natarajan KN, Saraiva LR, Proserpio V, Teichmann SA, Stegle O, et al. Computational assignment of cell-cycle stage from single-cell transcriptome data. Methods (San Diego, Calif). 2015;85:54-61. Epub 2015/07/06. doi: 10.1016/j.ymeth.2015.06.021. PubMed PMID: 26142758.
12. Sebastian A, Hum NR, Martin KA, Gilmore SF, Peran I, Byers SW, et al. Single-Cell Transcriptomic Analysis of Tumor-Derived Fibroblasts and Normal Tissue-Resident Fibroblasts Reveals Fibroblast Heterogeneity in Breast Cancer. Cancers. 2020;12(5):1307. PubMed PMID: doi:10.3390/cancers12051307.
13. Hao Y, Hao S, Andersen-Nissen E, Mauck III WM, Zheng S, Butler A, et al. Integrated analysis of multimodal single-cell data. Cell. 2021;184(13):3573-87. e29.
14. Xu C, Su Z. Identification of cell types from single-cell transcriptomes using a novel clustering method. Bioinformatics. 2015;31(12):1974-80. doi: 10.1093/bioinformatics/btv088. PubMed PMID: 25805722; PubMed Central PMCID: PMCPMC6280782.
15. Macosko EZ, Basu A, Satija R, Nemesh J, Shekhar K, Goldman M, et al. Highly Parallel Genome-wide Expression Profiling of Individual Cells Using Nanoliter Droplets. Cell. 2015;161(5):1202-14. Epub

2015/05/23. doi: 10.1016/j.cell.2015.05.002. PubMed PMID: 26000488; PubMed Central PMCID: PMCPMC4481139.
16. McInnes L, Healy J, Melville J. Umap: Uniform manifold approximation and projection for dimension reduction. arXiv preprint arXiv:180203426. 2018.
17. Ilicic T, Kim JK, Kolodziejczyk AA, Bagger FO, McCarthy DJ, Marioni JC, et al. Classification of low quality cells from single-cell RNA-seq data. Genome Biol. 2016;17(1):29. doi: 10.1186/s13059-016-0888-1. PubMed PMID: 26887813; PubMed Central PMCID: PMCPMC4758103.
18. Loeser RF, Olex AL, McNulty MA, Carlson CS, Callahan M, Ferguson C, et al. Disease progression and phasic changes in gene expression in a mouse model of osteoarthritis. PloS one. 2013;8(1):e54633.
19. Sebastian A, Murugesh DK, Mendez ME, Hum NR, Rios-Arce ND, McCool JL, et al. Global Gene Expression Analysis Identifies Age-Related Differences in Knee Joint Transcriptome during the Development of Post-Traumatic Osteoarthritis in Mice. International Journal of Molecular Sciences. 2020;21(1):364. PubMed PMID: doi:10.3390/ijms21010364.
20. Sunkara V, Heinz GA, Heinrich FF, Durek P, Mobasheri A, Mashreghi M-F, et al. Combining segmental bulk-and single-cell RNA-sequencing to define the chondrocyte gene expression signature in the murine knee joint. bioRxiv. 2020.
21. Amanatullah DF, Yamane S, Reddi AH. Distinct patterns of gene expression in the superficial, middle and deep zones of bovine articular cartilage. Journal of Tissue Engineering and Regenerative Medicine. 2014;8(7):505-14. doi: https://doi.org/10.1002/term.1543.
22. Sebastian A, McCool JL, Hum NR, Murugesh DK, Wilson SP, Christiansen BA, et al. Single-Cell RNA-Seq Reveals Transcriptomic Heterogeneity and Post-Traumatic Osteoarthritis-Associated Early Molecular Changes in Mouse Articular Chondrocytes. Cells. 2021;10(6):1462. doi: 10.3390/cells10061462. PubMed PMID: 34200880; PubMed Central PMCID: PMCPMC8230441.
23. Culemann S, Gruneboom A, Nicolas-Avila JA, Weidner D, Lammle KF, Rothe T, et al. Locally renewing resident synovial macrophages provide a protective barrier for the joint. Nature. 2019;572(7771):670-5. Epub 08/07. doi: 10.1038/s41586-019-1471-1. PubMed PMID: 31391580; PubMed Central PMCID: PMCPMC6805223.
24. Wu C-L, Dicks A, Steward N, Tang R, Katz DB, Choi Y-R, et al. Single cell transcriptomic analysis of human pluripotent stem cell chondrogenesis. Nature Communications. 2021;12(1):362. doi: 10.1038/s41467-020-20598-y.
25. Ding J, Adiconis X, Simmons SK, Kowalczyk MS, Hession CC, Marjanovic ND, et al. Systematic comparison of single-cell and single-nucleus RNA-sequencing methods. Nature Biotechnology. 2020;38(6):737-46. doi: 10.1038/s41587-020-0465-8.
26. Zhu L, Koneva L, Attar M, Webber J, Sansom S, Vincent T. SINGLE NUCLEI RNA-SEQUENCING OF PORCINE ARTICULAR CARTILAGE UNCOVERS THE CHONDROCYTES CLUSTERS THAT CHANGE IN RESPONSE TO MECHANICAL INJURY. Osteoarthritis and Cartilage. 2022;30:S27.
27. Thavaratnam K, Gracey E, Ratneswaran A, Vohra S, Lively S, Dupont S, et al. SINGLE NUCLEUS RNA SEQUENCING PROFILING IDENTIFIES DISTINCT CELLULAR POPULATIONS IN THE SYNOVIUM OF EARLY AND LATE STAGE RADIOGRAPHIC KNEE OA. Osteoarthritis and Cartilage. 2022;30:S118.
28. Schaum N, Karkanias J, Neff NF, May AP, Quake SR, Wyss-Coray T, et al. Single-cell transcriptomics of 20 mouse organs creates a Tabula Muris: The Tabula Muris Consortium. Nature. 2018;562(7727):367.
29. He S, Wang L-H, Liu Y, Li Y-Q, Chen H-T, Xu J-H, et al. Single-cell transcriptome profiling of an adult human cell atlas of 15 major organs. Genome biology. 2020;21(1):1-34.
30. Almanzar N, Antony J, Baghel AS, Bakerman I, Bansal I, Barres BA, et al. A single-cell transcriptomic atlas characterizes ageing tissues in the mouse. Nature. 2020;583(7817):590-5. doi: 10.1038/s41586-020-2496-1.

31. Travaglini KJ, Nabhan AN, Penland L, Sinha R, Gillich A, Sit RV, et al. A molecular cell atlas of the human lung from single-cell RNA sequencing. Nature. 2020;587(7835):619-25. doi: 10.1038/s41586-020-2922-4.
32. He H, Suryawanshi H, Morozov P, Gay-Mimbrera J, Del Duca E, Kim HJ, et al. Single-cell transcriptome analysis of human skin identifies novel fibroblast subpopulation and enrichment of immune subsets in atopic dermatitis. Journal of Allergy and Clinical Immunology. 2020;145(6):1615-28. doi: 10.1016/j.jaci.2020.01.042.
33. Qi F, Qian S, Zhang S, Zhang Z. Single cell RNA sequencing of 13 human tissues identify cell types and receptors of human coronaviruses. Biochemical and Biophysical Research Communications. 2020;526(1):135-40. doi: https://doi.org/10.1016/j.bbrc.2020.03.044.
34. Sebastian A, Hum NR, McCool JL, Wilson SP, Murugesh DK, Martin KA, et al. Single-cell RNA-Seq reveals changes in immune landscape in post-traumatic osteoarthritis. Frontiers in immunology. 2022;13:938075. Epub 2022/08/16. doi: 10.3389/fimmu.2022.938075. PubMed PMID: 35967299; PubMed Central PMCID: PMCPMC9373730.
35. Tonegawa S. Somatic generation of antibody diversity. Nature. 1983;302(5909):575-81. doi: 10.1038/302575a0.
36. Furman BD, Zeitlin JH, Buchanan MW, Huebner JL, Kraus VB, Yi JS, et al. Immune cell profiling in the joint following human and murine articular fracture. Osteoarthritis and Cartilage. 2021;29(6):915-23. doi: https://doi.org/10.1016/j.joca.2021.02.565.
37. Gelse K, Pfander D, Obier S, Knaup KX, Wiesener M, Hennig FF, et al. Role of hypoxia-inducible factor 1alpha in the integrity of articular cartilage in murine knee joints. Arthritis Research & Therapy. 2008;10(5):R111. doi: 10.1186/ar2508.
38. Pippenger BE, Duhr R, Muraro MG, Pagenstert GI, Hügle T, Geurts J. Multicolor flow cytometry-based cellular phenotyping identifies osteoprogenitors and inflammatory cells in the osteoarthritic subchondral bone marrow compartment. Osteoarthritis and Cartilage. 2015;23(11):1865-9. doi: https://doi.org/10.1016/j.joca.2015.07.021.
39. Dancey J, Deubelbeiss KA, Harker LA, Finch CA. Neutrophil kinetics in man. The Journal of clinical investigation. 1976;58(3):705-15.
40. Woodell-May JE, Sommerfeld SD. Role of Inflammation and the Immune System in the Progression of Osteoarthritis. Journal of orthopaedic research : official publication of the Orthopaedic Research Society. 2020;38(2):253-7. Epub 2019/08/31. doi: 10.1002/jor.24457. PubMed PMID: 31469192.
41. Kalaitzoglou E, Griffin TM, Humphrey MB. Innate Immune Responses and Osteoarthritis. Current rheumatology reports. 2017;19(8):45. Epub 2017/07/19. doi: 10.1007/s11926-017-0672-6. PubMed PMID: 28718060.
42. Berenbaum F. Osteoarthritis as an inflammatory disease (osteoarthritis is not osteoarthrosis!). Osteoarthritis Cartilage. 2013;21(1):16-21. Epub 2012/12/01. doi: 10.1016/j.joca.2012.11.012. PubMed PMID: 23194896.
43. Scanzello CR, Plaas A, Crow MK. Innate immune system activation in osteoarthritis: is osteoarthritis a chronic wound? Curr Opin Rheumatol. 2008;20(5):565-72. Epub 2008/08/14. doi: 10.1097/BOR.0b013e32830aba34. PubMed PMID: 18698179.
44. Orlowsky EW, Kraus VB. The role of innate immunity in osteoarthritis: when our first line of defense goes on the offensive. The Journal of rheumatology. 2015;42(3):363-71. Epub 2015/01/17. doi: 10.3899/jrheum.140382. PubMed PMID: 25593231; PubMed Central PMCID: PMCPMC4465583.
45. van den Brink SC, Sage F, Vértesy Á, Spanjaard B, Peterson-Maduro J, Baron CS, et al. Single-cell sequencing reveals dissociation-induced gene expression in tissue subpopulations. Nature Methods. 2017;14(10):935-6. doi: 10.1038/nmeth.4437.

46. Mizuhashi K, Ono W, Matsushita Y, Sakagami N, Takahashi A, Saunders TL, et al. Resting zone of the growth plate houses a unique class of skeletal stem cells. Nature. 2018;563(7730):254-8.
47. Shah KM, Stern MM, Stern AR, Pathak JL, Bravenboer N, Bakker AD. Osteocyte isolation and culture methods. BoneKEy reports. 2016;5.
48. Gulati GS, Murphy MP, Marecic O, Lopez M, Brewer RE, Koepke LS, et al. Isolation and functional assessment of mouse skeletal stem cell lineage. Nat Protoc. 2018;13(6):1294-309. Epub 05/10. doi: 10.1038/nprot.2018.041. PubMed PMID: 29748647.
49. Aronowitz JA, Lockhart RA, Hakakian CS. Mechanical versus enzymatic isolation of stromal vascular fraction cells from adipose tissue. SpringerPlus. 2015;4(1):713. doi: 10.1186/s40064-015-1509-2.
50. Banyard DA, Sarantopoulos CN, Borovikova AA, Qiu X, Wirth GA, Paydar KZ, et al. Phenotypic analysis of stromal vascular fraction after mechanical shear reveals stress-induced progenitor populations. Plastic and reconstructive surgery. 2016;138(2):237e.
51. Senesi L, De Francesco F, Farinelli L, Manzotti S, Gagliardi G, Papalia GF, et al. Mechanical and enzymatic procedures to isolate the stromal vascular fraction from adipose tissue: preliminary results. Frontiers in cell and developmental biology. 2019;7:88.
52. van den Brink SC, Sage F, Vértesy Á, Spanjaard B, Peterson-Maduro J, Baron CS, et al. Single-cell sequencing reveals dissociation-induced gene expression in tissue subpopulations. Nat Methods. 2017;14(10):935-6. Epub 2017/09/30. doi: 10.1038/nmeth.4437. PubMed PMID: 28960196.
53. Marsh SE, Walker AJ, Kamath T, Dissing-Olesen L, Hammond TR, de Soysa TY, et al. Dissection of artifactual and confounding glial signatures by single-cell sequencing of mouse and human brain. Nature Neuroscience. 2022;25(3):306-16. doi: 10.1038/s41593-022-01022-8.
54. Adam M, Potter AS, Potter SS. Psychrophilic proteases dramatically reduce single-cell RNA-seq artifacts: a molecular atlas of kidney development. Development. 2017;144(19):3625-32. doi: 10.1242/dev.151142.
55. Steinberg J, Southam L, Fontalis A, Clark MJ, Jayasuriya RL, Swift D, et al. Linking chondrocyte and synovial transcriptional profile to clinical phenotype in osteoarthritis. Annals of the Rheumatic Diseases. 2021;80(8):1070. doi: 10.1136/annrheumdis-2020-219760.
56. Sanjurjo-Rodriguez C, Baboolal TG, Burska AN, Ponchel F, El-Jawhari JJ, Pandit H, et al. Gene expression and functional comparison between multipotential stromal cells from lateral and medial condyles of knee osteoarthritis patients. Scientific Reports. 2019;9(1):9321. doi: 10.1038/s41598-019-45820-w.
57. Song J, Lee M, Kim D, Han J, Chun C-H, Jin E-J. MicroRNA-181b regulates articular chondrocytes differentiation and cartilage integrity. Biochemical and biophysical research communications. 2013;431(2):210-4.
58. López-Armada MJ, Caramés B, Lires-Deán M, Cillero-Pastor B, Ruiz-Romero C, Galdo F, et al. Cytokines, tumor necrosis factor-α and interleukin-1β, differentially regulate apoptosis in osteoarthritis cultured human chondrocytes. Osteoarthritis and Cartilage. 2006;14(7):660-9. doi: https://doi.org/10.1016/j.joca.2006.01.005.
59. Huang Y, Zhang P. Evaluation of machine learning approaches for cell-type identification from single-cell transcriptomics data. Briefings in Bioinformatics. 2021;22(5). doi: 10.1093/bib/bbab035.
60. Oller-Moreno S, Kloiber K, Machart P, Bonn S. Algorithmic advances in machine learning for single-cell expression analysis. Current Opinion in Systems Biology. 2021;25:27-33. doi: https://doi.org/10.1016/j.coisb.2021.02.002.
61. Kuo D, Ding J, Cohn IS, Zhang F, Wei K, Rao DA, et al. HBEGF+ macrophages in rheumatoid arthritis induce fibroblast invasiveness. Science Translational Medicine. 2019;11(491):eaau8587. doi: doi:10.1126/scitranslmed.aau8587.

62. Zhang F, Wei K, Slowikowski K, Fonseka CY, Rao DA, Kelly S, et al. Defining inflammatory cell states in rheumatoid arthritis joint synovial tissues by integrating single-cell transcriptomics and mass cytometry. Nature immunology. 2019;20(7):928-42.
63. Zhang H, Cai D, Bai X. Macrophages regulate the progression of osteoarthritis. Osteoarthritis and Cartilage. 2020;28(5):555-61. doi: https://doi.org/10.1016/j.joca.2020.01.007.
64. Wu CL, Harasymowicz NS, Klimak MA, Collins KH, Guilak F. The role of macrophages in osteoarthritis and cartilage repair. Osteoarthritis and Cartilage. 2020;28(5):544-54. doi: https://doi.org/10.1016/j.joca.2019.12.007.
65. Bailey KN, Furman BD, Zeitlin J, Kimmerling KA, Wu CL, Guilak F, et al. Intra-articular depletion of macrophages increases acute synovitis and alters macrophage polarity in the injured mouse knee. Osteoarthritis and Cartilage. 2020;28(5):626-38. doi: https://doi.org/10.1016/j.joca.2020.01.015.
66. Takayanagi H. Osteoimmunology: shared mechanisms and crosstalk between the immune and bone systems. Nature Reviews Immunology. 2007;7(4):292-304. doi: 10.1038/nri2062.
67. Pan J, Wang B, Li W, Zhou X, Scherr T, Yang Y, et al. Elevated cross-talk between subchondral bone and cartilage in osteoarthritic joints. Bone. 2012;51(2):212-7. Epub 2011/12/27. doi: 10.1016/j.bone.2011.11.030. PubMed PMID: 22197997; PubMed Central PMCID: PMCPMC3335971.
68. Wu CL, Harasymowicz NS, Klimak MA, Collins KH, Guilak F. The role of macrophages in osteoarthritis and cartilage repair. Osteoarthritis Cartilage. 2020;28(5):544-54. Epub 2020/01/12. doi: 10.1016/j.joca.2019.12.007. PubMed PMID: 31926267; PubMed Central PMCID: PMCPMC7214213.
69. Chou CH, Jain V, Gibson J, Attarian DE, Haraden CA, Yohn CB, et al. Synovial cell cross-talk with cartilage plays a major role in the pathogenesis of osteoarthritis. Sci Rep. 2020;10(1):10868. Epub 2020/07/04. doi: 10.1038/s41598-020-67730-y. PubMed PMID: 32616761; PubMed Central PMCID: PMCPMC7331607 C.B.Y. and R.M.L. are employees of Unity Biotechnology and played a role in the conceptualization of the study and in preparation of the manuscript. This work was funded in part by Unity Biotechnology, however, Unity Biotechnology had no role in the preparation of the manuscript, data collection or decision to publish this study. V.B.K. has been a periodic consultant for Unity Biotechnology providing periodic advice on clinical study design, unrelated to this study and has no competing interests to declare.
70. Liu-Bryan R. Synovium and the innate inflammatory network in osteoarthritis progression. Current rheumatology reports. 2013;15(5):323.
71. Benigni G, Dimitrova P, Antonangeli F, Sanseviero E, Milanova V, Blom A, et al. CXCR3/CXCL10 Axis Regulates Neutrophil-NK Cell Cross-Talk Determining the Severity of Experimental Osteoarthritis. Journal of immunology (Baltimore, Md : 1950). 2017;198(5):2115-24. Epub 2017/01/22. doi: 10.4049/jimmunol.1601359. PubMed PMID: 28108560.
72. Brown TD, Johnston RC, Saltzman CL, Marsh JL, Buckwalter JA. Posttraumatic osteoarthritis: a first estimate of incidence, prevalence, and burden of disease. Journal of orthopaedic trauma. 2006;20(10):739-44.
73. Lo J, Chan L, Flynn S. A systematic review of the incidence, prevalence, costs, and activity and work limitations of amputation, osteoarthritis, rheumatoid arthritis, back pain, multiple sclerosis, spinal cord injury, stroke, and traumatic brain injury in the United States: a 2019 update. Archives of physical medicine and rehabilitation. 2021;102(1):115-31.
74. Thomas AC, Hubbard-Turner T, Wikstrom EA, Palmieri-Smith RM. Epidemiology of Posttraumatic Osteoarthritis. J Athl Train. 2017;52(6):491-6. Epub 2016/05/05. doi: 10.4085/1062-6050-51.5.08. PubMed PMID: 27145096; PubMed Central PMCID: PMCPMC5488839.
75. Delco ML, Kennedy JG, Bonassar LJ, Fortier LA. Post-traumatic osteoarthritis of the ankle: a distinct clinical entity requiring new research approaches. Journal of Orthopaedic Research. 2017;35(3):440-53.

76. Dilley JE, Bello MA, Roman N, McKinley T, Sankar U. Post-traumatic osteoarthritis: A review of pathogenic mechanisms and novel targets for mitigation. Bone Reports. 2023;18:101658. doi: https://doi.org/10.1016/j.bonr.2023.101658.
77. Furman BD, Kimmerling KA, Zura RD, Reilly RM, Zlowodzki MP, Huebner JL, et al. Brief report: articular ankle fracture results in increased synovitis, synovial macrophage infiltration, and synovial fluid concentrations of inflammatory cytokines and chemokines. Arthritis & rheumatology. 2015;67(5):1234-9.
78. Simon D, Mascarenhas R, Saltzman BM, Rollins M, Bach BR, MacDonald P. The Relationship between Anterior Cruciate Ligament Injury and Osteoarthritis of the Knee. Advances in Orthopedics. 2015;2015:1-11. doi: 10.1155/2015/928301.
79. Riordan EA, Little C, Hunter D. Pathogenesis of post-traumatic OA with a view to intervention. Best Practice & Research Clinical Rheumatology. 2014;28(1):17-30.
80. Lotz MK. New developments in osteoarthritis: Posttraumatic osteoarthritis: pathogenesis and pharmacological treatment options. Arthritis Research & Therapy. 2010;12(3):211. doi: 10.1186/ar3046.
81. Pearson MJ, Herndler-Brandstetter D, Tariq MA, Nicholson TA, Philp AM, Smith HL, et al. IL-6 secretion in osteoarthritis patients is mediated by chondrocyte-synovial fibroblast cross-talk and is enhanced by obesity. Scientific Reports. 2017;7(1):3451. doi: 10.1038/s41598-017-03759-w.
82. Bigoni M, Sacerdote P, Turati M, Franchi S, Gandolla M, Gaddi D, et al. Acute and late changes in intraarticular cytokine levels following anterior cruciate ligament injury. Journal of Orthopaedic Research. 2013;31(2):315-21. doi: https://doi.org/10.1002/jor.22208.
83. Irie K, Uchiyama E, Iwaso H. Intraarticular inflammatory cytokines in acute anterior cruciate ligament injured knee. The Knee. 2003;10(1):93-6. doi: 10.1016/S0968-0160(02)00083-2.
84. Lieberthal J, Sambamurthy N, Scanzello CR. Inflammation in joint injury and post-traumatic osteoarthritis. Osteoarthritis Cartilage. 2015;23(11):1825-34. Epub 2015/11/03. doi: 10.1016/j.joca.2015.08.015. PubMed PMID: 26521728; PubMed Central PMCID: PMCPMC4630675.
85. Punzi L, Galozzi P, Luisetto R, Favero M, Ramonda R, Oliviero F, et al. Post-traumatic arthritis: overview on pathogenic mechanisms and role of inflammation. RMD open. 2016;2(2):e000279. Epub 2016/09/22. doi: 10.1136/rmdopen-2016-000279. PubMed PMID: 27651925; PubMed Central PMCID: PMCPMC5013366.
86. Christiansen B, Anderson M, Lee C, Williams J, Yik J, Haudenschild D. Musculoskeletal changes following non-invasive knee injury using a novel mouse model of post-traumatic osteoarthritis. Osteoarthritis and cartilage. 2012;20(7):773-82.
87. Fukui T, Yik JHN, Doyran B, Davis J, Haudenschild AK, Adamopoulos IE, et al. Bromodomain-containing-protein-4 and cyclin-dependent-kinase-9 inhibitors interact synergistically in vitro and combined treatment reduces post-traumatic osteoarthritis severity in mice. Osteoarthritis Cartilage. 2021;29(1):68-77. Epub 2020/11/10. doi: 10.1016/j.joca.2020.07.012. PubMed PMID: 33164842; PubMed Central PMCID: PMCPMC7785706.
88. Petersen KR, David A. Streett, Alida T. Gerritsen, Samuel S. Hunter, and Matthew L. Settles. HTStream. GitHub. 2023.
89. Robinson MD, Oshlack A. A scaling normalization method for differential expression analysis of RNA-seq data. Genome Biology. 2010;11(3):R25. doi: 10.1186/gb-2010-11-3-r25.
90. Ritchie ME, Phipson B, Wu D, Hu Y, Law CW, Shi W, et al. limma powers differential expression analyses for RNA-sequencing and microarray studies. Nucleic Acids Research. 2015;43(7):e47-e. doi: 10.1093/nar/gkv007.
91. Xie Z, Bailey A, Kuleshov MV, Clarke DJ, Evangelista JE, Jenkins SL, et al. Gene set knowledge discovery with Enrichr. Current protocols. 2021;1(3):e90.
92. Ashburner M, Ball CA, Blake JA, Botstein D, Butler H, Cherry JM, et al. Gene Ontology: tool for the unification of biology. Nature Genetics. 2000;25(1):25-9. doi: 10.1038/75556.

93. Consortium TGO, Aleksander SA, Balhoff J, Carbon S, Cherry JM, Drabkin HJ, et al. The Gene Ontology knowledgebase in 2023. Genetics. 2023;224(1). doi: 10.1093/genetics/iyad031.
94. Leale DM, Li L, Settles ML, Mitchell K, Froenicke L, Yik JH, et al. A two-stage digestion of whole murine knee joints for single-cell RNA sequencing. Osteoarthritis and Cartilage Open. 2022;4(4):100321.
95. Gu Z. Complex heatmap visualization. Imeta. 2022;1(3):e43.
96. Gu Z, Eils R, Schlesner M. Complex heatmaps reveal patterns and correlations in multidimensional genomic data. Bioinformatics. 2016;32(18):2847-9. doi: 10.1093/bioinformatics/btw313.
97. Law CW, Chen Y, Shi W, Smyth GK. voom: precision weights unlock linear model analysis tools for RNA-seq read counts. Genome Biology. 2014;15(2):R29. doi: 10.1186/gb-2014-15-2-r29.
98. Jin S, Guerrero-Juarez CF, Zhang L, Chang I, Ramos R, Kuan C-H, et al. Inference and analysis of cell-cell communication using CellChat. Nature Communications. 2021;12(1):1088. doi: 10.1038/s41467-021-21246-9.
99. Knights AJ, Farrell EC, Ellis OM, Lammlin L, Junginger LM, Rzeczycki PM, et al. Synovial fibroblasts assume distinct functional identities and secrete R-spondin 2 in osteoarthritis. Annals of the Rheumatic Diseases. 2023;82(2):272-82. doi: 10.1136/ard-2022-222773.
100. Amirtham SM, Ozbey O, Kachroo U, Ramasamy B, Vinod E. Optimization of immunohistochemical detection of collagen type II in osteochondral sections by comparing decalcification and antigen retrieval agent combinations. Clinical anatomy (New York, NY). 2020;33(3):343-9. Epub 2019/08/06. doi: 10.1002/ca.23441. PubMed PMID: 31381185.
101. Schumacher BL, Block JA, Schmid TM, Aydelotte MB, Kuettner KE. A novel proteoglycan synthesized and secreted by chondrocytes of the superficial zone of articular cartilage. Archives of biochemistry and biophysics. 1994;311(1):144-52.
102. Gougos A, Letarte M. Primary structure of endoglin, an RGD-containing glycoprotein of human endothelial cells. Journal of Biological Chemistry. 1990;265(15):8361-4. doi: https://doi.org/10.1016/S0021-9258(19)38892-1.
103. Smith MD. The normal synovium. The open rheumatology journal. 2011;5(1).
104. Minegishi Y, Coustan-Smith E, Rapalus L, Ersoy F, Campana D, Conley ME. Mutations in Igα (CD79a) result in a complete block in B-cell development. The Journal of clinical investigation. 1999;104(8):1115-21.
105. Schatz DG, Oettinger MA, Baltimore D. The V(D)J recombination activating gene, RAG-1. Cell. 1989;59(6):1035-48. Epub 1989/12/22. doi: 10.1016/0092-8674(89)90760-5. PubMed PMID: 2598259.
106. Grieshaber-Bouyer R, Radtke FA, Cunin P, Stifano G, Levescot A, Vijaykumar B, et al. The neutrotime transcriptional signature defines a single continuum of neutrophils across biological compartments. Nature Communications. 2021;12(1):2856. doi: 10.1038/s41467-021-22973-9.
107. Mazzone T. Apolipoprotein E secretion by macrophages: its potential physiological functions. Current opinion in lipidology. 1996;7(5):303-7.
108. Hsiao CJ, Tung P, Blischak JD, Burnett JE, Barr KA, Dey KK, et al. Characterizing and inferring quantitative cell cycle phase in single-cell RNA-seq data analysis. Genome research. 2020;30(4):611-21.
109. Mack M, Cihak J, Simonis C, Luckow B, Proudfoot AE, Plachý J, et al. Expression and characterization of the chemokine receptors CCR2 and CCR5 in mice. Journal of immunology (Baltimore, Md : 1950). 2001;166(7):4697-704. Epub 2001/03/20. doi: 10.4049/jimmunol.166.7.4697. PubMed PMID: 11254730.
110. Marzaioli V, Canavan M, Floudas A, Flynn K, Mullan R, Veale DJ, et al. CD209/CD14+ dendritic cells characterization in rheumatoid and psoriatic arthritis patients: activation, synovial infiltration, and therapeutic targeting. Frontiers in immunology. 2022;12:5792.

111. Guilliams M, Mildner A, Yona S. Developmental and Functional Heterogeneity of Monocytes. Immunity. 2018;49(4):595-613. Epub 2018/10/18. doi: 10.1016/j.immuni.2018.10.005. PubMed PMID: 30332628.
112. Dick SA, Wong A, Hamidzada H, Nejat S, Nechanitzky R, Vohra S, et al. Three tissue resident macrophage subsets coexist across organs with conserved origins and life cycles. Science immunology. 2022;7(67):eabf7777.
113. Workman CJ, Wang Y, El Kasmi KC, Pardoll DM, Murray PJ, Drake CG, et al. LAG-3 regulates plasmacytoid dendritic cell homeostasis. The Journal of Immunology. 2009;182(4):1885-91.
114. Li Y, Qi X, Liu B, Huang H. The STAT5–GATA2 pathway is critical in basophil and mast cell differentiation and maintenance. The Journal of Immunology. 2015;194(9):4328-38.
115. Simon MM, Kramer MD. [4] Granzyme A. Methods in Enzymology. 244: Academic Press; 1994. p. 68-79.
116. McCoy JM, Walkenhorst DE, McCauley KS, Elaasar H, Everett JR, Mix KS. Orphan nuclear receptor NR4A2 induces transcription of the immunomodulatory peptide hormone prolactin. Journal of Inflammation. 2015;12(1):13. doi: 10.1186/s12950-015-0059-2.
117. Borden KL, Volpon L. The diversity, plasticity, and adaptability of cap-dependent translation initiation and the associated machinery. RNA biology. 2020;17(9):1239-51.
118. Mars JC, Ghram M, Culjkovic-Kraljacic B, Borden KLB. The Cap-Binding Complex CBC and the Eukaryotic Translation Factor eIF4E: Co-Conspirators in Cap-Dependent RNA Maturation and Translation. Cancers (Basel). 2021;13(24). Epub 20211208. doi: 10.3390/cancers13246185. PubMed PMID: 34944805; PubMed Central PMCID: PMCPMC8699206.
119. Takahashi S. Molecular functions of metallothionein and its role in hematological malignancies. Journal of hematology & oncology. 2012;5(1):1-8.
120. Pinto SM, Subbannayya Y, Rex DAB, Raju R, Chatterjee O, Advani J, et al. A network map of IL-33 signaling pathway. Journal of cell communication and signaling. 2018;12(3):615-24. Epub 2018/05/01. doi: 10.1007/s12079-018-0464-4. PubMed PMID: 29705949; PubMed Central PMCID: PMCPMC6039344.
121. Nakata K, Hanai T, Take Y, Osada T, Tsuchiya T, Shima D, et al. Disease-modifying effects of COX-2 selective inhibitors and non-selective NSAIDs in osteoarthritis: a systematic review. Osteoarthritis and Cartilage. 2018;26(10):1263-73. doi: https://doi.org/10.1016/j.joca.2018.05.021.
122. Sieker JT, Proffen BL, Waller KA, Chin KE, Karamchedu NP, Akelman MR, et al. Transcriptional profiling of articular cartilage in a porcine model of early post-traumatic osteoarthritis. Journal of orthopaedic research : official publication of the Orthopaedic Research Society. 2018;36(1):318-29. Epub 2017/07/04. doi: 10.1002/jor.23644. PubMed PMID: 28671352; PubMed Central PMCID: PMCPMC5752630.
123. Chang JC, Sebastian A, Murugesh DK, Hatsell S, Economides AN, Christiansen BA, et al. Global molecular changes in a tibial compression induced ACL rupture model of post-traumatic osteoarthritis. Journal of orthopaedic research : official publication of the Orthopaedic Research Society. 2017;35(3):474-85. Epub 2016/04/19. doi: 10.1002/jor.23263. PubMed PMID: 27088242; PubMed Central PMCID: PMCPMC5363336.
124. Sebastian A, Chang JC, Mendez ME, Murugesh DK, Hatsell S, Economides AN, et al. Comparative Transcriptomics Identifies Novel Genes and Pathways Involved in Post-Traumatic Osteoarthritis Development and Progression. International Journal of Molecular Sciences. 2018;19(9):2657. PubMed PMID: doi:10.3390/ijms19092657.
125. Liu C-C, Lee H-C, Peng Y-S, Tseng AH, Wu J-L, Tsai W-Y, et al. Transcriptome Analysis Reveals Novel Genes Associated with Cartilage Degeneration in Posttraumatic Osteoarthritis Progression. CARTILAGE. 2019;13(2_suppl):1249S-62S. doi: 10.1177/1947603519847744.

126. McCoy AM, Kemper AM, Boyce MK, Brown MP, Trumble TN. Differential gene expression analysis reveals pathways important in early post-traumatic osteoarthritis in an equine model. BMC Genomics. 2020;21(1):843. doi: 10.1186/s12864-020-07228-z.
127. Ayturk UM, Sieker JT, Haslauer CM, Proffen BL, Weissenberger MH, Warman ML, et al. Proteolysis and cartilage development are activated in the synovium after surgical induction of post traumatic osteoarthritis. PLOS ONE. 2020;15(2):e0229449. doi: 10.1371/journal.pone.0229449.
128. Vincent TL. IL-1 in osteoarthritis: time for a critical review of the literature. F1000Research. 2019;8. Epub 2019/06/30. doi: 10.12688/f1000research.18831.1. PubMed PMID: 31249675; PubMed Central PMCID: PMCPMC6589928.
129. Ha J, Choi H-S, Lee Y, Kwon H-J, Song YW, Kim H-H. CXC Chemokine Ligand 2 Induced by Receptor Activator of NF-κB Ligand Enhances Osteoclastogenesis. The Journal of Immunology. 2010;184(9):4717-24. doi: 10.4049/jimmunol.0902444.
130. Pan P, Liu X, Wu L, Li X, Wang K, Wang X, et al. TREM-1 promoted apoptosis and inhibited autophagy in LPS-treated HK-2 cells through the NF-κB pathway. International journal of medical sciences. 2021;18(1):8-17. Epub 2021/01/05. doi: 10.7150/ijms.50893. PubMed PMID: 33390769; PubMed Central PMCID: PMCPMC7738954.
131. Peng A, Lu X, Huang J, He M, Xu J, Huang H, et al. Rheumatoid arthritis synovial fibroblasts promote TREM-1 expression in monocytes via COX-2/PGE2 pathway. Arthritis Research & Therapy. 2019;21(1):169. doi: 10.1186/s13075-019-1954-3.
132. Qiao L, Gu J, Ni Y, Wu J, Zhang D, Gu Y. RNA-Seq Reveals the mRNAs, miRNAs, and lncRNAs Expression Profile of Knee Joint Synovial Tissue in Osteoarthritis Patients. Journal of Clinical Medicine. 2023;12(4):1449. PubMed PMID: doi:10.3390/jcm12041449.
133. Kienle K, Lämmermann T. Neutrophil swarming: an essential process of the neutrophil tissue response. Immunological Reviews. 2016;273(1):76-93. doi: https://doi.org/10.1111/imr.12458.
134. Won Y, Shin Y, Chun C-H, Cho Y, Ha C-W, Kim J-H, et al. Pleiotropic roles of metallothioneins as regulators of chondrocyte apoptosis and catabolic and anabolic pathways during osteoarthritis pathogenesis. Annals of the Rheumatic Diseases. 2016;75(11):2045-52. doi: 10.1136/annrheumdis-2015-208406.
135. Zafarullah M, Martel-Pelletier J, Cloutier JM, Gedamu L, Pelletier JP. Expression of c-fos, c-jun, jun-B, metallothionein and metalloproteinase genes in human chondrocyte. FEBS letters. 1992;306(2-3):169-72. Epub 1992/07/20. doi: 10.1016/0014-5793(92)80992-p. PubMed PMID: 1633872.
136. Ma Y, Du J, Yin Z, Dai H, Wei Y, Xia Y, et al. Metallothionein-1 is Positively Correlated with Inflammation and Ankylosing Spondylitis Activity. Journal of inflammation research. 2022;15:5935-44. Epub 2022/10/25. doi: 10.2147/jir.s382827. PubMed PMID: 36274830; PubMed Central PMCID: PMCPMC9585266.
137. Backman JT, Siegle I, Fritz P. Immunohistochemical localization of metallothionein in synovial tissue of patients with chronic inflammatory and degenerative joint disease. Virchows Archiv. 1998;433(2):153-60. doi: 10.1007/s004280050230.
138. Wang C, Gong Z, Hu S, Zhang G. Metallothionein-1 is associated with osteoarthritis disease activity and suppresses proinflammatory cytokines production in synovial cells. International Immunopharmacology. 2019;75:105815. doi: https://doi.org/10.1016/j.intimp.2019.105815.
139. Sebastian A, Chang JC, Mendez ME, Murugesh DK, Hatsell S, Economides AN, et al. Comparative Transcriptomics Identifies Novel Genes and Pathways Involved in Post-Traumatic Osteoarthritis Development and Progression. Int J Mol Sci. 2018;19(9). Epub 2018/09/13. doi: 10.3390/ijms19092657. PubMed PMID: 30205482; PubMed Central PMCID: PMCPMC6163882.
140. Sebastian A, Murugesh DK, Mendez ME, Hum NR, Rios-Arce ND, McCool JL, et al. Global Gene Expression Analysis Identifies Age-Related Differences in Knee Joint Transcriptome during the

Development of Post-Traumatic Osteoarthritis in Mice. International Journal of Molecular Sciences [Internet]. 2020; 21(1).
141. Loeser RF, Olex AL, McNulty MA, Carlson CS, Callahan MF, Ferguson CM, et al. Microarray analysis reveals age-related differences in gene expression during the development of osteoarthritis in mice. Arthritis & Rheumatism. 2012;64(3):705-17. doi: https://doi.org/10.1002/art.33388.
142. Rai V, Dilisio MF, Samadi F, Agrawal DK. Counteractive Effects of IL-33 and IL-37 on Inflammation in Osteoarthritis. International journal of environmental research and public health. 2022;19(9). Epub 2022/05/15. doi: 10.3390/ijerph19095690. PubMed PMID: 35565085; PubMed Central PMCID: PMCPMC9100324.
143. He Z, Song Y, Yi Y, Qiu F, Wang J, Li J, et al. Blockade of IL-33 signalling attenuates osteoarthritis. Clinical & translational immunology. 2020;9(10):e1185. Epub 2020/11/03. doi: 10.1002/cti2.1187. PubMed PMID: 33133598; PubMed Central PMCID: PMCPMC7587452.
144. Millar NL, Gilchrist DS, Akbar M, Reilly JH, Kerr SC, Campbell AL, et al. MicroRNA29a regulates IL-33-mediated tissue remodelling in tendon disease. Nature Communications. 2015;6(1):6774. doi: 10.1038/ncomms7774.
145. Lunderius-Andersson C, Enoksson M, Nilsson G. Mast Cells Respond to Cell Injury through the Recognition of IL-33. Frontiers in immunology. 2012;3:82. Epub 2012/05/09. doi: 10.3389/fimmu.2012.00082. PubMed PMID: 22566963; PubMed Central PMCID: PMCPMC3342375.
146. Siqueira MBP, Frangiamore S, Klika AK, Gajewski N, Barsoum WK, Higuera CA. Comparison of Synovial Fluid Cytokine Levels between Traumatic Knee Injury and End-Stage Osteoarthritis. J Knee Surg. 2017;30(02):128-33. Epub 04/28. doi: 10.1055/s-0036-1583269.
147. Zhang Y, Liu D, Vithran DTA, Kwabena BR, Xiao W, Li Y. CC chemokines and receptors in osteoarthritis: new insights and potential targets. Arthritis Research & Therapy. 2023;25(1):113. doi: 10.1186/s13075-023-03096-6.
148. Jia C, Li X, Pan J, Ma H, Wu D, Lu H, et al. Silencing of Angiopoietin-Like Protein 4 (Angptl4) Decreases Inflammation, Extracellular Matrix Degradation, and Apoptosis in Osteoarthritis via the Sirtuin 1/NF-κB Pathway. Oxidative medicine and cellular longevity. 2022;2022:1135827. Epub 2022/09/09. doi: 10.1155/2022/1135827. PubMed PMID: 36071864; PubMed Central PMCID: PMCPMC9442503.
149. Chou C-H, Jain V, Gibson J, Attarian DE, Haraden CA, Yohn CB, et al. Synovial cell cross-talk with cartilage plays a major role in the pathogenesis of osteoarthritis. Scientific Reports. 2020;10(1):10868. doi: 10.1038/s41598-020-67730-y.
150. Driban JB, Hootman JM, Sitler MR, Harris KP, Cattano NM. Is Participation in Certain Sports Associated With Knee Osteoarthritis? A Systematic Review. Journal of Athletic Training. 2017;52(6):497-506. doi: 10.4085/1062-6050-50.2.08.
151. Showery JE, Kusnezov NA, Dunn JC, Bader JO, Belmont PJ, Waterman BR. The Rising Incidence of Degenerative and Posttraumatic Osteoarthritis of the Knee in the United States Military. The Journal of Arthroplasty. 2016;31(10):2108-14. doi: 10.1016/j.arth.2016.03.026.
152. Wang L-J, Zeng N, Yan Z-P, Li J-T, Ni G-X. Post-traumatic osteoarthritis following ACL injury. Arthritis Research & Therapy. 2020;22(1):57. doi: 10.1186/s13075-020-02156-5.
153. Yelin E, Weinstein S, King T. The burden of musculoskeletal diseases in the United States. Seminars in Arthritis and Rheumatism. 2016;46(3):259-60. doi: 10.1016/j.semarthrit.2016.07.013.
154. Atarod Pilambaraei M, O'Brien EJO, Frank CB, Shrive NG. There is significant load sharing and physical interaction between the anteromedial and posterolateral bundles of the ovine ACL under anterior tibial loads. The Knee. 2012;19(6):797-803. doi: 10.1016/j.knee.2012.03.001.
155. Ferdowsian HR, Durham DL, Kimwele C, Kranendonk G, Otali E, Akugizibwe T, et al. Signs of Mood and Anxiety Disorders in Chimpanzees. PLoS One. 2011;6(6):e19855. doi: 10.1371/journal.pone.0019855.

156. Pasold J, Osterberg A, Peters K, Taipaleenma H, Vollmar B, Mu B. Reduced expression of Sfrp1 during chondrogenesis and in articular chondrocytes correlates with osteoarthritis in STR / ort mice. Exp Cell Res. 2013;319:649-59. doi: 10.1016/j.yexcr.2012.12.012.
157. Tapper JE, Fukushima S, Azuma H, Sutherland C, Marchuk L, Thornton GM, et al. Dynamic in vivo three-dimensional (3D) kinematics of the anterior cruciate ligament/medial collateral ligament transected ovine stifle joint. Journal of Orthopaedic Research. 2008;26(5):660-72. doi: 10.1002/jor.20557.
158. Osterhoff G, Löffler S, Steinke H, Feja C, Josten C, Hepp P. Comparative anatomical measurements of osseous structures in the ovine and human knee. The Knee. 2011;18(2):98-103. doi: 10.1016/j.knee.2010.02.001.
159. Reichert JC, Saifzadeh S, Wullschleger ME, Epari DR, Schütz MA, Duda GN, et al. The challenge of establishing preclinical models for segmental bone defect research. Biomaterials. 2009;30(12):2149-63. doi: 10.1016/j.biomaterials.2008.12.050.
160. Flynn C, Hurtig M, Lamoure E, Cummins E, Roati V, Lowerison M, et al. Modeling and Staging of Osteoarthritis Progression Using Serial CT Imaging and Arthroscopy. CARTILAGE. 2018;11(3):338-47. doi: 10.1177/1947603518789997.
161. Holzmuller W, Rehm KE, Perren SM. Mechanical properties of PDS-augmented patellar tendon transplants for reconstruction of the anterior cruciate ligament. Unfallchirurg. 1992;95(6):306-10.
162. Tapper JE, Fukushima S, Azuma H, Thornton GM, Ronsky JL, Shrive NG, et al. Dynamic in vivo kinematics of the intact ovine stifle joint. Journal of Orthopaedic Research. 2006;24(4):782-92. doi: 10.1002/jor.20051.
163. Schinhan M, Gruber M, Vavken P, Dorotka R, Samouh L, Chiari C, et al. Critical-size defect induces unicompartmental osteoarthritis in a stable ovine knee. Journal of Orthopaedic Research. 2012;30(2):214-20. doi: 10.1002/jor.21521.
164. Cake MA, Smith MM, Young AA, Smith SM, Ghosh P, Read RA. Synovial pathology in an ovine model of osteoarthritis: Effect of intraarticular hyaluronan (Hyalgan®). Clinical and Experimental Rheumatology. 2008;26(4):561-7.
165. Atarod M, Ludwig TE, Frank CB, Schmidt TA, Shrive NG. Cartilage boundary lubrication of ovine synovial fluid following anterior cruciate ligament transection: a longitudinal study. Osteoarthritis and Cartilage. 2015;23(4):640-7. doi: 10.1016/j.joca.2014.12.017.
166. Moya-Angeler J, Gonzalez-Nieto J, Sanchez Monforte J, Altonaga JR, Vaquero J, Forriol F. Surgical induced models of joint degeneration in the ovine stifle: Magnetic resonance imaging and histological assessment. The Knee. 2016;23(2):214-20. doi: 10.1016/j.knee.2015.11.017.
167. Shekarforoush M, Barton KI, Beveridge JE, Scott M, Martin CR, Muench G, et al. Alterations in Joint Angular Velocity Following Traumatic Knee Injury in Ovine Models. Annals of Biomedical Engineering. 2019;47(3):790-801. doi: 10.1007/s10439-019-02203-6.
168. Barton KI, Heard BJ, Sevick JL, Martin CR, Shekarforoush SMM, Chung M, et al. Posttraumatic Osteoarthritis Development and Progression in an Ovine Model of Partial Anterior Cruciate Ligament Transection and Effect of Repeated Intra-articular Methylprednisolone Acetate Injections on Early Disease. The American Journal of Sports Medicine. 2018;46(7):1596-605. doi: 10.1177/0363546518765098.
169. Heard BJ, Solbak NM, Achari Y, Chung M, Hart DA, Shrive NG, et al. Changes of early post-traumatic osteoarthritis in an ovine model of simulated ACL reconstruction are associated with transient acute post-injury synovial inflammation and tissue catabolism. Osteoarthritis and Cartilage. 2013;21(12):1942-9. doi: 10.1016/j.joca.2013.08.019.
170. Heard BJ, Beveridge JE, Atarod M, O'Brien EJ, Rolian C, Frank CB, et al. Analysis of change in gait in the ovine stifle: normal, injured, and anterior cruciate ligament reconstructed. BMC Musculoskeletal Disorders. 2017;18(1). doi: 10.1186/s12891-017-1576-3.

171. Appleyard RC, Ghosh P, Swain VM. Biomechanical, histological and immunohistological studies of patellar cartilage in an ovine model of osteoarthritis induced by lateral meniscectomy. Osteoarthritis and Cartilage. 1999;7(3):281-94. doi: 10.1053/joca.1998.0202.
172. Appleyard RC, Burkhardt D, Ghosh P, Read R, Cake M, Swain MV, et al. Topographical analysis of the structural, biochemical and dynamic biomechanical properties of cartilage in an ovine model of osteoarthritis. Osteoarthritis and Cartilage. 2003;11(1):65-77. doi: 10.1053/joca.2002.0867.
173. Gruchenberg K, Ignatius A, Friemert B, von Lübken F, Skaer N, Gellynck K, et al. In vivo performance of a novel silk fibroin scaffold for partial meniscal replacement in a sheep model. Knee Surgery, Sports Traumatology, Arthroscopy. 2015;23(8):2218-29. doi: 10.1007/s00167-014-3009-2.
174. Gruchenberg K, Ignatius A, Friemert B, von Lübken F, Skaer N, Gellynck K, et al. Correction to: In vivo performance of a novel silk fibroin scaffold for partial meniscal replacement in a sheep model (Knee Surgery, Sports Traumatology, Arthroscopy, (2015), 23, 8, (2218-2229), 10.1007/s00167-014-3009-2). Knee Surgery, Sports Traumatology, Arthroscopy. 2018;26(7):2216. doi: 10.1007/s00167-018-4878-6.
175. Al Faqeh H, Nor Hamdan BMY, Chen HC, Aminuddin BS, Ruszymah BHI. The potential of intra-articular injection of chondrogenic-induced bone marrow stem cells to retard the progression of osteoarthritis in a sheep model. Experimental Gerontology. 2012;47(6):458-64. doi: 10.1016/j.exger.2012.03.018.
176. Funakoshi Y, Hariu M, Tapper JE, Marchuk LL, Shrive NG, Kanaya F, et al. Periarticular ligament changes following ACL/MCL transection in an ovine stifle joint model of osteoarthritis. Journal of Orthopaedic Research. 2007;25(8):997-1006. doi: 10.1002/jor.20370.
177. Tapper JE BC, Funakoshi Y, et al. . Evidence supporting a new hypothesis for the development of osteoarthritis. . ORS Trans 325. 2004:2004.
178. Manunta A, Zedde P, Pilicchi S, Rocca S, Pool R, Dattena M, et al. The use of embryonic cells in the treatment of osteochondral defects of the knee: an ovine in vivo study. Joints. 2016;04(02):070-9. doi: 10.11138/jts/2016.4.2.070.
179. Lohmander LS, Englund PM, Dahl LL, Roos EM. The long-term consequence of anterior cruciate ligament and meniscus injuries: Osteoarthritis. American Journal of Sports Medicine. 2007;35(10):1756-69. doi: 10.1177/0363546507307396.
180. Buoncristiani AM, Tjoumakaris FP, Starman JS, Ferretti M, Fu FH. Anatomic Double-Bundle Anterior Cruciate Ligament Reconstruction. Arthroscopy: The Journal of Arthroscopic & Related Surgery. 2006;22(9):1000-6. doi: 10.1016/j.arthro.2006.06.005.
181. Coughlin TR, Kennedy OD. The role of subchondral bone damage in post-traumatic osteoarthritis. Annals of the New York Academy of Sciences. 2016;1383(1):58-66. doi: 10.1111/nyas.13261.
182. Beveridge JE, Atarod M, Heard BJ, O'Brien EEJ, Frank CB, Shrive NG. Relationship between increased in vivo meniscal loads and abnormal tibiofemoral surface alignment in ACL deficient sheep is varied. Journal of Biomechanics. 2016;49(16):3824-32. doi: 10.1016/j.jbiomech.2016.10.017.
183. Atarod M, Frank CB, Shrive NG. Decreased posterior cruciate and altered collateral ligament loading following ACL transection: A longitudinal study in the ovine model. Journal of Orthopaedic Research. 2014;32(3):431-8. doi: 10.1002/jor.22529.
184. Roychowdhury S, Fitzgerald SW, Sonin AH, Peduto AJ, Miller FH, Hoff FL. Using MR imaging to diagnose partial tears of the anterior cruciate ligament: value of axial images. American Journal of Roentgenology. 1997;168(6):1487-91. doi: 10.2214/ajr.168.6.9168712.
185. Gardner EJ, Noyes FR, Jetter AW, Grood ES, Harms SP, Levy MS. Effect of Anteromedial and Posterolateral Anterior Cruciate Ligament Bundles on Resisting Medial and Lateral Tibiofemoral Compartment Subluxations. Arthroscopy: The Journal of Arthroscopic & Related Surgery. 2015;31(5):901-10. doi: 10.1016/j.arthro.2014.12.009.

186. Sonnery-Cottet B, Colombet P. Partial tears of the anterior cruciate ligament. Orthopaedics & Traumatology: Surgery & Research. 2016;102(1):S59-S67. doi: 10.1016/j.otsr.2015.06.032.
187. Butler RJ, Minick KI, Ferber R, Underwood F. Gait mechanics after ACL reconstruction: Implications for the early onset of knee osteoarthritis. British Journal of Sports Medicine. 2009;43(5):366-70. doi: 10.1136/bjsm.2008.052522.
188. Spindler KP, Parker RD, Andrish JT, Kaeding CC, Wright RW, Marx RG, et al. Prognosis and predictors of ACL reconstructions using the MOON cohort: A model for comparative effectiveness studies. Journal of Orthopaedic Research. 2012;31(1):2-9. doi: 10.1002/jor.22201.
189. Brophy RH, Wright RW, Matava MJ. Cost Analysis of Converting from Single-Bundle to Double-Bundle Anterior Cruciate Ligament Reconstruction. The American Journal of Sports Medicine. 2009;37(4):683-7. doi: 10.1177/0363546508328121.
190. Kim SH, Kim SJ, Choi CH, Kim D, Jung M. Optimal condition to create femoral tunnel considering combined influence of knee flexion and transverse drill angle in anatomical single-bundle acl reconstruction using medial portal technique: 3D simulation study. BioMed Research International. 2018;2018. doi: 10.1155/2018/2643247.
191. Mishra P, Lal A, Mohindra M, Mehta N, Joshi D, Chaudhary D. Incidence, management and outcome assessment of post operative infection following single bundle and double bundle acl reconstruction. Journal of Clinical Orthopaedics and Trauma. 2018;9(2):167-71. doi: 10.1016/j.jcot.2017.09.017.
192. Li W, Song Y, Song B, Yang R, Xing T, Chen Z, et al. Comparison of anterior cruciate ligament reconstruction methods between reverse “Y” plasty reconstruction and traditional single-bundle technique—A cadaveric study. Journal of Orthopaedic Translation. 2018;14:1-7. doi: 10.1016/j.jot.2018.03.002.
193. Asano H, Muneta T, Ikeda H, Yagishita K, Kurihara Y, Sekiya I. Arthroscopic evaluation of the articular cartilage after anterior cruciate ligament reconstruction: A short-term prospective study of 105 patients. Arthroscopy: The Journal of Arthroscopic & Related Surgery. 2004;20(5):474-81. doi: 10.1016/j.arthro.2004.03.006.
194. Lohmander LS, Östenberg A, Englund M, Roos H. High prevalence of knee osteoarthritis, pain, and functional limitations in female soccer players twelve years after anterior cruciate ligament injury. Arthritis & Rheumatism. 2004;50(10):3145-52. doi: 10.1002/art.20589.
195. Lotz MK, Kraus VB. Correction: Posttraumatic osteoarthritis: Pathogenesis and pharmacological treatment options. Arthritis Research and Therapy. 2010;12(6). doi: 10.1186/ar3177.
196. Sellam J, Berenbaum F. The role of synovitis in pathophysiology and clinical symptoms of osteoarthritis. Nature Reviews Rheumatology. 2010;6(11):625-35. doi: 10.1038/nrrheum.2010.159.
197. Scanzello CR, Goldring SR. The role of synovitis in osteoarthritis pathogenesis. Bone. 2012;51(2):249-57. doi: 10.1016/j.bone.2012.02.012.
198. Kessler MA, Behrend H, Henz S, Stutz G, Rukavina A, Kuster MS. Function, osteoarthritis and activity after ACL-rupture: 11 years follow-up results of conservative versus reconstructive treatment. Knee Surgery, Sports Traumatology, Arthroscopy. 2008;16(5):442-8. doi: 10.1007/s00167-008-0498-x.
199. Ajuied A, Wong F, Smith C, Norris M, Earnshaw P, Back D, et al. Anterior cruciate ligament injury and radiologic progression of knee osteoarthritis: A systematic review and meta-analysis. American Journal of Sports Medicine. 2014;42(9):2242-52. doi: 10.1177/0363546513508376.
200. Mickiewicz B, Heard BJ, Chau JK, Chung M, Hart DA, Shrive NG, et al. Metabolic profiling of synovial fluid in a unilateral ovine model of anterior cruciate ligament reconstruction of the knee suggests biomarkers for early osteoarthritis. Journal of Orthopaedic Research. 2014;33(1):71-7. doi: 10.1002/jor.22743.

201. Heard BJ, Achari Y, Chung M, Shrive NG, Frank CB. Early joint tissue changes are highly correlated with a set of inflammatory and degradative synovial biomarkers after ACL autograft and its sham surgery in an ovine model. Journal of Orthopaedic Research. 2011;29(8):1185-92. doi: 10.1002/jor.21404.
202. Hexter AT, Hing KA, Haddad FS, Blunn G. Decellularized porcine xenograft for anterior cruciate ligament reconstruction: A histological study in sheep comparing cross-pin and cortical suspensory femoral fixation. Bone & joint research. 2020;9(6):293-301. Epub 2020/07/31. doi: 10.1302/2046-3758.96.bjr-2020-0030.r2. PubMed PMID: 32728430; PubMed Central PMCID: PMCPMC7376309.
203. Adams BG, Houston MN, Cameron KL. The epidemiology of meniscus injury. Sports medicine and arthroscopy review. 2021;29(3):e24-e33.
204. Kilcoyne KG, Dickens JF, Haniuk E, Cameron KL, Owens BD. Epidemiology of meniscal injury associated with ACL tears in young athletes. Orthopedics. 2012;35(3):208-12.
205. Englund M, Roos EM, Roos HP, Lohmander LS. Patient-relevant outcomes fourteen years after meniscectomy: Influence of type of meniscal tear and size of resection. Rheumatology. 2001;40(6):631-9. doi: 10.1093/rheumatology/40.6.631.
206. Roos EM, Östenberg A, Roos H, Ekdahl C, Lohmander LS. Long-term outcome of meniscectomy: symptoms, function, and performance tests in patients with or without radiographic osteoarthritis compared to matched controls. Osteoarthritis and Cartilage. 2001;9(4):316-24. doi: 10.1053/joca.2000.0391.
207. Roos EM, Thorlund JB. It is time to stop meniscectomy. British Journal of Sports Medicine. 2017;51(6):490-1. doi: 10.1136/bjsports-2016-097273.
208. Burger C, Mueller M, Wlodarczyk P, Goost H, Tolba RH, Rangger C, et al. The sheep as a knee osteoarthritis model: early cartilage changes after meniscus injury and repair. Laboratory Animals. 2007;41(4):420-31. doi: 10.1258/002367707782314265.
209. Cake MA, Read RA, Corfield G, Daniel A, Burkhardt D, Smith MM, et al. Comparison of gait and pathology outcomes of three meniscal procedures for induction of knee osteoarthritis in sheep. Osteoarthritis and Cartilage. 2013;21(1):226-36. doi: 10.1016/j.joca.2012.10.001.
210. Young AA, McLennan S, Smith MM, Smith SM, Cake MA, Read RA, et al. Proteoglycan 4 downregulation in a sheep meniscectomy model of early osteoarthritis. Arthritis Research and Therapy. 2006;8(2):4-9. doi: 10.1186/ar1898.
211. Lubis AMT, Aprianto P, Pawitan JA, Priosoeryanto BP, Dewi TIT, Kamal AF. Intra-articular injection of secretome, derived from umbilical cord mesenchymal stem cell, enhances the regeneration process of cartilage in early-stage osteo-arthritis: an animal study. Acta Orthopaedica. 2023;94:300-6. doi: 10.2340/17453674.2023.12359.
212. Rongen JJ, van Tienen TG, van Bochove B, Grijpma DW, Buma P. Biomaterials in search of a meniscus substitute. Biomaterials. 2014;35(11):3527-40. doi: 10.1016/j.biomaterials.2014.01.017.
213. Sandmann GH, Adamczyk C, Garcia EG, Doebele S, Buettner A, Milz S, et al. Biomechanical comparison of menisci from different species and artificial constructs. BMC Musculoskeletal Disorders. 2013;14(1). doi: 10.1186/1471-2474-14-324.
214. Chevrier A, Nelea M, Hurtig MB, Hoemann CD, Buschmann MD. Meniscus structure in human, sheep, and rabbit for animal models of meniscus repair. Journal of Orthopaedic Research. 2009;27(9):1197-203. doi: 10.1002/jor.20869.
215. Gigout A, Werkmann D, Menges S, Brenneis C, Henson F, Cowan KJ, et al. R399E, A Mutated Form of Growth and Differentiation Factor 5, for Disease Modification of Osteoarthritis. Arthritis & Rheumatology. 2023;75(3):375-86. doi: https://doi.org/10.1002/art.42343.
216. Cojocaru DG, Hondke S, Krüger JP, Bosch C, Croicu C, Florescu S, et al. Meniscus-shaped cell-free polyglycolic acid scaffold for meniscal repair in a sheep model. Journal of Biomedical Materials Research - Part B Applied Biomaterials. 2019;(December 2018):1-10. doi: 10.1002/jbm.b.34435.

217. Ma N, Wang T, Bie L, Zhao Y, Zhao L, Zhang S, et al. Comparison of the effects of exercise with chondroitin sulfate on knee osteoarthritis in rabbits. Journal of Orthopaedic Surgery and Research. 2018;13(1). doi: 10.1186/s13018-018-0722-4.
218. Xu H, Bouta EM, Wood RW, Schwarz EM, Wang Y, Xing L. Utilization of longitudinal ultrasound to quantify joint soft-tissue changes in a mouse model of posttraumatic osteoarthritis. Bone Research. 2017;5(1). doi: 10.1038/boneres.2017.12.
219. Ude CC, Sulaiman SB, Min-Hwei N, Hui-Cheng C, Ahmad J, Yahaya NM, et al. Cartilage Regeneration by Chondrogenic Induced Adult Stem Cells in Osteoarthritic Sheep Model. PLoS ONE. 2014;9(6):e98770. doi: 10.1371/journal.pone.0098770.
220. Ude CC, Shamsul BS, Ng MH, Chen HC, Ohnmar H, Amaramalar SN, et al. Long-term evaluation of osteoarthritis sheep knee, treated with TGF-β3 and BMP-6 induced multipotent stem cells. Experimental Gerontology. 2018;104:43-51. doi: 10.1016/j.exger.2018.01.020.
221. Frank CB, Beveridge JE, Huebner KD, Heard BJ, Tapper JE, O'Brien EJO, et al. Complete ACL/MCL deficiency induces variable degrees of instability in sheep with specific kinematic abnormalities correlating with degrees of early osteoarthritis. Journal of orthopaedic research : official publication of the Orthopaedic Research Society. 2012;30(3):384-92. doi: 10.1002/jor.21549.
222. Márcio de Oliveira Carneiro CHB, Neto JB. Platelet-Rich Plasma Gel promotes regeneration of articular cartilage in knees of sheeps. Acta Ortop Bras. 2013;21(2):80-6.
223. Kitamura N, Yokota M, Kurokawa T, Gong JP, Yasuda K. In vivo cartilage regeneration induced by a double-network hydrogel: Evaluation of a novel therapeutic strategy for femoral articular cartilage defects in a sheep model. Journal of Biomedical Materials Research - Part A. 2016;104(9):2159-65. doi: 10.1002/jbm.a.35745.
224. Schinhan M, Toegel S, Weinmann D, Schneider E, Chiari C, Gruber M, et al. Biological Regeneration of Articular Cartilage in an Early Stage of Compartmentalized Osteoarthritis: 12-Month Results. The American Journal of Sports Medicine. 2020;48(6):1338-46. doi: 10.1177/0363546520906411. PubMed PMID: 32150451.
225. Hunt N, Sanchez-Ballester J, Pandit R, Thomas R, Strachan R. Chondral lesions of the knee: A new localization method and correlation with associated pathology. Arthroscopy. 2001;17(5):481-90. doi: 10.1053/jars.2001.19977.
226. Fischenich KM, Pauly HM, Button KD, Fajardo RS, DeCamp CE, Haut RC, et al. A study of acute and chronic tissue changes in surgical and traumatically-induced experimental models of knee joint injury using magnetic resonance imaging and micro-computed tomography. Osteoarthritis and Cartilage. 2017;25(4):561-9. doi: 10.1016/j.joca.2016.10.010.
227. McMillan S, Chhabra A, Hassebrock JD, Ford E, Amin NH. Risks and Complications Associated With Intra-articular Arthroscopy of the Knee and Shoulder in an Office Setting. Orthopaedic Journal of Sports Medicine. 2019;7(9):232596711986984. doi: 10.1177/2325967119869846.
228. Jiang XD, Zheng HL, Yang YP. Outcome of posterior wall blowout in anterior cruciate ligament (ACL) reconstruction via anteromedial portal approach: A retrospective research in 20 patients with 6 years follow-up. Chinese Journal of Traumatology - English Edition. 2019;22(1):24-8. doi: 10.1016/j.cjtee.2018.12.002.
229. Lutz C, Baverel L, Colombet P, Cournapeau J, Dalmay F, Lefevre N, et al. Pain after out-patient vs. in-patient ACL reconstruction: French prospective study of 1076 patients. Orthopaedics & Traumatology: Surgery & Research. 2016;102(8):S265-S70. doi: 10.1016/j.otsr.2016.08.009.
230. O'Brien EJO, Beveridge JE, Huebner KD, Heard BJ, Tapper JE, Shrive NG, et al. Osteoarthritis develops in the operated joint of an ovine model following ACL reconstruction with immediate anatomic reattachment of the native ACL. Journal of Orthopaedic Research. 2013;31(1):35-43. doi: 10.1002/jor.22187.

231. Chen W-P, Bao J-P, Hu P-F, Feng J, Wu L-D. Alleviation of osteoarthritis by Trichostatin A, a histone deacetylase inhibitor, in experimental osteoarthritis. Molecular Biology Reports. 2010;37(8):3967-72. doi: 10.1007/s11033-010-0055-9.
232. Barton KI, Shekarforoush M, Heard BJ, Sevick JL, Vakil P, Atarod M, et al. Use of pre-clinical surgically induced models to understand biomechanical and biological consequences of PTOA development. Journal of Orthopaedic Research. 2017;35(3):454-65. doi: 10.1002/jor.23322.
233. Xiaoqiang E YCHMYQGDJXZB. Dendritic cells of synovium in experimental model of osteoarthritis of rabbits. Cell Physiol Biochem. 2012;30(1):23-32.
234. Moskowitz RW, Davis W, Sammarco J, Martens M, Baker J, Mayor M, et al. Experimentally Induced Degenerative Joint Lesions Following Partial Meniscectomy in the Rabbit. Arthritis & Rheumatism. 1973;16(3):397-405. doi: 10.1002/art.1780160317.
235. Zhang Z-Z, Wang S-J, Zhang J-Y, Jiang W-B, Huang A-B, Qi Y-S, et al. 3D-Printed Poly(ε-caprolactone) Scaffold Augmented With Mesenchymal Stem Cells for Total Meniscal Substitution: A 12- and 24-Week Animal Study in a Rabbit Model. The American Journal of Sports Medicine. 2017;45(7):1497-511. doi: 10.1177/0363546517691513.
236. Stein SEC, von Luebken F, Warnecke D, Gentilini C, Skaer N, Walker R, et al. The challenge of implant integration in partial meniscal replacement: an experimental study on a silk fibroin scaffold in sheep. Knee Surgery, Sports Traumatology, Arthroscopy. 2019;27(2):369-80. doi: 10.1007/s00167-018-5160-7.
237. Stein SEC, von Luebken F, Warnecke D, Gentilini C, Skaer N, Walker R, et al. The challenge of implant integration in partial meniscal replacement: an experimental study on a silk fibroin scaffold in sheep. Knee Surgery, Sports Traumatology, Arthroscopy. 2018;27(2):369-80. doi: 10.1007/s00167-018-5160-7.
238. Kolaczek S, Hewison C, Caterine S, Berardelli R, Beveridge T, Herman B, et al. 3D strain in native medial meniscus is comparable to medial meniscus allograft transplant. Knee Surgery, Sports Traumatology, Arthroscopy. 2019;27(2):349-53. doi: 10.1007/s00167-018-5075-3.
239. Guisasola Ii, Vaquero J, Forriol F. Knee Immobilization on Meniscal Healing After Suture. Clinical Orthopaedics and Related Research. 2002;395:227-33. doi: 10.1097/00003086-200202000-00027.
240. Beveridge JE, Heard BJ, Brown JJY, Shrive NG, Frank CB. A new measure of tibiofemoral subchondral bone interactions that correlates with early cartilage damage in injured sheep. Journal of Orthopaedic Research. 2014;32(10):1371-80. doi: 10.1002/jor.22685.
241. Mizuta HMD, Ph D, Kudo SMD, Ph D, Nakamura EMD, Ph D, et al. Brief report Expression of the PTH / PTHrP receptor in chondrogenic cells during the repair of full-thickness defects of articular cartilage. Osteoarthritis and Cartilage. 2006;14:944-52. doi: 10.1016/j.joca.2006.03.009.
242. Mizuta H, Kudo S, Nakamura E, Takagi K, Hiraki Y. Expression of the PTH/PTHrP receptor in chondrogenic cells during the repair of full-thickness defects of articular cartilage. Osteoarthritis and Cartilage. 2006;14(9):944-52. doi: 10.1016/j.joca.2006.03.009.
243. Orth P, Meyer HL, Goebel L, Eldracher M, Ong MF, Cucchiarini M, et al. Improved repair of chondral and osteochondral defects in the ovine trochlea compared with the medial condyle. Journal of Orthopaedic Research. 2013;31(11):1772-9. doi: 10.1002/jor.22418.
244. Hoemann C, Kandel R, Roberts S, Saris DBF, Creemers L, Mainil-Varlet P, et al. International Cartilage Repair Society (ICRS) Recommended Guidelines for Histological Endpoints for Cartilage Repair Studies in Animal Models and Clinical Trials. CARTILAGE. 2011;2(2):153-72. doi: 10.1177/1947603510397535.
245. Bell AD, Lascau-Coman V, Sun J, Chen G, Lowerison MW, Hurtig MB, et al. Bone-Induced Chondroinduction in Sheep Jamshidi Biopsy Defects with and without Treatment by Subchondral Chitosan-Blood Implant. CARTILAGE. 2012;4(2):131-43. doi: 10.1177/1947603512463227.

246. Hoemann CD, Hurtig M, Rossomacha E, Sun J, Chevrier A, Shive MS, et al. Chitosan-Glycerol Phosphate/Blood Implants Improve Hyaline Cartilage Repair in Ovine Microfracture Defects. The Journal of Bone & Joint Surgery. 2005;87(12):2671-86. doi: 10.2106/jbjs.d.02536.
247. Bell AD, Hurtig MB, Quenneville E, Rivard G-é, Hoemann CD. Effect of a Rapidly Degrading Presolidified 10 kDa Chitosan / Blood Implant and Subchondral Marrow Stimulation Surgical Approach on Cartilage Resurfacing in a Sheep Model. Cartilage. 2017;8(4):417–31. doi: 10.1177/1947603516676872.
248. Chen H, Hoemann CD, Sun J, Chevrier A, McKee MD, Shive MS, et al. Depth of subchondral perforation influences the outcome of bone marrow stimulation cartilage repair. Journal of Orthopaedic Research. 2011;29(8):1178-84. doi: 10.1002/jor.21386.
249. Chubinskaya S, Hurtig M, Rueger DC. OP-1/BMP-7 in cartilage repair. International Orthopaedics. 2007;31(6):773-81. doi: 10.1007/s00264-007-0423-9.
250. Caron JP. Osteoarthritis. In: Ross MW, Dyson SJ, editors. Diagnosis and Management of Lameness in the Horse. 2nd ed. St Louis: Elsevier Saunders; 2011. p. 655-68.
251. USDA. Lameness and Laminitis in U.S. Horses United States Department of Agriculture: USDA:APHIS:VS; 2000 [updated 2000]. Available from: http://www.aphis.usda.gov/animal_health/nahms/equine/downloads/equine98/Equine98_dr_Lameness.pdf.
252. Caron JP, Genovese RL. Principles and Practices of Joint Disease Treatment. In: Ross MW, Dyson SJ, editors. Diagnosis and Management of Lameness in the Horse. Philadelphia: Elsevier; 2003. p. 746-64.
253. McIlwraith CW, Frisbie DD, Kawcak CE. The horse as a model of naturally occurring osteoarthritis. Bone Joint Res. 2012;1(11):297-309. Epub 2013/04/24. doi: 10.1302/2046-3758.111.2000132. PubMed PMID: 23610661; PubMed Central PMCID: PMCPMC3626203.
254. McIlwraith CW. The use of intra-articular corticosteroids in the horse: what is known on a scientific basis? Equine Vet J. 2010;42(6):563-71. Epub 2010/08/19. doi: 10.1111/j.2042-3306.2010.00095.x. PubMed PMID: 20716199.
255. McIlwraith CW, Lattermann C. Intra-articular Corticosteroids for Knee Pain-What Have We Learned from the Equine Athlete and Current Best Practice. J Knee Surg. 2019;32(1):9-25. Epub 2018/12/19. doi: 10.1055/s-0038-1676449. PubMed PMID: 30562835.
256. Zanotto GM, Frisbie DD. Current joint therapy usage in equine practice: changes in the last 10 years. Equine Vet J. 2021. Epub 2021/06/19. doi: 10.1111/evj.13489. PubMed PMID: 34143532.
257. Haudenschild DR, Carlson AK, Zignego DL, Yik JHN, Hilmer JK, June RK. Inhibition of early response genes prevents changes in global joint metabolomic profiles in mouse post-traumatic osteoarthritis. Osteoarthritis Cartilage. 2019;27(3):504-12. Epub 2018/12/21. doi: 10.1016/j.joca.2018.11.006. PubMed PMID: 30572121; PubMed Central PMCID: PMCPMC6391201.
258. Hu Z, Yik JH, Cissell DD, Michelier PV, Athanasiou KA, Haudenschild DR. Inhibition of CDK9 prevents mechanical injury-induced inflammation, apoptosis and matrix degradation in cartilage explants. Eur Cell Mater. 2016;30:200-9. Epub 2016/02/11. doi: 10.22203/ecm.v030a14. PubMed PMID: 26859911; PubMed Central PMCID: PMCPMC4750484.
259. Yik JH, Hu Z, Kumari R, Christiansen BA, Haudenschild DR. Cyclin-dependent kinase 9 inhibition protects cartilage from the catabolic effects of proinflammatory cytokines. Arthritis Rheumatol. 2014;66(6):1537-46. Epub 2014/01/29. doi: 10.1002/art.38378. PubMed PMID: 24470357; PubMed Central PMCID: PMCPMC4127300.
260. Hargreaves DC, Horng T, Medzhitov R. Control of inducible gene expression by signal-dependent transcriptional elongation. Cell. 2009;138(1):129-45. Epub 2009/07/15. doi: 10.1016/j.cell.2009.05.047. PubMed PMID: 19596240; PubMed Central PMCID: PMCPMC2828818.

261. Zippo A, Serafini R, Rocchigiani M, Pennacchini S, Krepelova A, Oliviero S. Histone crosstalk between H3S10ph and H4K16ac generates a histone code that mediates transcription elongation. Cell. 2009;138(6):1122-36. Epub 2009/09/22. doi: 10.1016/j.cell.2009.07.031. PubMed PMID: 19766566.
262. Yik JH, Chen R, Nishimura R, Jennings JL, Link AJ, Zhou Q. Inhibition of P-TEFb (CDK9/Cyclin T) kinase and RNA polymerase II transcription by the coordinated actions of HEXIM1 and 7SK snRNA. Mol Cell. 2003;12(4):971-82. Epub 2003/10/29. doi: 10.1016/s1097-2765(03)00388-5. PubMed PMID: 14580347.
263. Yik JH, Chen R, Pezda AC, Samford CS, Zhou Q. A human immunodeficiency virus type 1 Tat-like arginine-rich RNA-binding domain is essential for HEXIM1 to inhibit RNA polymerase II transcription through 7SK snRNA-mediated inactivation of P-TEFb. Mol Cell Biol. 2004;24(12):5094-105. Epub 2004/06/01. doi: 10.1128/MCB.24.12.5094-5105.2004. PubMed PMID: 15169877; PubMed Central PMCID: PMCPMC419863.
264. Hu Z, Chen Y, Song L, Yik JHN, Haudenschild DR, Fan S. Flavopiridol Protects Bone Tissue by Attenuating RANKL Induced Osteoclast Formation. Front Pharmacol. 2018;9:174. Epub 2018/05/19. doi: 10.3389/fphar.2018.00174. PubMed PMID: 29773986; PubMed Central PMCID: PMCPMC5944179.
265. Wu T, Qin Z, Tian Y, Wang J, Xu C, Li Z, et al. Recent Developments in the Biology and Medicinal Chemistry of CDK9 Inhibitors: An Update. J Med Chem. 2020;63(22):13228-57. Epub 2020/09/01. doi: 10.1021/acs.jmedchem.0c00744. PubMed PMID: 32866383.
266. Cassandri M, Fioravanti R, Pomella S, Valente S, Rotili D, Del Baldo G, et al. CDK9 as a Valuable Target in Cancer: From Natural Compounds Inhibitors to Current Treatment in Pediatric Soft Tissue Sarcomas. Front Pharmacol. 2020;11:1230. Epub 2020/09/10. doi: 10.3389/fphar.2020.01230. PubMed PMID: 32903585; PubMed Central PMCID: PMCPMC7438590.
267. Wiernik PH. Alvocidib (flavopiridol) for the treatment of chronic lymphocytic leukemia. Expert Opin Investig Drugs. 2016;25(6):729-34. Epub 2016/03/22. doi: 10.1517/13543784.2016.1169273. PubMed PMID: 26998706.
268. ClinicalTrials.gov. ClinicalTrials.gov 2021 [cited 2021 07/02/2021]. Available from: https://clinicaltrials.gov/ct2/results?cond=&term=flavopiridol&cntry=&state=&city=&dist=.
269. Innocenti F, Stadler WM, Iyer L, Ramirez J, Vokes EE, Ratain MJ. Flavopiridol metabolism in cancer patients is associated with the occurrence of diarrhea. Clin Cancer Res. 2000;6(9):3400-5. Epub 2000/09/22. PubMed PMID: 10999721.
270. Sedlacek H, Czech J, Naik R, Kaur G, Worland P, Losiewicz M, et al. Flavopiridol (L86 8275; NSC 649890), a new kinase inhibitor for tumor therapy. Int J Oncol. 1996;9(6):1143-68. Epub 1996/12/01. doi: 10.3892/ijo.9.6.1143. PubMed PMID: 21541623.
271. Jager W, Zembsch B, Wolschann P, Pittenauer E, Senderowicz AM, Sausville EA, et al. Metabolism of the anticancer drug flavopiridol, a new inhibitor of cyclin dependent kinases, in rat liver. Life Sci. 1998;62(20):1861-73. Epub 1998/05/26. doi: 10.1016/s0024-3205(98)00152-0. PubMed PMID: 9600328.
272. Knych HK, Vidal MA, Casbeer HC, McKemie DS. Pharmacokinetics of triamcinolone acetonide following intramuscular and intra-articular administration to exercised Thoroughbred horses. Equine Vet J. 2013;45(6):715-20. Epub 2013/04/12. doi: 10.1111/evj.12059. PubMed PMID: 23574452.
273. Kraus VB, Conaghan PG, Aazami HA, Mehra P, Kivitz AJ, Lufkin J, et al. Synovial and systemic pharmacokinetics (PK) of triamcinolone acetonide (TA) following intra-articular (IA) injection of an extended-release microsphere-based formulation (FX006) or standard crystalline suspension in patients with knee osteoarthritis (OA). Osteoarthritis Cartilage. 2018;26(1):34-42. Epub 2017/10/13. doi: 10.1016/j.joca.2017.10.003. PubMed PMID: 29024802.
274. Zimmermann T, Kunisch E, Pfeiffer R, Hirth A, Stahl H-D, Sack U, et al. Isolation and characterization of rheumatoid arthritis synovial fibroblasts from primary culture—primary culture cells markedly differ from fourth-passage cells. Arthritis Research & Therapy. 2000;3:1-20.

275. Practitioners AAoE. Guide for veterinary service and judging of equestrian events. 4th ed ed. Lexington KY: AAEP; 1991.
276. Huber PJ, Ronchetti E. Robust statistics. Second edition. ed. Hoboken, N.J: Wiley; 2009.
277. Auer JrA, Stick JA, Kümmerle JM, Prange T. Equine surgery. Fifth edition ed. St. Louis, Missouri: Elsevier; 2019. p. 1348-63.
278. Gunatillake P, Mayadunne R, Akhikari R. Recent Developments in Biodegradable Synthetic Polymers. Amsterdam: Elsevier; 2006.
279. Ko KW, Choi B, Kang EY, Shin SW, Baek SW, Han DK. The antagonistic effect of magnesium hydroxide particles on vascular endothelial activation induced by acidic PLGA degradation products. Biomater Sci. 2021;9(3):892-907. Epub 2020/11/28. doi: 10.1039/d0bm01656j. PubMed PMID: 33245077.
280. Habib GS. Systemic effects of intra-articular corticosteroids. Clin Rheumatol. 2009;28(7):749-56. Epub 2009/03/03. doi: 10.1007/s10067-009-1135-x. PubMed PMID: 19252817.
281. Seshadri V, Coyle CH, Chu CR. Lidocaine potentiates the chondrotoxicity of methylprednisolone. Arthroscopy. 2009;25(4):337-47. Epub 2009/04/04. doi: 10.1016/j.arthro.2009.01.003. PubMed PMID: 19341919; PubMed Central PMCID: PMCPMC6548446.
282. Kobza AO, Herman D, Papaioannou A, Lau AN, Adachi JD. Understanding and Managing Corticosteroid-Induced Osteoporosis. Open Access Rheumatol. 2021;13:177-90. Epub 2021/07/10. doi: 10.2147/OARRR.S282606. PubMed PMID: 34239333; PubMed Central PMCID: PMCPMC8259736.
283. Derendorf H, Mollmann H, Voortman G, van den Ouweland FA, van de Putte LB, Gevers G, et al. Pharmacokinetics of rimexolone after intra-articular administration. J Clin Pharmacol. 1990;30(5):476-9. Epub 1990/05/01. doi: 10.1002/j.1552-4604.1990.tb03488.x. PubMed PMID: 2347958.
284. Paik J, Duggan ST, Keam SJ. Triamcinolone Acetonide Extended-Release: A Review in Osteoarthritis Pain of the Knee. Drugs. 2019;79(4):455-62. Epub 2019/03/09. doi: 10.1007/s40265-019-01083-3. PubMed PMID: 30847805; PubMed Central PMCID: PMCPMC6437125.
285. Bodick N, Williamson T, Strand V, Senter B, Kelley S, Boyce R, et al. Local Effects Following Single and Repeat Intra-Articular Injections of Triamcinolone Acetonide Extended-Release: Results from Three Nonclinical Toxicity Studies in Dogs. Rheumatol Ther. 2018;5(2):475-98. Epub 2018/09/12. doi: 10.1007/s40744-018-0125-3. PubMed PMID: 30203389; PubMed Central PMCID: PMCPMC6251841.
286. Ni W, Zhang F, Zheng L, Wang L, Liang Y, Ding Y, et al. Cyclin-Dependent Kinase 9 (CDK9) Inhibitor Atuveciclib Suppresses Intervertebral Disk Degeneration via the Inhibition of the NF-kappaB Signaling Pathway. Front Cell Dev Biol. 2020;8:579658. Epub 2020/10/06. doi: 10.3389/fcell.2020.579658. PubMed PMID: 33015073; PubMed Central PMCID: PMCPMC7511812.
287. Yang Z, Yik JH, Chen R, He N, Jang MK, Ozato K, et al. Recruitment of P-TEFb for stimulation of transcriptional elongation by the bromodomain protein Brd4. Mol Cell. 2005;19(4):535-45. Epub 2005/08/20. doi: 10.1016/j.molcel.2005.06.029. PubMed PMID: 16109377.